Selective Catalytic Reduction of NOx on Ships

Christensen, Steen Riis

Publication date:
2018

Document Version
Publisher's PDF, also known as Version of record

Selective Catalytic Reduction of NOx on Ships

Ph.D. Thesis

Steen Riis Christensen

ORCID: 0000-0002-1684-6321

DTU Chemical Engineering
Department of Chemical and Biochemical Engineering

Handed in 31st of August 2018

Preface

This thesis entitled "Selective Catalytic Reduction of NO_x on ships" is submitted in partial fulfillment of the requirements for a Ph.D. degree at the Technical University of Denmark. The thesis accounts for the most significant results achieved from the independent scientific research that I, Steen Riis Christensen, have conducted. Besides the research, the requirements for completion of the Ph.D. program also includes 25-30 ETCS points in courses, teaching, dissemination and the public defense of this thesis.

This project is part of the private-public society partnership named Blue INNOship and is a collaboration between the CHEC research center at DTU Chemical and Biochemical Engineering, Umicore Denmark ApS, Haldor Topsøe A/S, Alfa Laval Aalborg and Maersk Maritime Technology. The project is funded by the participating companies, and by innovation fund Denmark and the danish maritime fond.

The work was completed at the CHEC research center at the Department of Chemical and Biochemical Engineering in close collaboration with Haldor Topsøe A/S (HTAS) (from 1/9-15 to 30/11-17), until the stationary DeNOx department was acquired by Umicore Denmark Aps (from 1/12-17 and ahead), with whom the close collaboration continued. The project was also performed in collaboration with Alfa Laval Aalborg and Maersk Maritime Technology. The research project was supervised by Professor Anker Degn Jensen (DTU), Senior Scientist Brian Brun Hansen (DTU), and Senior R&D Manager Kim Hougaard Pedersen (Umicore). I would like to thank all of my supervisors for their great effort and dedication. We have throughout the Ph.D. had many good discussion from model theory, to practical knowhow and English grammar, all of which I have enjoyed and learned a lot from. A big thanks is also given to former supervisor Keld Johansen (HTAS), and Joakim Reimer Thøgersen (Umicore).

I would like to thanks the CHEC technicians, Nikolaj Nissen and Anders Kjersgaard, for their great technical assistance, and also for their warm moot and funny humor. I would also like to thanks the workshop at KT, without their great work and genious help during design of setups, the research would never had reached the level it did. A special thanks is dedicated to Søren Madsen and Jens Poulsen.

A special thanks is dedicated to Jesper Sargent Larsen, research specialist at Umicore Denmark, without his help, the measurement of pressurized SO_2 oxidation, using "his" setup would never had been possible.

My gratitudes is also dedicated to Søren Mølgaard and Jens Peter Hansen from Alfa Laval for their great support and help in conducting full-scale experiments at the 2 MW marine diesel engine, as part of their test and training center in Aalborg.

My appreciation is also given to the people at Haldor Topsøe; Søren Birk Rasmussen for IR and Raman spectroscopy studies and Bjarne Møller and Henrik Lyng for help during experiments at Haldor Topsøe.

I would also like to thanks my great colleagues at CHEC, for good and funny conversations, both professionally and socially. I would also like to thanks my two former officemates Trine Dabros Arndal and Thomas Klint Torp, for good times and valuable discussion. A special thanks is dedicated to my friends; Kasper H. Lejre, Magnus Z. Stummann, and Anna Leth-Espensen, who's company I have had the great pleasure of sharing since we all started at DTU in 2010.

Last but never least, I would like to thanks the love of my life and my wife, Line Riis Christensen, for always being there for me, and for always being ready to listen to a probably boring conversation about pressurized SCR.

Steen Riis Christensen
Kongens Lyngby
August 31st, 2018

Abstract

This thesis is dedicated to investigating the effects of installing a selective catalytic reduction (SCR) reactor upstream of a turbocharger on a two-stroke marine diesel engine, at which elevated pressure of up to 5 bar is present. The installation of an SCR reactor is of interest in order to comply with IMO Tier III regulation when sailing within NO_x emission control areas.

The first part of the thesis investigates the effect of increased pressure on the main SCR reaction, which was studied using a catalyst containing about 1 wt% V_2O_5/10 wt% WO_3/TiO_2 supplied by Umicore Denmark ApS. The SCR reaction was studied across granulated catalysts (150-300 microns) in steady state experiments, for which the NO_x conversion was found independent of the pressure when the residence time was kept constant. This shows that the kinetics of the SCR reaction were not affected by the increased pressure of up to 5 bar.
NH_3 temperature programmed desorption (TPD) experiments were also conducted for the granulated catalyst. The results showed that the adsorption of NH_3 increased with pressure. The desorption profiles were modeled using a Temkin isotherm (i.e. a coverage dependent desorption enthalpi). The steady state SCR experiments were also modeled, and the SCR reaction was found independent of the catalyst surface concentration of NH_3, when the surface coverage was higher than 14%. This low surface coverage also explains why the SCR reaction was unaffected by the increased NH_3 adsorption because the active part of the catalyst was already covered with NH_3.
At a marine engine, the catalyst will be used in the form of a monolith. Therefore, SCR experiments at elevated pressure using a monolith was also conducted. Using a constant residence time, the NO_x conversion was found to be lowered by up to 5% points, at an increased pressure of 3 bar and above 250℃, due to increased mass transfer limitations. The change in mass transfer limitation is due to inverse proportionality between the binary diffusion constant and the pressure.

The second part of this thesis investigated how the oxidation of SO_2 into SO_3 was affected by increased pressure. SO_2 oxidation is known to be slightly catalyzed by the vanadium-based SCR catalyst. When the residence time was kept constant, the conversion of SO_2 was found independent of the pressure in the 1-4.5 bar range investigated. Hence the increased pressure does not affect the reaction kinetics. The reaction rate was found to be first order in SO_2 and zero order in SO_3. The rate of SO_2 oxidation was found to be promoted by NO_2, probably due to a catalyzed reaction between NO_2 and SO_2.

The last part of this thesis investigated the formation and condensation of ammonium sulfates. The sticky nature of ammonium bisulfate (ABS) was found to be prohibited by the presence of soot, probably because the soot absorbed ABS.
The deactivation of SCR monoliths due to condensation of sulfates was also studied. The bulk condensation temperature was found to be best calculated by the expression presented by Muzio et al.[1]. Experiments where an SCR catalyst was exposed to SO_3, H_2O and NH_3 showed the importance of taking pore condensation into account because the catalyst was deactivated above the bulk dew point temperature due to pore condensation. The deactivated catalyst was regenerated by elevating the temperature to 350-400℃, however, the regeneration was found insufficient at these temperatures.

This thesis contributes with new insights into the possibility of using SCR reactors positioned upstream of a marine turbocharger, where increased pressure is also present. Because no direct pressure dependency was found for either the kinetics of the SCR reaction or the kinetics of the oxidation of SO_2, the most dominating factor for deciding where to install the reactor is the correct temperature to ensure that ABS does not condense within the catalyst. Such temperatures will typically only be available upstream of the turbocharger at two-stroke marine diesel engines, and therefore also at an increased pressure of up to 5 bar.

Resumé

Denne afhandling beskriver forskning, udført indenfor drift og design af en højtryks (<5 bar) selektiv katalytisk reduktions (SCR) reaktor placeret før turboladeren på en totakts skibsmotor. Interessen for at installere en SCR reaktor på et skib drives af IMO Tier III lovgivning om reduceret NO_x udledning når der sejles indenfor NO_x emissions kontrollerede områder.

Den første del af afhandlingen undersøger effekten af det forøgede tryk på selve SCR reaktionen, målt for en SCR katalysator leveret af Umicore Danmark ApS, indeholdende ca. 1 wt% V_2O_5 / 10 wt% WO_3 / TiO_2. SCR reaktionen blev undersøgt ved brug af små granulerede katalysator partikler (150-300 mikrometer) i steady-state forsøg, hvorfra NO_x omdannelsen blev fundet uafhængig af trykket når opholdstiden var konstant. Dette viste at kinetikken for SCR reaktionen ikke blev påvirket af det øgede tryk på op til 5 bar.
NH_3 temperatur programmeret desorberings (TPD) forsøg blev også udført for den granulerede katalysator, og viste at adsorptionen af NH_3 blev forøget med det øgede tryk. NH_3 TPD forsøgene blev modelleret med brug af en Temkin isoterm, for hvilken desorberings entalpien afhang af NH_3 dækningsgraden. Steady-state SCR forsøgene blev også modelleret og SCR reaktionen blev fundet uafhængig af NH_3 dækningsgraden, allerede ved en dækningsgrad på 14%. Denne relativt lave kristiske dækningsgrad forklarede også hvorfor SCR reaktionen ikke blev påvirket af den øgede mængde NH_3 på katalysatoren ved forøget tryk, da den aktive del af katalysatoren allerede var dækket med NH_3.
Det undersøgte katalytiske pulver vil i praksis blive påført et monolit bæremateriale og derpå installeret ombord. Tryksatte monolith SCR forsøg viste, at når opholdstiden i katalysatoren blev holdt konstant, faldt NO_x omdannelsen med op til 5% point ved 3 bar og over 250℃, grundet masse transports begrænsninger. Ændringen i masse transport ved højere tryk, skyldes et fald i den binære diffusions konstant, som er omvendt proportional med trykket.

Del to af afhandlingen undersøger effekten af øget tryk på oxidationen af SO_2 til SO_3. SO_2 oxidationen er kendt for, at i mindre grad, at være katalyseret af en vanadium baseret SCR katalysator. For konstant opholdstid, blev omsætningsgraden af SO_2 også fundet konstant, uafhængigt af trykket på 1-4.5 bar. Derfor konkluderes det at kinetikken ikke påvirkes af det øgede tryk. Raten for SO_2 oxidation blev fundet til at være første orden mht. SO_2 og nulte orden mht. SO_3. Raten for SO_2 oxidation, blev forøget ved tilførsel af NO_2, sandsynligvis grundet en katalyseret reaktion imellem NO_2 og SO_2.

Den sidste del af afhandlingen undersøger dannelsen og kondenseringen af ammonium bisulfat (ABS) og ammonium sulfat. Det blev fundet at den klistrende effekt af ABS blev mindsket når sod var tilstede, hvilket måske kunne forklares ved at sod absorbere ABS.
Deaktiveringen af SCR monoliter grundet kondensering af sulfater blev også undersøgt. Gas kondensationen blev fundet bedst beskrevet af udtrykket foreslået af Muzio et al.[1]. Forsøg blev udført hvor en SCR katalysator blev udsat for SO_3, H_2O og NH_3, hvilket viste hvor vigtigt det er at tage højde for kondensation af ABS inde i katalysator porerne, fordi katalysatoren blev deaktiveret ved en temperatur højere end gas kondensations temperaturen, grundet pore kondensation af ABS. Den deaktiverede katalysator blev regenereret ved at øge temperaturen til 350-400℃, men katalysatoren kunne ikke fuldt regenereres ved disse temperaturer.

Denne afhandling tilføjer ny viden indenfor mulighederne for at installere SCR reaktoren ved højere tryk og temperaturer (før turboladeren) end praksis idag. Eftersom der ikke blev fundet nogen direkte effekt af det øgede tryk på hverken SCR kinetik eller SO_2 oxidations kinetik, er det vigtigste at sikre at temperaturen er høj nok så katalysatoren ikke deaktiveres af kondensering af ABS. Den høje temperatur som dette kræver, er typisk kun tilgængelig før turboladeren på store totakts skibsmotorer, hvor et højere tryk på op til 5 bar også vil være tilstede.

Abbreviations

Chemicals

$CaCO_3$	Calcium carbonate
CaO	Burnt lime
$Ca(OH)_2$	Hydrated lime
H_2SO_4	Sulfuric Acid
HCNO	Isocyanic acid
$NH_2{-}CO{-}NH_2$	Urea
NH_3	Ammonia
$(NH_4)_2SO_4$	Ammonium Sulfate - AS
NH_4HSO_4	Ammonium Bisulfate - ABS
NO	Nitrogen Oxide
NO_2	Nitrogen Dioxide
NO_x	Total amount of NO and NO_2
SO_2	Sulfur Dioxide
SO_3	Sulfur Trioxide
SO_x	Total amount of SO_2, SO_3 and H_2SO_4
TiO_2	Titania, unless else is stated referring to anatase
V_2O_5	Vandium Pentaoxide, active component of V-SCR catalyst
WO_3	Wolfram Trioxide, stabilizer for V-SCR catalyst

General

ABS	Ammonium bisulfate
ANR	Molar ammonia to NO_x ratio
AS	Ammonium sulfate
ASR	Molar ammonia to sulfuric acid ratio

ATR-FTIR	Attenuated total reflectance - FTIR
BET	Brunauer–Emmett–Teller
CBV	Cylinder & SCR bypass valve
CPSI	Channels pr. square inch
CSTR	Continuous stirred tank reactor
DeNOx	NO_x reduction
DOC	Diesel oxidation catalyst
DPF	Diesel particulate filter
EGB	Turbine bypass valve
EGR	Exhaust gas recirculation
EIAPP certificate	Engine international air pollution prevention certificate
ESC	European Stationary Cycle
EURO-MOT	European association of internal combustion engine manufacturers
FTIR	Fourier transformed infrared spectroscopy
HD	Heavy Duty
HFO	Heavy fuel oil
IAPP Certificate	International air polution precention certificate
IMO	International maritime organization
MDO	Marine diesel oil
MEPC	Marine environment protection committee
MFC	Mass flow controller
NECA	NO_x emission control area
NTO	Not to exceed emission limit
PBR	Packed bed reactor
PM	Particulate matter
RMSE	Residual mean sum of squares
RSS	Residual sum of squares
SCR	Selective catalytic reduction
SECA	SO_x emission control area
SFOC	Specific fuel oil consumption

TGA	Thermogravimetric analysis
TPD	Temperature programmed desorption
V-SCR	Vanadium based SCR catalyst
VOC	Volatile organic compounds

Symbols

α	Temkin parameter	$[-]$
ΔH_{ad}	Heat of adsorption	$\left[\mathrm{J/mol}\right]$
ϵ	Porosity	$[-]$
γ	Pore radius	
Ω	$\frac{1-\epsilon}{\epsilon} \cdot \Omega'$	$\left[\mathrm{mol/m^3_{reactor}}\right]$
Ω'	NH_3 adsorption capacity	$\left[\mathrm{mol/m^3_{particle}}\right]$
ρ	Density	$\left[\mathrm{kg/m^3}\right]$
σ	Surface tension	
θ_i	Surface coverage of species i	$[-]$
θ^*_{NH3}	Critical surface coverage of NH_3	$[-]$
A	Preexponential factor for a regular Arrhenius expression	
C_i	Concentration of species i	$\left[\mathrm{mol/m^3}\right]$
d_h	Hydraulic diameter	$[m]$
$d_{particle}$	Diameter of catalyst particle	$[m]$
$D_{reactor}$	Inner diameter of reactor	[m]
E_a	Activation energy of NH_3 adsorption	$\left[\mathrm{J/mol}\right]$
E_d^0	Activation energy of NH_3 desorption	$\left[\mathrm{J/mol}\right]$
$E_{A,NO}$	Activation energy for the standard SCR reaction	$\left[\mathrm{J/mol}\right]$
Gz	Graetz number	
k'_{NO}	Mass based intrinsic rate constant	
$k(T_{ref})$	Intrinsic rate constant calculated at the reference temperature T_{ref}	
k_a^0	Preexponential NH_3 adsorption constant	$\left[\mathrm{m^3/(mol \cdot s)}\right]$
k_d^0	Preexponential NH_3 desorption constant	$\left[\mathrm{1/s}\right]$
k_i	Intrinsic rate constant of component i	

$K_{i,0}$	Preexponential factor for K_i	$[1/\mathrm{Pa}]$
K_i	Adsorption equilibrium constant of component i	$[1/\mathrm{Pa}]$
P_i	Partial pressure of species i	$[Pa]$
P_{ABS}	ABS potential, i.e. the product of P_{NH3} and P_{SO4}	
P_{SO4}	Partial pressure of both SO_3 and H_2SO_4	
R	Gas constant	$[\mathrm{J}/(\mathrm{mol}\cdot\mathrm{K})]$
r_a	Rate of NH_3 adsorption	$[1/\mathrm{s}]$
r_d	Rate of NH_3 desorption	$[1/\mathrm{s}]$
Re	Reynolds number	
Sc	Schmidts number	
T	Temperature	[K]
V	Volume of reactor	$[\mathrm{m}^3]$
v_0	Volumetric flow rate	$[\mathrm{m}^3/\mathrm{s}]$
V_m	Molar volume	[Nl/mol]
w_{cat}	Mass of catalyst	[kg]
y_{calc}	Calculated value based upon model	[ppm]
y_{meas}	Measured value	[ppm]

Contents

Preface iii

Abstract v

Resumé vii

Abbreviations ix

Contents xiii

I Introduction to the Thesis xvii

1 Introduction and Background 1
- 1.1 Marpol 73/78 Annex VI . . . 2
  - 1.1.1 Regulation 13 - Emission of NO_x . . . 2
  - 1.1.2 Regulation 14 - Emissions of SO_x . . . 3
  - 1.1.3 Regulation 4 - Equivalent Compliance . . . 4
  - 1.1.4 How to Comply with IMO Tier III . . . 4
- 1.2 Selective Catalytic Reduction . . . 5
  - 1.2.1 The NO_x Reduction Chemistry . . . 6
  - 1.2.2 Addition of the Reductant . . . 8
  - 1.2.3 SCR Catalyst . . . 9
  - 1.2.4 SCR Mechanism . . . 10
  - 1.2.5 Catalyst Poisoning . . . 12
- 1.3 SCR of NO_x on Ships . . . 16
  - 1.3.1 SCR Reactor on 2- and 4-Stroke Engines . . . 17
  - 1.3.2 SCR Reactor Before Turbocharger . . . 20
  - 1.3.3 Downstream Negative Effects of an SCR Reactor . . . 22
- 1.4 Real Life Test of SCR on Ships . . . 23
- 1.5 Literature Conclusion . . . 26

2 High Pressure SCR 27
- 2.1 Introduction . . . 27
- 2.2 Experimental . . . 29
  - 2.2.1 Packed Bed Reactor . . . 29
  - 2.2.2 Monolith Setup . . . 31
- 2.3 Results . . . 33

2.3.1 NH_3 TPD . . . 33
2.3.2 Steady State SCR . . . 40
2.3.3 Full Monolith Experiment . . . 48
2.4 Conclusion . . . 52

3 Pressurized SO_2 Oxidation across V-Based SCR Catalyst - Article 55
3.1 Abstract . . . 56
3.2 Introduction . . . 56
3.3 Experimental Methods . . . 59
3.3.1 Apparatus . . . 59
3.3.2 Catalysts . . . 60
3.4 Results and Discussion . . . 61
3.4.1 Pressurized SO_2 Oxidation . . . 61
3.4.2 SO_2 Oxidation and H_2O . . . 64
3.4.3 SO_2 Inlet Concentration . . . 65
3.4.4 SO_2 Kinetic Model . . . 66
3.4.5 Fitting Results . . . 67
3.4.6 Fitted Kinetics Compared to Literature Values . . . 69
3.4.7 SO_2 Oxidation in the presence of NO_x . . . 71
3.5 Conclusion . . . 73

4 Ammonium Sulfates 75
4.1 Introduction . . . 75
4.2 Full Scale Measurements at Alfa Laval Aalborg . . . 79
4.2.1 Experimental Facility . . . 80
4.2.2 Method . . . 81
4.2.3 Results . . . 82
4.2.4 Conclusion . . . 84
4.3 Formation of AS and ABS . . . 86
4.3.1 Experimental Facility . . . 86
4.3.2 Method . . . 87
4.3.3 Results . . . 88
4.3.4 Conclusion . . . 90
4.4 ABS and Soot - A study on Soot Blowing Efficiency . . . 91
4.4.1 Experimental . . . 91
4.4.2 Results . . . 92
4.4.3 Conclusion . . . 93
4.5 SCR and ABS Deactivation - A Bench-Scale Investigation . . . 94
4.5.1 Experimental . . . 94
4.5.2 Clean SCR Profile . . . 95
4.5.3 Test of ABS Bulk Dew Point . . . 96
4.5.4 Regeneration of Deactivated Catalyst . . . 100
4.5.5 ABS Deactivation as a Function of Temperature . . . 102
4.5.6 Deactivation with both ABS and NOx . . . 104
4.6 Installation of an SCR reactor on a Ship . . . 106
4.6.1 Conclusion . . . 108

5 Conclusion and Future Work **109**
5.1 Future Work 112

Bibliography **115**

A SCR Engine Test **A-1**

B NH_3 TPD - Fitting **B-1**

C Limitations in a PBR **C-1**
C.1 Diffusion Limitations C-1
C.2 Dispersion C-3
C.2.1 Axial Dispersion C-3
C.2.2 Radial Dispersion C-3

D Online Resources for SO_2 Ox. Article **D-1**
D.1 Mass Transfer Limitations D-1

I Introduction to the Thesis

This chapter gives an overview of the structure of the Ph.D. thesis, the publication made, and the student project that was supervised.

Publications and Conference Contributions

Published International Peer-Reviewed Journals

S. R. Christensen, B.B. Hansen, K. Johansen, K. H. Pedersen, J. R. Thøgersen, and A. D. Jensen (2018), "SO_2 Oxidation Across Marine V_2O_5-WO_3-TiO_2 SCR Catalysts: a Study at Elevated Pressure for Preturbine SCR Configuration", *Emission Control Science and Technology*, DOI: 10.1007/s40825-018-0092-8

Articles in Preparation

S. R. Christensen, B.B. Hansen, K. H. Pedersen, J. R. Thøgersen, and A. D. Jensen, "High Pressure SCR of NO_x Across Marine V_2O_5-WO_3-TiO_2 SCR Catalyst: a Study at Elevated Pressure for Preturbine SCR Configuration", *In Preparation to be submitted.*

Oral Conference Contributions

S. R. Christensen, B.B. Hansen, K. H. Pedersen, and A. D. Jensen: "High Pressure Pre-turbine SCR reactor for NO_x reduction on Ships". Presented at 18^{th} Nordic Symposium on Catalysis (NSC), 2018, Copenhagen, Denmark

Poster Conference Contributions

S. M. Christensen, B. B. Hansen, K. Johansen, and **A. D. Jensen**: "Selective Catalytic Reduction of NO_x on Ships". Presented at 13^{th} European Congress on Catalysis (Europacat), 2017, Florance, Italy.

Supervision of Student Projects

Laurits Bøggild Krogsbøll, Bachelor's thesis: "High Pressure Pre-turbine SCR for NO_x reduction on Ships", January-June 2017

Structure of the Thesis

Each experimental chapter (Chapter 2, 3, and 4) is initiated by a short literature section, in order to establish the correct knowledge base of the reader.

Chapter 1: Is a literature survey, written to introduce the reader within the general concepts of marine legislation, selective catalytic reduction, and selective catalytic reduction on ships.

Chapter 2: Is an experimental chapter, for which high pressure SCR experiments were conducted using both packed bed reactors and monolith catalysts. The chapter is in the process of being rewritten into an article.

Chapter 3: Is a copy of the published article "SO_2 Oxidation Across Marine V_2O_5-WO_3-TiO_2 SCR Catalysts: a Study at Elevated Pressure for Preturbine SCR Configuration".

Chapter 4: Is an experimental chapter, in which the formation and decomposition of ammonium sulfates and also the important study about deactivation of an SCR catalyst caused by ammonium sulfates are discussed.

Chapter 5: Is the conclusion on the Ph.D. thesis and proposed future work.

1 Introduction and Background

In the 1890s Rudolf Diesel invented a new type of internal combustion engine, that today is known as a diesel engine[2]. The diesel engine has a good fuel economy, due to a high air-fuel compression ratio, resulting in a high energy output and low (g/km) emissions of carbon dioxide CO_2, compared to the counterpart of a gasoline engine[2]. However, during combustion other emissions such as nitrogen oxides (NO_x), sulfur oxides (SO_x), and particulate matter (PM) are formed as also shown by Figure 1.1.

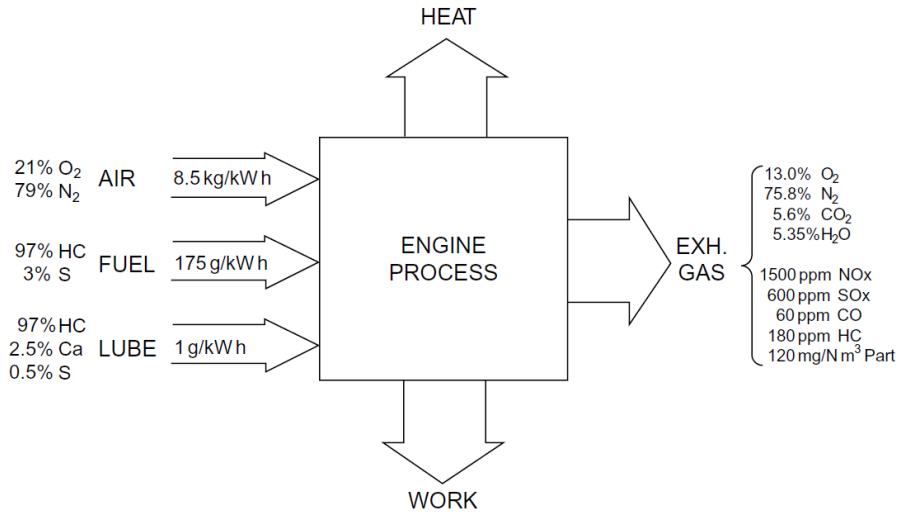

Figure 1.1: Typical exhaust emissions from a modern low-speed diesel engine[3].

SO_x emissions are produced due to the presence of sulfur within the fuel, which is completly oxidized into SO_2 during the combustion, and up to 10% of the SO_2 is further oxidized into SO_3[4]. NO_x on the other hand, is not present in the fuel but is produced within the high temperature combustion zone. NO_x is mainly produced through the Zeldovich mechanism[5, 6], in which oxygen and nitrogen radicals react and produce NO, which can further react with oxygen producing NO_2, however, NO_2 i usually less than 10% of the overall NO_x[7].

In todays modern society, shipping of goods is the life blood of the global economy, and the international shipping industry is responsible for the carriage of more than 80% of world trade[8, 9]. More than 90%[10] of all ocean going vessels are today powered by large diesel engines, and hence a substantial amount of pollution originate from the maritime sector. It has been estimated that global transport

makes up 30% of anthropogenic NO_x emissions[11] out of which the marine sector accounts for the half[12]. The emission of NO_x is known to cause eutrophication and acidification at sea and land and causes health issues such as lung and hearth complains[11, 13–15]. Due to the health care problems connected with emissions of NO_x, SO_x, and PM, the automotive industry has since 1975 decreased the amount of emitted gases with multiple orders of magnitude for instance through the EU legislations for passenger cars such as EuroI (1992)-EuroVI (2014)[16]. The global nature of the marine sector means that it has been more difficult to agree on how and what to regulate, however, with the enforcement of MARPOL 73/78 Annex VI in 2005[17], the reduction of NO_x and SO_x has been put on the agenda.

1.1 Marpol 73/78 Annex VI

Marpol 73/78 Annex VI entered into force the 19th of May 2005 in order to reduce the air pollutions from ships. Marpol Annex VI applies to all ships, fixed and floating rigs and other platforms. Annex VI requires that ships of 400 gross tons and above, which are engaged in international voyages involving the countries who have ratified the conventions to have an International Air Polution Prevention Certificate (IAPP Certificate). Furthermore, the diesel engine used at the ship needs an Engine International Air Pollution Prevention Certificate (EIAPP Certificate). The EIAPP certificate is issued during an initial test at the engine manufactures test cite, and should be periodical tested to ensure compliance. Six main regulations are introduced with respect to air pollution[17]:

- **Regulation 12:** Emissions from ozone depleting substances from refrigerating plant and fire fighting equipment
- **Regulation 13:** (NO_x) emissions from diesel engines
- **Regulation 14:** (SO_x) emissions from diesel engines
- **Regulation 15:** Volatile organic compounds (VOC) emissions from cargo oil tanks of oil tankers
- **Regulation 16:** Emissions from shipboard incinerators
- **Regulation 18:** Fuel oil quality

Out of the six regulation shown, regulation 13 (NO_x) and regulation 14 (SO_x) will be further discussed here.

1.1.1 Regulation 13 - Emission of NO_x

Regulation 13 states the maximum allowed NO_x emission for diesel engines depending on the size of the engine and when the diesel engine was installed on the ship. Regulation 13 applies for[17]:

- A diesel engine that has a greater power output than 130 kW, which has been installed on a ship constructed after the 1st of January 2000

- A diesel engine that undergoes a major conversion after the 1st of January 2000
- A diesel engine with a power output greater than 5000 kW and a per cylinder displacement at or above 90 liter constructed after the 1st of January 1990 but prior to the 1st of January 2000

The diesel engines that falls under the above mentioned characteristics needs to follow the NO_x emission as shown in Figure 1.2

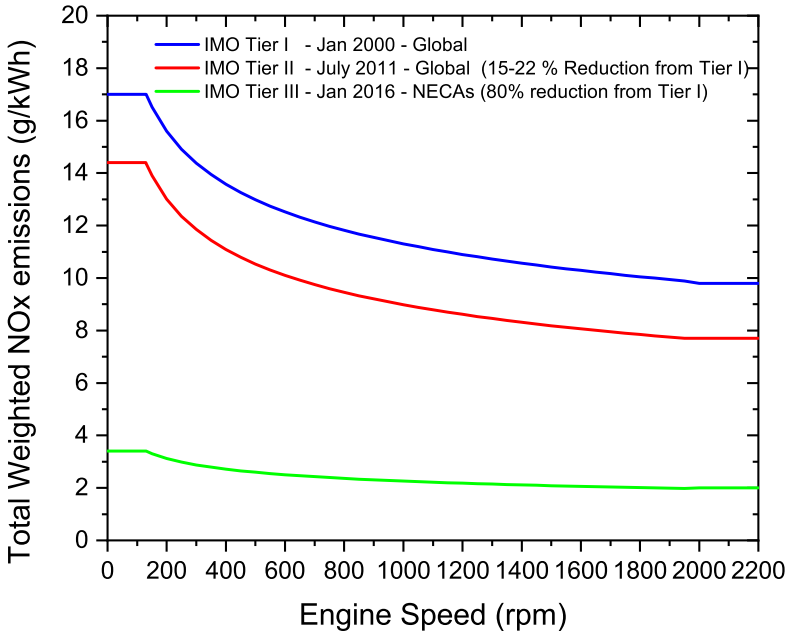

Figure 1.2: The allowed weighted NO_x emissions[17]. The weighting depends on the type of engine and follows different test cycles as given by the Marpol Annex VI Appendix II[18]. The month and year for each Tier, states the time for which the regulation applies to all new build ships or major conversion of the engine. It should be noted that Tier III is not a global requirement, hence outside NECA Tier II applies.

Figure 1.2 shows the allowed weighted NO_x emission based on the engine speed. The weighted NO_x emission refers to the different test cycle that Marpol have created depending on the type of engine as given by Marpol Annex VI appendix II[18]. Figure 1.2 also shows three different Tier's together with a date. Tier I and Tier II are global requirements and apply to all engines installed after 1st of January 2000 or 1st of July 2011 respectively. Tier III only applies to engines constructed after 1st of January 2016 and only when the ship is operated within NO_x Emission Control Area's (NECA's), outside of the NECA Tier II applies. NECA's are at the moment comprised of the North American coast line and the US Caribbean coast line and more areas are expected to come[19].

1.1.2 Regulation 14 - Emissions of SO_x

Emissions of SO_x and particulate matter are regulated through regulation 14, which state the maximum allowed sulfur content of the marine fuel oil regardless of the use

on board (i.e. combustion engines, boilers, gas turbince etc.)[17]. The maximum allowed sulfur content of a marine fuel oil is shown in Figure 1.3 together with implementation dates. Contrary to the NO_x regulation, the regulation of SO_x applies to all ships independent on keel laying dates, because it is possible to comply with the regulation without making any changes to the ship/engine other than fueling with a fuel oil containing less sulfur.

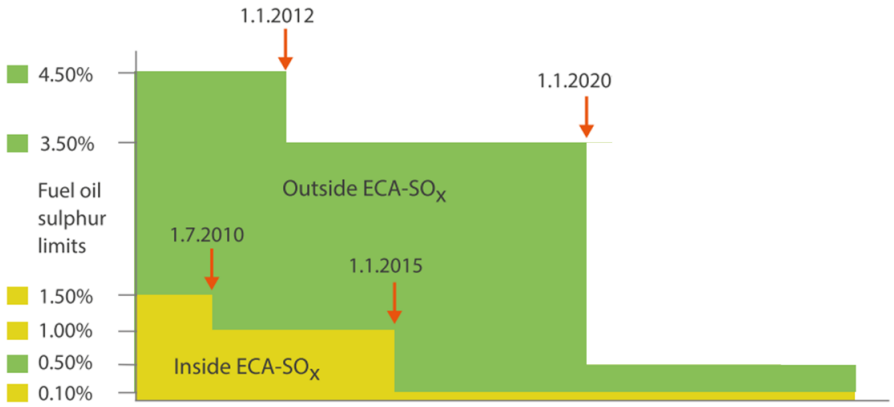

Figure 1.3: The maximum allowed sulfur content of a fuel oil depending on the date, and whether sailing is within or outside of a SECA (ECA-SO_x). Adapted from [20].

Figure 1.3 shows that different amount of sulfur are allowed depending on whether sailing within or outside of a SO_x Emission control area (SECA), which at the moment means the Baltic Sea, the North Sea, the North American coast line and the US Caribbean coast line[20].

Regulation 14 requires that in case a fuel changed is performed in order to comply with SECA regulation, the changed should be performed in such a time that all fuel lines have been flushed with the new fuel when the ship enters the SECA. Furthermore, the time and placement of the fuel changed must be written in the logbook.

1.1.3 Regulation 4 - Equivalent Compliance

Marpol Annex VI introduced a new regulation 4, which allow ship owners to comply with regulation 13 and 14 by means of "Equivalent compliance". This means that the engine out NO_x and SO_x emission does not need to comply with the regulation, as long as the final outlet of exhaust gas comply with the regulations. For SO_x emissions, this means that it is possible to use fuel oil with a higher sulfur concentration than stated by regulation 14, as long as the exhaust gas is cleaned, for instance using a scrubber, to the same extent, as if the low sulfur fuel oil was used.

1.1.4 How to Comply with IMO Tier III

The european association of internal combustion engine manufacturers (EUROMOT), and the two largest marine engine manufacturers MAN Diesel & Turbo and

Wärtsilä corporation have made it clear that multiple solutions exist to comply with IMO Tier III regulation 13, and at the moment the most favorable solutions are exhaust gas recirculation (EGR), selective catalytic reduction (SCR), or dual-fuel engines[21]. EGR, as the name implies, recirculates part of the exhaust gas back to the combustion chamber. This decreases the concentration of oxygen and increases the heat capacity by increasing the amount of H_2O present within the combustion chamber. Therefore, the NO_x production is reduced due to a decrease in combustion temperature[10, 22]. Another possibility is to use an SCR catalyst, across which the NO_x can be reduced to harmless nitrogen and water. The possibility of using SCR will be the focus of the coming sections, and the remaining part of this thesis.

To comply with regulation 14 the ship owner can either use a cleaner fuel oil, a different fuel or a scrubber which remove the SO_x content from the exhaust gas downstream of the engine. The scrubber can either be a dry scrubber[23] or a wet scrubber[24] both of which will also remove particulate matter. The dry scrubber uses a packed bed reactor of calcium carbonate ($CaCO_3$), burnt lime (CaO) or hydrated lime ($Ca(OH)_2$)[23], which react with SO_x across the bed. The wet scrubber on the other hand is based on the principle of a spray tower, where water is prayed as small droplets into the exhaust gas, at which SO_x reacts with alkaline species present in the water. If the scrubber is operated as "open loop", seawater is used which has a natural buffering capacity due to bicarbonate (HCO_3^-). Alternatively, "close loop", can be used in which fresh water is used and an alkaline specie such as sodium carbonate is added (Na_2CO_3).

Because the dry scrubber is dry and the reactions are exothermic the exhaust gas temperature is increased a bit across the scrubber, and hence the installation of an SCR unit can be done downstream of the dry scrubber, at which place less sulfur is present. However, the weight of a dry scrubber is substantially larger than a wet scrubber, for instance a 20 MW dry scrubber weights approximately 211 tonnes compared to an equivalent wet scrubber which weighs around 10 tonnes[20]. The wet scrubber cools the exhaust gas to around 50℃[24], and hence the SCR unit cannot be installed downstream of a wet scrubber, but needs to be installed in the high sulfur environment upstream of the scrubber.

1.2 Selective Catalytic Reduction

The Selective Catalytic Reduction (SCR) of NO_x (NO+ NO_2) using a N-containing specie as reductant was first used in Japan during the 1970s and later introduced in the US during the 1980s[25–27]. SCR of NO_x utilizes a catalyst, usually an oxide based catalyst, at which the reaction between NO_x and ammonia (NH_3) takes place and selectively forms harmless nitrogen (N_2) and water (H_2O) according to Equation 1.1, 1.2, and 1.3.

SCR of NO_x was first introduced at stationary applications such as power plants, waste incinerators and within the cement industries[27]. The reduction of NO_x was performed using NH_3 and high efficiencies were achieved ($> 90\%$ NO_x reduction)[28].

The later use of SCR of NO_x on heavy duty diesel vehicles was done due to the introduction of Euro4 (2005) and Euro5 (2009) emission standards which called for a high reduction in tail-pibe NO_x[29]. For mobile applications an aqueous solution of urea (30-40wt%) instead of NH_3 has been used as a reductant, a liquid which decomposes into NH_3 and CO_2 upon heating[30]. With the introduction of Marpol 73/78 annex VI Tier III[17], the maritime sector needs efficient ways of reducing both SO_x and NO_x. Therefore, this thesis will focus on optimizing the use of SCR of NO_x on ships and how the SCR reactor will affect up- and downstream equipment.

This section will focus on the SCR catalyst used within the maritime sector, the NO_x reduction chemistry, how to add the reductant, possible side reactions, reaction mechanism, and catalyst poisoning.

1.2.1 The NO_x Reduction Chemistry

The SCR of NO_x is comprised of three reactions[26, 30, 31]. The main reaction is known as the standard SCR reaction and involves oxygen and equimolar amounts of NO and NH_3 as shown in Equation 1.1. It is called the standard SCR reaction because approximately 90% of the engine out NO_x from diesel engines is present as NO[26, 30–33]. The fast SCR reaction is the reduction of 2 moles of both NO and NO_2 which are reduced using 4 moles of NH_3 as shown in Equation 1.2. It is known as the fast SCR because the reaction rate of the fast SCR is substantially faster than the standard SCR at low temperatures (< 300℃)[26, 27, 30, 31]. The fast SCR is usually only interesting for systems where a strong oxidation catalyst, such as Platinum, is present upstream of the SCR reactor, such as on road transport vehicles. An oxidation catalyst is not used within high sulfur applications such as ships fuel by MDO (Marine diesel oil, ∼1.5-2 wt% S.) or HFO (Heavy fuel oil, >2 wt S.)[34]. Therefore, the fast SCR is expected to play small role for the marine SCR chemistry. The last SCR reaction is the slow SCR reaction and is the reduction of NO_2 with NH_3 as shown in Equation 1.3, and is even slower than the standard SCR, and hence the NO_2/NO_x ratio should not be higher than 0.5.

$$\text{Standard SCR:} \quad 4NH_3 + 4NO + O_2 \longrightarrow 4N_2 + 6H_2O \tag{1.1}$$

$$\text{Fast SCR:} \quad 4NH_3 + 2NO + 2NO_2 \longrightarrow 4N_2 + 6H_2O \tag{1.2}$$

$$\text{Slow SCR:} \quad 4NH_3 + 3NO_2 \longrightarrow 3.5N_2 + 6H_2O \tag{1.3}$$

The SCR reactions shows optimal NO_x reduction efficiency (DeNOx) and selectivity in a temperature window of 300-400℃[33, 35], however, it depends on the catalytic loading and catalyst, as will be considered during explanation of the catalyst components, Section 1.2.3. At higher temperatures the catalyst tends to form byproducts such as NO and N_2O, or NH_3 can be oxidized to N_2 without reducing any NO_x as shown by the unwanted side reactions in Equation 1.4, 1.5, and 1.6.

$$4NH_3 + 5O_2 \longrightarrow 4NO + 6H_2O \tag{1.4}$$

$$4NH_3 + 3O_2 \longrightarrow 2N_2 + 6H_2O \tag{1.5}$$

$$2NH_3 + 2O_2 \longrightarrow N_2O + 3H_2O \tag{1.6}$$

The byproducts will either form pollution (NO and N_2O) or create the need for more NH_3 for a given NO_x reduction and hence induce a higher cost of operation.

NO_x reduction as a function of temperature across different catalysts are shown in Figure 1.4. The figure shows typical examples of a fast increase in activity, from approximately 30% NO_x reduction at 225℃ and up to approximately 90% NO_x reduction at 300℃. The NO_x reduction is usually around 90% between 300-400℃ when using V-SCR catalyst, and above approximately 400℃ NH_3 oxidation becomes the dominating reaction, according to Equation 1.4, and hence the NO_x reduction decreases. The only catalyst showing a higher initial activity is the 3 wt% V_2O_5 extruded catalyst, probably due to the increased catalytic material being present at an extruded catalyst. Koebel et al.[36] showed that at a temperature below 250℃ the NO_x takes place within the catalyst, however, at higher temperatures, at which fast kinetics are present, the reaction becomes diffusion limited, and hence reaction only occurs at the surface of the catalyst.

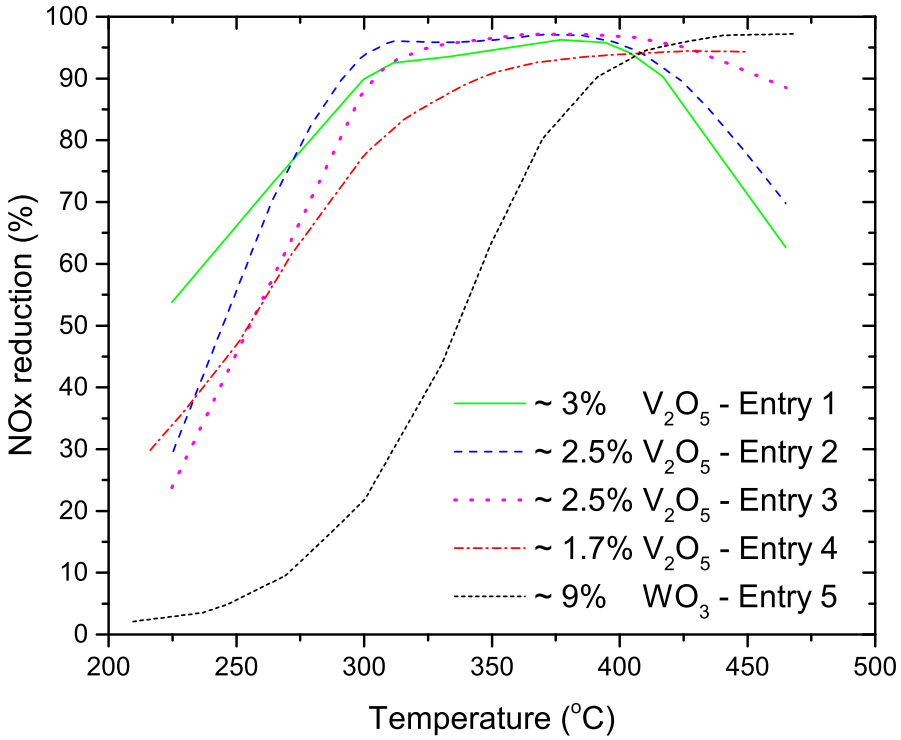

Figure 1.4: NO_x reduction as a function of temperature, using different types of catalyst and testing methods. Further explanation is given in Table 1.1 based on the entry number given in the figure. Entry 1-3 are tested at an engine setup, at which NH_3 is controlled to give an NH_3 slip of 10 ppm[37]. Entry 4 is tested using model gas containing 10% O_2, 5% H_2O, 1000 ppm NO, balanced N_2, and NH_3 corresponding to 10 ppm NH_3 slip with a GHSV = 52 000 hr^{-1}[33]. Entry 5 is tested using a Packed Bed Reactor (PBR), and model gas containing 800 ppm NH_3, 800 ppm NO, 1% O_2 and balance He at a flowrate of 216 Nl/hr[26].

Figure 1.4 also shows that WO_3 also exhibit some NO_x reduction capability, however, it should be noted that entry 5 is based on a PBR experiment compared to the other entries which are based on monoliths, hence non intrinsic rates.

It should be noted that Entry 2 shows a higher activity compared to entry 3 below 300℃, even though entry 3 contains 400 cpsi and hence almost double the amount of active component (2200 g. vs. 1400 g[37]). This is probably due to a higher surface area of cordierite compared to the metal substrate.

Table 1.1: Specifications for the catalysts tested in Figure 1.4.

Entry	Citation	Catalyst	Catalyst tybe	Test	Cpsi	Substrate
1	Koebel et al. [37]	3% $V_2O_5/WO_3/TiO_2$	Ext. Mono	Engine	300	-
2	Koebel et al. [37]	2.5% $V_2O_5/WO_3/TiO_2$	Coat. Mono	Engine	300	Cordierite
3	Koebel et al. [37]	2.5% $V_2O_5/WO_3/TiO_2$	Coat. Mono	Engine	400	Metal
4	Krocher et al. [33]	1.7% $V_2O_5/WO_3/TiO_2$	Ext. Mono	Model gas	400	-
5	Forzatti et al. [26]	9% WO_3/TiO_2	Grounded	Model gas	-	-

1.2.2 Addition of the Reductant

For stationary applications gaseous NH_3 is normally used as reductant, however, for mobile applications such as the transport or maritime sector, gaseous NH_3 is considered too dangerous and instead urea ($NH_2{-}CO{-}NH_2$) is used, usually as an aqueous solution[30, 38]. A 30-40 wt% urea in water solutions is typically used[30], for which it should be noted that the eutectic composition is 32.5 wt% with a freezing point of -11℃. With the relative high freezing point the storage of urea also needs a heating system to ensure that the urea solution does not solidify.

The urea solution is sprayed into the hot exhaust gas upstream of the SCR reactor, as very fine droplets. The first reaction taking place is the evaporation of water, a highly energy requiring reaction ($\Delta H_{H_2O,vap} = 2270\frac{kJ}{kg}$), leaving small urea melt droplets as shown in Equation 1.7[30, 32, 33].

$$NH_2{-}CO{-}NH_2(aq) \longrightarrow NH_2{-}CO{-}NH_2(melt) + x\ H_2O \tag{1.7}$$

The urea melt is heated and decomposes readily in the exhaust gas at temperatures above 200℃ into NH_3 and isocyanic acid (HNCO) according to reaction 1.8[30, 32, 33].

$$NH_2{-}CO{-}NH_2(melt) \longrightarrow NH_3(g) + HNCO(g) \quad \Delta H_{298\,K} = 186kJ \tag{1.8}$$

$$HNCO(g) + H_2O(g) \longrightarrow NH_3(g) + CO_2(g) \quad \Delta H_{298\,K} = -96kJ \tag{1.9}$$

The HNCO formed in Equation 1.8 then reacts with water present in the exhaust gas forming a mole of NH_3 according to Equation 1.9. HNCO has been found to be quite stable in the gas phase, and hence the hydrolysis of HNCO does not take place in the gas phase. As stated by Kleemann et al.[39], the hydrolysis is easily catalyzed by various oxides such as silica, alumina, and titania and will, therefore, also be catalyzed by typical V-SCR catalyst. The fact that the hydrolysis takes place at the V-SCR catalyst reduces the NO_x efficiency since less catalyst will be available for NO_x reduction. The requirement of small reactor sizes for mobile applications also means that the physical space available for the above reactions to take place is very limited. Beside the limiting time of reaction, the use of urea instead of NH_3

complicates the system due to possible side reactions forming higher molecular species such as cyanuric acid, biuret or melamine. The temperature of the SCR should therefore preferably be above 200℃. At fast heating rates above 200℃, the higher molecular species are normally not observed[30, 32, 33]. Furthermore, the addition of urea causes a temperature decrease of the exhaust gas of approximately 10-15℃[32], which especially impact the SCR reactions at low temperatures.

Even though problems can arise when using urea it has found use within heavy duty (HD) diesel trucks, and urea is distributed under the sales name Adblue®. Research is still ongoing in both control systems, nozzles for addition of the urea-water mixture, and low pressure loss static mixers in order to ensure mixing between NO_x and NH_3.

1.2.3 SCR Catalyst

The first SCR catalyst used was based on platinum[26, 28], however, due to the high redox activity and low selectivity of the catalyst, this catalyst could not be used at temperatures above 250℃[40]. During the 1970s a switch from noble metals to metal oxide based catalysts was done. The new generation of catalysts were based on vanadium pentaoxide (V_2O_5) on a surface of alumina, silica or titania. Due to a superior activity, selectivity and stability under normal operating conditions most SCR catalysts are today based on vanadia added to a high surface area form of titania (anatase) and stabilized by the addition of wolfram trioxide (WO_3)[26]. A new type of catalyst also used today is the ion exchanged zeolite type, either exchanged with copper or iron. Zeolites have great thermal stability, however, they are easily deactivated by sulfur and hence cannot be used at ships using heavy fuel oil, and will therefore not be considered here. For more information about zeolites used for SCR see for instance [41–43].

V_2O_5 is the active component of the vanadium based SCR (V-SCR) catalyst. V_2O_5 provide surface sites at which NH_3 can adsorb (V-OH sites) and sites at which the adsorbed NH_3 can be activated. It is usually present in 1-5 wt% of the catalyst depending on the system. A higher loading of V_2O_5 will also promote the undesired oxidation of SO_2 but also give a higher activity of the catalyst, and hence, can be useful for low sulfur and low temperature processes. Forzatti et al.[26] have for instance shown that a V_2O_5(0.78 wt%)/TiO_2 based catalyst could achieved 50% NO_x conversion at 317℃, however, increasing the V_2O_5 content to 1.4 wt% reduced the temperature to 287℃ for the same degree of conversion. The V_2O_5 content is rarely above 6 wt% since the catalyst then tends to lose its stability and its selectivity towards N_2 at higher temperatures and with increasing load of V_2O_5.

V_2O_5 is usually stabilized by wolfram trioxide (WO_3) and spread over a surface of anatase. For pure TiO_2 the transformation of anatase into rutile, a low surface area form of TiO_2, is observed at approximately 700℃, however, the transformation is catalyzed by V_2O_5 and can be observed at lower temperatures depending on the loading. The transformation can be hindered by adding WO_3, at which the transformation of pure TiO_2 mixed with 9 wt% WO_3 is first observed at 900℃[26–28].

Beside delaying the transformation of anatase, WO_3 also adds to the surface acidity which increases the surface coverage of NH_3. Furthermore WO_3 also suppresses the unwanted SO_2 oxidation[26]. Approximately 10 wt% of WO_3 is therefore usually added to an SCR catalyst.

The combination of V_2O_5(0-5 wt%)/WO_3($\sim$ 10 wt%)/TiO_2 as a catalyst is very attractive for the SCR of NO_x due to high surface area, strong redox activity, high surface acidity, and high selectivity. The catalyst is either added to a monolith using a washcoat or the catalyst is made as an extruded monolith. The monolith structure has the great advantage compared to a packed bed reactor, that it delivers the same geometrical surface area without adding the same large pressure drop, and with the straight channels present in the monolith clogging due to dust can be avoided by designing the size of the channels appropriately. At temperatures below 250℃ the SCR reactions are relatively slow compared to the diffusion of NO_x and NH_3 and therefore the reactions are governed by kinetic control. Above 250℃ the reactions are fast, and increased diffusion control will be observed by a decrease in NO_x reduction efficiency[44]. Therefore at high temperatures the SCR reactions will only take place at the surface of the catalyst. The oxidation of SO_2 on the other hand is kinetically limited across the full SCR temperature range 200-500℃, and hence will be enhanced by a thicker catalyst layer[26, 27]. Therefore when using SCR technology in high sulfur and high dust areas a low content of V_2O_5 is added to a large surface area of catalyst, created with relative high channel sizes.

1.2.4 SCR Mechanism

Different mechanisms have been proposed for the reduction of NO_x by NH_3, however, the most accepted mechanism today is the dual site Eley-Rideal mechanism which was proposed by Inomata et al.[45].

Inomata et al. observed that when oxygen was present in higher concentration than 1% v/v the catalyst was found to be in a fully oxidized state. Furthermore, by pulse experiments it was found that a catalyst treated with NH_3 resulted in considerable amount of N_2 when reacted with NO (1000 ppm)+O_2 (1%) or only NO (1000 ppm) at 250℃, however, with the pure NO being slowest. If the catalyst on the other hand was treated with NO first, no N_2 was obtained as product at 250℃ when NH_3 was added with or without O_2. This clarifies that the reaction mechanism is initiated by NH_3 adsorbed on the catalyst surface, and that NO reacts from the gas phase or as weakly bounded to the surface[45].

Topsøe et al.[46] used in-situ FTIR to support the research performed by Inomata et al. They proposed a catalytic cycle, as shown in Figure 1.5 at which the first step (step 1) is the adsorption of NH_3 on a Brønsted acid site (V$-$OH) located adjacent to a redox active site (V=O). Topsøe et al. measured the concentration of both lewis acid sites and Brønsted acid sites, and found that the SCR activity was only dependent on the Brønsted acid sites[46].

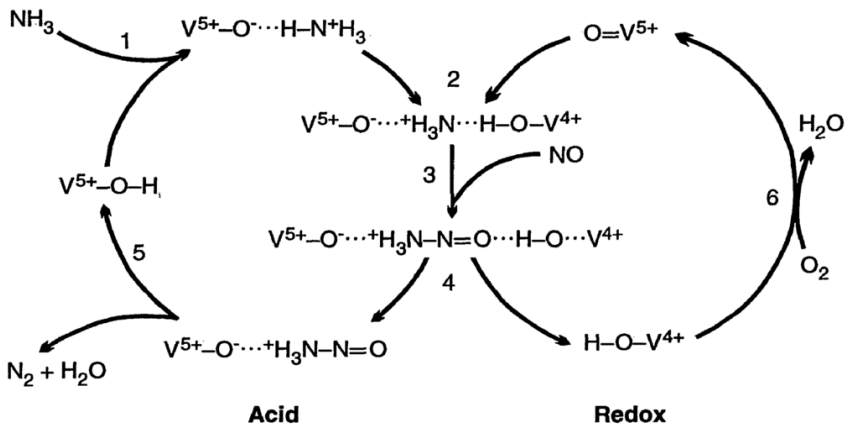

Figure 1.5: The catalytic cycle proposed by Topsøe et al.[46] which shows the reduction of NO using NH_3 on a V_2O_5 based catalyst.

The strongly adsorbed NH_3 which is adsorbed as NH_4^+(ad) is activated by adjacent vanadyl sites (V=O) (step 2). Went et al.[47] observed that both monomeric and polymeric vanadate species are active in the NO_x reduction, however, the polymeric vanadates are more active and with an increasing concentration of O_2 tends to form N_2O, hence, at normal conditions with higher concentration of O_2 (>2% v/v) the polymeric vanadates should be avoided. Topsøe et al.[48] observed that the formation of polymeric vanadyl sites are depending on both the temperature and vanadia concentration. Topsøe et al.[48] tested three catalysts with 6 wt%, 2 wt%, and 0.6 wt% V_2O_5, polymeric vanadia sites was only observed in the 6 wt% V_2O_5 catalyst as a broad band at 923 cm^{-1} using Raman spectroscopy. Therefore the V_2O_5 loading should be below 6 wt% to ensure selectivity towards N_2, however, the specific concentration at which polymeric vanadia sites are formed was not investigated, but they were not present in a 2 wt% V_2O_5 based catalyst.

The activated NH_4^+(ad) complex then reacts with gaseous or weakly bond NO (step 3). The reaction causes (step 4) the formation of a reduced form of the catalyst ($V^{4+}-OH$) which was observed by Topsøe et al.[46] using online FTIR, however, the other product (see Figure 1.5) was not observed and is believed to be an intermediate which decomposes fast (step 5) forming the reaction products i.e. N_2 and H_2O. The last step (step 6) is the completion of the catalytic cycle by re-oxidation of the catalyst by gaseous O_2 and is considered fast at O_2 concentration higher than 1% v/v[45, 46, 49].

A new complete mechanism explaining both the standard SCR and the fast SCR reaction has been proposed by people at Topsøe A/S, in the article by Arnarson et al.[50]. The main difference is that the reoxidation of the catalyst is now believed to go through a reaction between both NO and O_2 producing NO_2 which then also is reduced to N_2. The initiation step for the reaction is a reduction reaction which require NH_3 and NO to be present and therefore the product of NO_2 will not be observed without NH_3 present, and if NH_3 is present, will be reacted through the fast SCR. Because this study is more interested in macro than micro kinetics, the reader is refereed to the article by Arnarson et al.[50] for more information.

The kinetic modeling of the reaction is usually done under the assumption of an oxygen concentration above 1% v/v and hence the reaction is independent of O_2 concentration[45]. Using the Eley-Rideal mechanism with NH_3 being adsorbed on the surface and NO reacting from the gas phase the rate of reaction can be written as in Equation 1.10[26]:

$$r_{\mathrm{NO}} = k_c \cdot C_{\mathrm{NO}} \cdot C_{\theta,\mathrm{NH_3}} \tag{1.10}$$

In which k_c is the intrinsic rate constant, C_{NO} is the gas-phase NO concentration, and $C_{\theta,\mathrm{NH_3}}$ is the surface concentration of NH_3. Equation 1.10 can be further evaluated by considering the equilibrium of water and NH_3 that are present on the surface as shown in Equation 1.11 and Equation 1.12. Water is considered since it adsorbs on the same Brønsted acid sites as NH_3 in a competitive adsorption[49].

$$C_{\theta,\mathrm{NH_3}} = K_{\mathrm{NH_3}} \cdot C_{\mathrm{NH_3}} \cdot C_{\theta,*} \tag{1.11}$$

$$C_{\theta,\mathrm{H_2O}} = K_{\mathrm{H_2O}} \cdot C_{\mathrm{H_2O}} \cdot C_{\theta,*} \tag{1.12}$$

In which $K_{\mathrm{NH_3}}$ and $K_{\mathrm{H_2O}}$ are the adsorption equilibrium constants for NH_3 and H_2O respectively, and $C_{\theta,*}$ is the concentration of vacant surface active sites. Equation 1.10 can now be changed by substitution of Equation 1.11, Equation 1.12, and the total surface site balance ($C_{\theta,*} + C_{\theta,\mathrm{NH_3}} + C_{\theta,\mathrm{H_2O}} = C_{\theta,\mathrm{total}}$) into Equation 1.13

$$r_{\mathrm{NO}} = k_c' \cdot C_{\mathrm{NO}} \cdot \frac{K_{\mathrm{NH_3}} \cdot C_{\mathrm{NH_3}}}{1 + K_{\mathrm{NH_3}} \cdot C_{\mathrm{NH_3}} + K_{\mathrm{H_2O}} \cdot C_{\mathrm{H_2O}}} \tag{1.13}$$

In which $k_c' = k_c \cdot C_{tot}$. The effect of competitive adsorption of water is constant above 5% v/v, which is typical for combustion processes, and hence for typical applications the final kinetic expression is usually further simplified as shown in Equation 1.14[26, 51, 52].

$$r_{\mathrm{NO}} = k_c' \cdot C_{\mathrm{NO}} \cdot \frac{K_{\mathrm{NH_3}} \cdot C_{\mathrm{NH_3}}}{1 + K_{\mathrm{NH_3}} \cdot C_{\mathrm{NH_3}}} \tag{1.14}$$

1.2.5 Catalyst Poisoning

This section focus on the possible poisoning and deactivation mechanisms that could limit the lifetime of a $V_2O_5/WO_3/TiO_2$ catalyst used on a ship such as hydrothermal aging, hydrocarbon poisoning, and sulfur poisoning.

1.2.5.1 Hydrothermal Aging

It is generally known that compared to zeolites the V-SCR catalysts are not as thermal stable[28, 41]. Girard et al.[53] tested the aging effect on two new undisclosed vanadium based catalysts washcoated on cordierite and compared the results with an extruded vanadia-titania catalyst. The aging was performed at 550℃ in 14% O_2, 5% H_2O, 5% CO_2 and balance N_2 for 75 hours. After aging, the extruded catalyst showed good DeNOx activity at low temperature, however, at 400℃ a sharp decrease in DeNOx activity was observed and at 480℃ a negative DeNOx activity was

observed due to NH_3 oxidation. The washcoated catalyst still resulted in approximately 80% NO_x reduction at 500℃. The production of N_2O was observed from all three catalyst above 400℃, however, the extruded catalyst produced approximately 15 ppm N_2O at 450℃ compared to below 5 ppm from the washcoated catalysts. Maunula et al.[54] showed that standard 2-3 wt% V_2O_5/10 wt% WO_3/TiO_2 could withstand temperatures below 600℃ without losing activity, and with the addition of silicon could be durable up to 700℃, with a slightly lower activity at medium temperatures.

Nova et al.[55] tested a 0.6 wt% V_2O_5/9 wt% WO_3/TiO_2 catalyst at different calcination temperatures. The catalyst was calcined at 500℃ for 2 hours and the BET surface area was measured to 63 m^2/g. The BET surface area decreased to 33 m^2/g after being calcined at 750℃ for 2 hours and 17 m^2/g after being calcined at 800℃ at 2 hours. Beside the decreased surface area, an increased mean radius of the pores present in the catalyst was observed. The mean radius after calcination at 500℃ was 109 Å, however increased to 195 Å after being calcined at 750℃. After calcination at 800℃ a bimodal distribution of pores was observed with a radius of 135 Å and 530 Å. The SCR activity was expected to be lowered with the loss of surface area, however, due to the formation of larger pores, the effective diffusion constant of the diffusion limited SCR reaction was almost doubled after calcination at 800℃ and the total activity of the catalyst was similar as shown in Table 1.2.

Table 1.2: Estimated kinetic parameters at a reaction temperature of 350℃, ANR=1.1, SO_2=500ppm, H_2O=10%, O_2=2% in N_2[55].

	Calcined @ 500℃	Calcined @ 750℃	Calcined @ 800℃
$D_{eff,NO}$ - (cm^2/s)	$1.5 \cdot 10^{-2}$	$2.5 \cdot 10^{-2}$	$2.7 \cdot 10^{-2}$
Effectiveness factor, η	$8.8 \cdot 10^{-2}$	$1.5 \cdot 10^{-1}$	$1.6 \cdot 10^{-1}$
k_c - (1/s)	$1.16 \cdot 10^3$	$7.10 \cdot 10^2$	$6.22 \cdot 10^2$
$\eta \cdot k_c$ - (1/s)	103	105	102

The catalyst calcined at 800℃ was found to be twice as active with respect to SO_2 oxidation, which was attributed to agglomeration of V species on the TiO_2 surface[55].

Without the addition of a diesel particulate filter (DPF) creating high exotherms during regeneration i.e. oxidizing particles to clean the filter, the temperature before the SCR catalyst at a ship will be below 500℃ at which V-SCR is considered thermally stable.

1.2.5.2 Hydrocarbon Poisoning

Girard et al.[53] tested a washcoated vanadia based catalyst and an extruded vanadia based catalyst and observed that they only had a decrease of 5% in NO_x conversion during exposure to 700 ppm propylene added to a simulated exhaust gas containing 350 ppm NO, 350 ppm NH_3, 14% O_2, 4.6% H_2O, and 5% CO_2 at 200℃

and 300℃. Schmieg et al.[56] tested two commercial vanadia based cordierite monoliths in the presence of either a (69%)propene/(31%)propane mixture or n-octane, added to simulated exhaust gas consisting of 125 ppm NO, 125 ppm NO_2 (fast SCR), 250 ppm NH_3, 5% CO_2, 5% H_2O, 8% O_2, and balance N_2. The hydrocarbons were either added as 300 ppm or 990 ppm. At 225℃ Schmieg et al. observed no deactivation at either catalysts and neither any oxidation of HC i.e. no increase in CO or CO_2 across the catalyst. At 450℃, oxidation and deactivation were observed both with the propene/propane mixture and the n-octane. The NO_x reduction was decreased from 90% NO_x conversion to 86% in the presence of 300 ppm propene/propane mixture and to 77% in the presence of 990 ppm propene/propane mixture. When using n-octane instead of the propene/propane mixture Scmieg et al. observed that the decrease in NO_x conversion was approximately 5% points lower than in the propene/propane case.

Gieshoff et al.[57] also tested a washcoated $V_2O_5/WO_3/TiO_2$ catalyst by addition of 10 ppm and 30 ppm n-decane to a model gas containing 500 ppm NO, 450 ppm NH_3, 1.3% H_2O, 5% O_2, and balance N_2. Gieshoff et al. observed a decrease in activity with the addition of n-decane. The temperature at which 50% NO_x conversion was observed was 250℃ without n-decane, 270℃ with 10 ppm n-decane, and 300℃ with 30 ppm n-decane. At temperatures above 380℃ no deactivation was observed showing the reversibility of the deactivation process. Gieshoff et al. measured an increase in CO and CO_2 after the SCR catalyst, however, no NO_x conversion was observed when NH_3 was not present and hence oxidation of HC is not part of the selective reduction of NO_x.

Table 1.3: Elemental composition of the catalysts tested by Japke et al.[58]. Catalyst 1 is a commercial catalyst and bulk values are based on analysis of a grounded catalyst sample.

Species	Cat. 1	Cat. 2	Cat. 3	Cat. 4
V (surface - XPS)[wt%]	1.6	0.7	1.7	1.5
V (Bulk)[wt%]	(0.5)	1	2.2	2.1
W (bulk)[wt%]	(2.6)	7.38	8.4	5.35
Si (Bulk)[wt%]	(15.6)	*l*0.5	*l*0.5	4.32
Ti (Bulk)[wt%]	(18.1)	50.5	49.3	44.5

Japke et al.[58] tested different vanadium based catalyst as shown in Table 1.3. Japke et al. observed that by the addition of 1000 ppm propylene the propylene oxidation was low (<20%) below 300℃ in the absence of SCR reaction. With both propylene and SCR reaction present no deactivation of the SCR reaction was observed below 300℃, however, above 300℃ where the propylene oxidation also was proceeding effectively, a large deactivation of the SCR reaction was observed. Japke et al. therefore proposed that the deactivation was due to adsorption of intermediates from the propylene oxidation on the NH_3 active sites. The deactivation mechanism is the same found by Lou et al.[59] for a copper beta zeolite. Below the onset temperature of propylene oxidation Lou et al. found no deactivation.

The deactivation caused by intermediates could explain why Girard et al.[53] and

Schmieg et al.[56] did not observe any deactivation below 300℃. Gieshoff et al.[57] also observed deactivation when oxidation of hydrocarbons was observed, however, at lower temperatures, which could be due to the use of a long chain hydrocarbon (n-decane) which is easily broken into smaller hydrocarbons and possible intermediates causing the deactivation.

As indicated by Japke et al. further studies should be made to fully understand the deactivation mechanism. As also noted by several authors vanadium based catalysts in general are less deactivated by hydrocarbons compared to zeolites and the deactivation is reversible and hence the catalyst can regain its activity after heating to higher temperatures depending on the hydrocarbon.

1.2.5.3 Sulfur Poisoning

Sulfur content in HFO can be as high as 3.5%[60] and is oxidized into SO_2 and a minor part into SO_3 ($< 10\%$[4]) during combustion. HFO is the most used fuel within the maritime sector, and even with the new sulfur legislation (IMO Tier III 1/1/2020), a sulfur content of 0.1 wt% sulfur is allowed in the marine fuel. Therefore an SCR catalyst need to have high resistance against sulfur poisoning.

$V_2O_5/WO_3/TiO_2$ based catalyst are generally considered to be sulfur robust. Sulfur poisoning is usually observed at low temperatures at which sulfates such as ammonium sulfate (AS) and ammonium bisulfate (ABS) condense and block the pores and the active sites of the catalyst[61–63]. Blakeman et al.[31] for instance tested a washcoated vanadia based SCR by using the automotive test, the European Stationary Cycle (ESC) before and after 50 hours of aging. The aging was performed without NH_3, at 240℃ using a 12 liter HD engine fueled with high sulfur fuel for vehicles (350 ppm sulfur). The NO_x conversion over the ESC was 86% before aging and 89% after. The increased activity of the catalyst is due to the formation of surface sulphates adding to the surface acidity, as will be further explained later in this section. Blakeman et al. also measured the DeNOx as a function of temperature before and after low temperature aging (260℃) using extra high sulfur fuel for vehicles (3600 ppm) with an NH_3 to NO_x ratio (ANR) of 0.8 while aging. With ANR = 0.8 NH_3 was present during aging and sulfates were formed and resulted in high deactivation i.e. 50% NO_x conversion was achieved at 275℃ before aging, but first at 350℃ after aging. At higher temperatures above 375℃ regeneration was observed. Walker et al.[64] also tested an undisclosed washcoated monolith, and Ura et al.[65] tested an undisclosed extruded catalyst and both found no deactivation when sulfur aging was performed at either high temperature or without NH_3.

SO_2 has been found by multiple authors[61–63, 66] to have a twofold effect. It promotes the DeNOx reaction under some conditions and deactivates under other. Kijlstra et al.[61] investigated this two fold effects of SO_2 on a 1.5 wt% V_2O_5/TiO_2 catalyst and a 6 wt% V_2O_5/TiO_2 catalyst. The low temperature deactivation was found to be due to condensation of ammonium sulfates, such as ammonium bisulfate (ABS) or ammonium sulfate (AS). Because the sulfates originates (See Equation 1.15 and 1.16) from the oxidation of SO_2 to SO_3, a kinetically hindered oxidation,

the deactivation was more severe at the high loaded vanadia catalyst.

$$SO_3 + 2NH_3 + H_2O \longrightarrow (NH_4)_2SO_4 \quad (1.15)$$

$$SO_3 + NH_3 + H_2O \longrightarrow NH_4HSO_4 \quad (1.16)$$

The sulfates created could be decomposed by heating the sample. If the regeneration was performed up to 400℃ the activity of the catalyst was restored without removing the promoting affect, however, by heating to 580℃ the promoting affect was lost as well indicating the difference in bonding strength between promoting species and sulfates[31, 61].

The promoting effect of SO_2 has been ascribed by several authors[61–63, 66] to be due to an increase in surface acidity close to the redox sites (V=O) and hence increasing the DeNOx until V=O sites becomes the limiting component. Kijlstra et al.[61] proposed that the increased surface acidity was due to formation of $(TiO)_3S{=}O$, which then further reacted with H_2O or available OH groups to form the acid $(TiO)_2SOOH$. Kijlstra et al. observed a higher degree of promotion for the low load vanadia catalyst and explained it through the availability of the titania support adjacent to redox sites as shown in Figure 1.6.

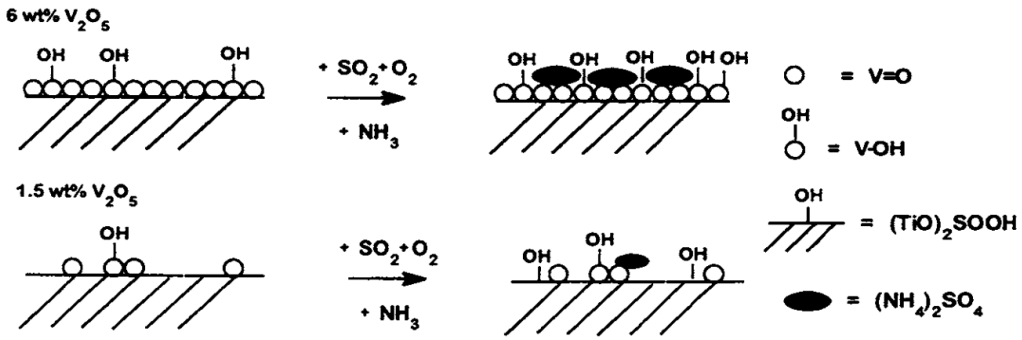

Figure 1.6: How a high loaded V-SCR is covered by vanadium and and hence the formation of support acid sites ($(TiO)_2SOOH$) are limited, and the promoting effect of SO_2 on high load V-SCR is therefore not observed[61].

The formation of AS and ABS is a large problem especially for downstream heat exchangers or other cold surfaces where the sulfates will precipitate. At higher temperatures the V-SCR catalysts are considered sulfur tolerant and is the preferred catalyst chosen when using HFO[53, 54, 67].

1.3 SCR of NO_x on Ships

The use of SCR of NO_x on ships was first introduced in the late 1980s. Even though more than twenty years have gone by, the literature within SCR for ships is sparse. This is especially due to the possibility of reaching the earlier NO_x emission limits, through cheaper methods such as internal engine modification such as water injection, EGR, or increased Miller Cycle all of which decreases the cylinder temperature and hence the formation of NO_x. The previous introduction of IMO

Tier I (2000[17]) and the addition of Tier II (2011[17]) resulted in a decrease in the allowed NO_x emissions of 15-20% compared to Tier I, however, with the introduction of IMO Tier III in 2016 it is believed that more of the NO_x reduction will be performed through the use of an SCR catalyst, due to the requirement of 80% NO_x reduction compared to IMO Tier I[17]. In a report made by the IMO Marine Environment Protection Committee (MEPC)[68] it is stated that the two most suited technologies for complying with Tier III NO_x reduction is either by the use of EGR or SCR technology.

During this section the focus will be on how to fit an SCR catalyst on both 2- and 4-stroke engines, how to add, control and ensure mixing of urea, and finally a case study with SCR implemented on-board a ship.

1.3.1 SCR Reactor on 2- and 4-Stroke Engines

One of the first applications of SCR reactors on ships was at two 8 MW 2-stroke engines in 1989 and 1990 on two Korean bulk carriers[69]. The two SCR reactors were placed upstream of the turbocharger to ensure high temperature and were designed to achieve around 90% NO_x reduction. Since the addition of SCR units to the two 8 MW engines, the use of SCR units on ships has slowly but steady increased as also shown on Figure 1.7. The industry within marine SCR reactors has especially increased within the last 10 years probably due to the enforcement of IMO Tier III in 2016.

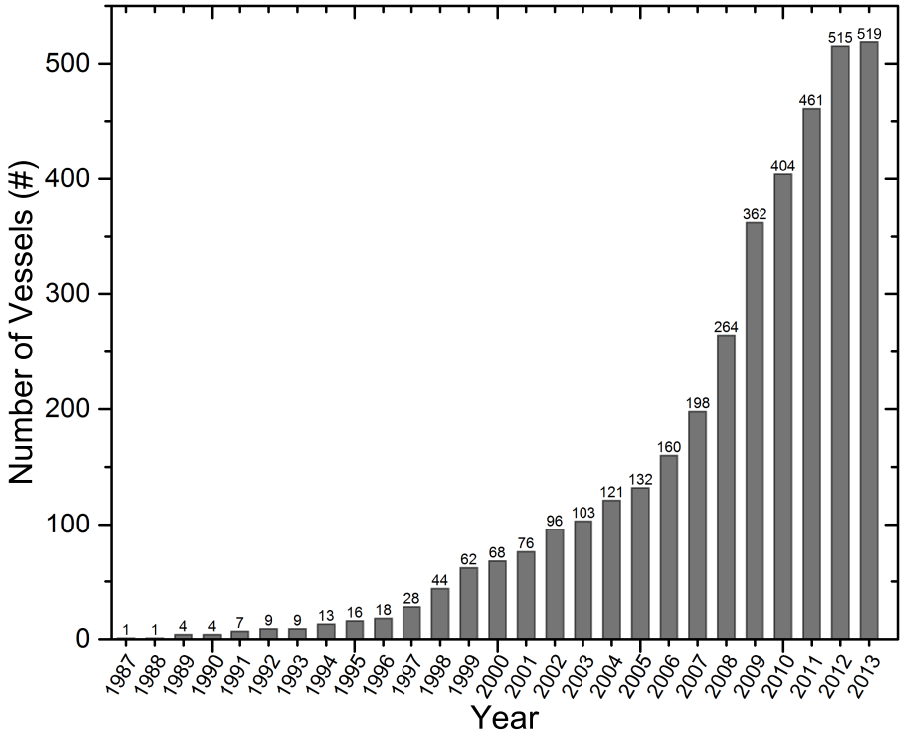

Figure 1.7: Number of vessels with SCR installed. Adopted from [11].

Most of the SCR reactors introduced on ships so far have been on 4-stroke engines,

due to a higher exhaust gas temperature after the turbocharger, at around 300-450℃[70, 71]. The exhaust gas temperature from a 4-stroke engine has a higher temperature due to the design of the four strokes. In a 4-stroke engine, one stroke pushes out the exhaust gas and another stroke draws fresh air into the combustion chamber, hence, a very well defined amount of air is introduced to the combustion chamber. In a 2-stroke engine the exhaust gas is pushed out by the inlet of fresh air in one stroke. To ensure depletion of the exhaust gas, a lot of fresh air is pushed through the combustion chamber at a high pressure, therefore, 2-stroke engines have a higher air to fuel ratio and hence a higher heat capacity inside the combustion chamber resulting in a lower exhaust gas temperature. If an SCR reactor is to be fitted at a 2-stroke engine, it is generally accepted that the temperature after the high efficient turbocharger is too low for SCR operation, especially when running on high sulfur fuel as shown in Figure 1.8 [14, 22, 70, 72–74].

Figure 1.8 shows the exhaust gas temperatures from two 2-stroke engines as a function of load both before and after the turbocharger. Figure 1.8 also shows the minimum required temperatures for an SCR reactor when 0.5 wt% S, 1.5 wt% S, and 2.5 wt% S are present in the fuel burned. The limits are present due to the formation of sulfates which will condense and block the surface of the catalyst. The condensation temperatures depends on the partial pressure of the sulfates and hence, the concentration of sulfur in the fuel, therefore, different limits are shown in Figure 1.8 depending on the fuel sulfur content. In order to achieve the correct temperature the SCR should be placed upstream the turbocharger at which the temperature is sufficient during some loads. It should be noted that, as shown in Figure 1.8, for some engine setups an engine load of 50% will result in a sufficient exhaust gas temperature even when using HFO containing 2.5 wt% sulfur and on others this will require an operation at around 80% load. Due to differences in the exhaust gas temperature the fitting of an SCR reactor is very engine specific and should be controlled to ensure correct temperature. A control structure is also needed since the volume and heat capacity of the catalyst will have an impact on the engine dynamics when decreasing or increasing the load on the engine[22, 69, 75] as will be considered in Section 1.3.2.

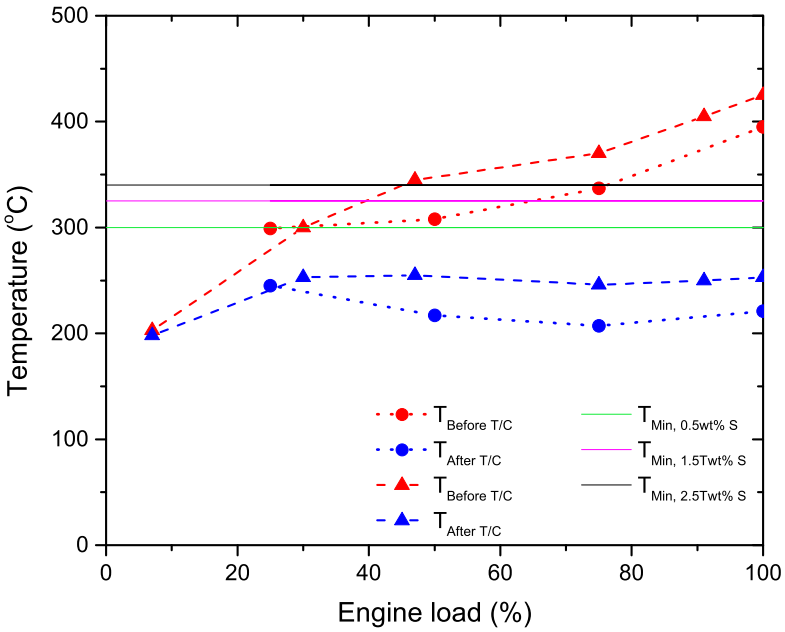

Figure 1.8: Temperature before (red) and after (blue) the turbocharger from two 2-stroke engines and the minimum required SCR temperature when running on fuel containing 0.5 wt% (green), 1.5 wt% (purple) and 2.5 wt% sulfur (black) based on Zheng et al.[76]. The circles are based on experiments performed by Man Turbo & Diesel[22] at a 6S50ME-C engine. The triangles are based on experiments performed by Fujibayashi et al.[70] at a 6S46MC-C7 engine.

1.3.1.1 Controlling and mixing Urea

A very important topic in order to ensure stable and efficient NO_x reduction is how to control the amount of urea added to the exhaust gas and how to ensure evaporation and mixing within the very short residence time from injection of urea and until the SCR reactor inlet. Koebel et al.[30] measured the NH_3/HNCO/Urea fraction before a V-SCR catalyst at a vehicle test bench as shown in Figure 1.9, with a reference residence time of 0.09 seconds at 440℃.

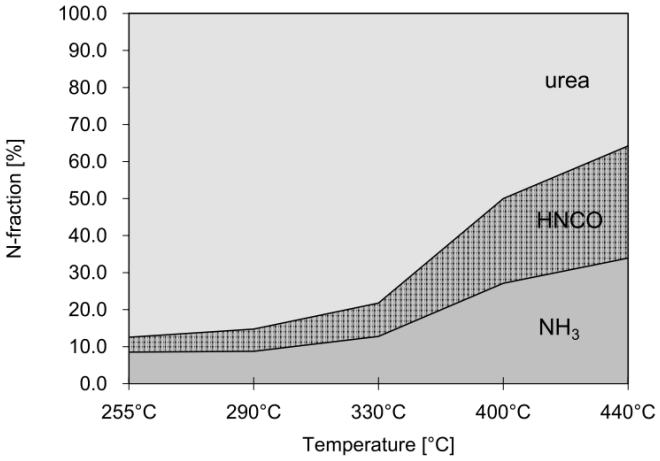

Figure 1.9: The fraction of NH3/HNCO/Urea before a V-SCR catalyst with a reference residence time of 0.09 seconds at 440℃[30].

The control structure for adding urea is usually based on feedforward control, feedback control or a mixture of the two[77]. Feedforward control is the measurement of NO_x out of the engine, before the SCR, and add urea accordingly, usually using an ANR below 0.9 to ensure high NO_x reduction while reducing NH_3 slip to below 10 ppm[71]. Since a NO_x sensor needs maintenance and calibration another feedforward control structure is based on engine mapping, where more simple measurements such as engine load, speed, temperature, and ambient temperature and humidity are measured by conventional sensors and the engine out NO_x is calculated and used for controlling the urea dosage[71]. Feedback control system is based on measuring the NO_x out of the reactor, and on this basis urea is dosed to ensure a certain low level of NO_x out of the SCR reactor. A feedback control system has the advantage of more precise control, however, is very dependent on correct real time measurements.

After addition of urea it is important to ensure good mixing before the SCR reactor. If sufficient mixing is not achieved insufficient NO_x reduction will occur together with ammonia slip, which also increases the possibility for sulfate formation downstream of the SCR reactor, which will condense at the boiler and reduce the efficiency. The problem of achieving good mixing is present due to the small time scale and the large geometries present within the maritime sector. First part of the mixing is to create small droplets preferably using an air-assisted jet to induce the urea[13, 71, 78]. Second part is the placement of a static mixer with as low pressure drop as possible which still gives sufficient mixing. Zheng et al.[79] states that in order to achieve sufficient mixing it is important to design each mixer and injector for the specific operation since external factors such as engine conditions, mounting angles, mixing length, and pipe diameter have to be taken into account, which can be a problem especially if the SCR reactor is placed upstream of the turbocharger where the space is even more limited.

1.3.2 SCR Reactor Before Turbocharger

The next sections discuss how to fit an SCR reactor before the turbocharger, how low load operation can be achieved with sufficient temperature for SCR operation, and how the reactor affects the engine dynamics.

1.3.2.1 Dynamic Effects and Low Load SCR

In order to use SCR for NO_x reduction at large 2-stroke engines Man Diesel and Turbo[22] and Hitachi Zosen Corporation[70] have developed a Tier III compliant system comprised of a 6.8 MW 2-stroke engine, fitted with an SCR reactor upstream of the turbocharger as shown in Figure 1.10(a). While inside a NECA exhaust gas is directed from the exhaust gas receiver through the urea vaporizer, SCR reactor and subsequent turbocharger by closing V1 and opening V3 and V2 (See Figure 1.10(b)). Urea is a large expense and therefore the system has been designed to bypass the SCR when not operating inside a NECA (See Figure 1.10(a) purple arrows) and can be obtained by closing V2 and V3 and opening V1.

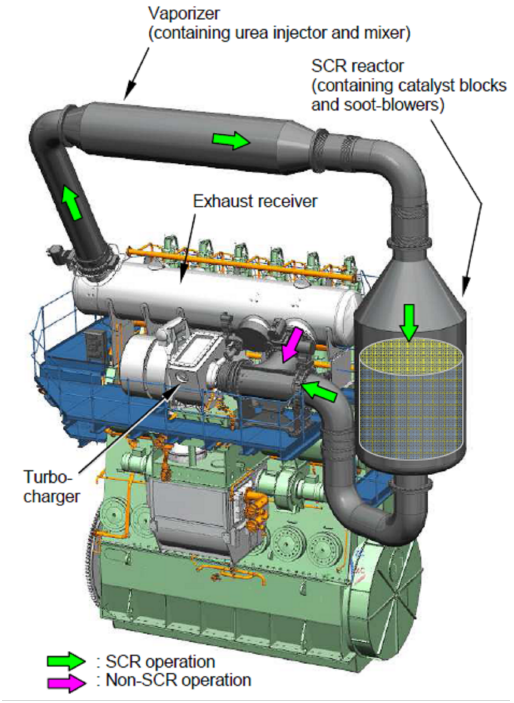

(a) Possible fitting of an SCR reactor upstream the turbocharger.

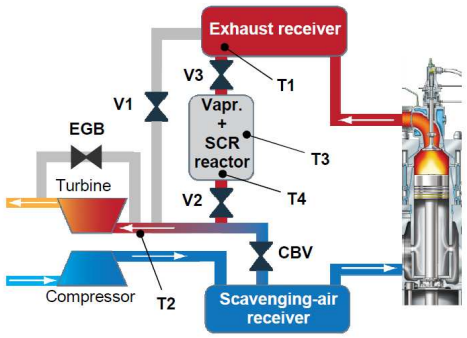

Symbol	Explanation	Remark
V1	SCR bypass valve	variable
V2	SCR sealing valve	variable
V3	SCR sealing valve	on/off
CBV	Cylinder & SCR bypass valve	variable
EGB	Turbine bypass valve	variable
T1	Exhaust gas temperature at exhaust receiver (inlet of SCR system)	
T2	Exhaust gas temperature at inlet of turbine	
T3	Exhaust gas temperature at inlet of reactor	
T4	Exhaust gas temperature at outlet of reactor	

(b) Schematic representation of the SCR reactor and controlling valves.

Figure 1.10: 6.8 MW 2-stroke marine diesel engine. Hitachi-MAN B&W 6S46MC-C7 equipped with SCR reactor upstream the turbocharger[70].

The importance of the aforementioned valves (V1,V2, and V3) is not only to control whether the engine is operated with or without the SCR reactor, the valves are also used to ensure steady and efficient operation of the turbocharger. Due to the large heat capacity of the SCR reactor the turbocharger would fluctuate in the case of a sudden change in engine load due to insufficient or excess scavenging-air pressure as also depicted in Figure 1.11(a), at which a load decrease was simulated by Fujibayashi et al.[70]. In case of a load decrease, less fuel is injected into the combustion chamber and therefore, the exhaust gas temperature is lowered. The lowered exhaust gas temperature also induces a lower volumetric flowrate which will push the turbine and therefore, the compressor will also push less scavenged-air into the next cycle. With a warm SCR reactor positioned before the turbine the cold exhaust gas will be heated and hence increase the volumetric flowrate through the turbine and therefore also increase the scavenging-air into the combustion chamber. This will cause fluctuation for the turbocharger as also shown in a simulation by Fujibayashi et al.[70]. The fluctuation of the turbocharger can be minimized either by bypassing the SCR reactor through V1 or bypassing the turbocharger through the turbine bypass valve (EGB) as shown in Figure 1.11(b). Since the exhaust gas going through V1 is not cleaned for NO_x, the control through the EGB valve is the preferred solution when decreasing the load[70].

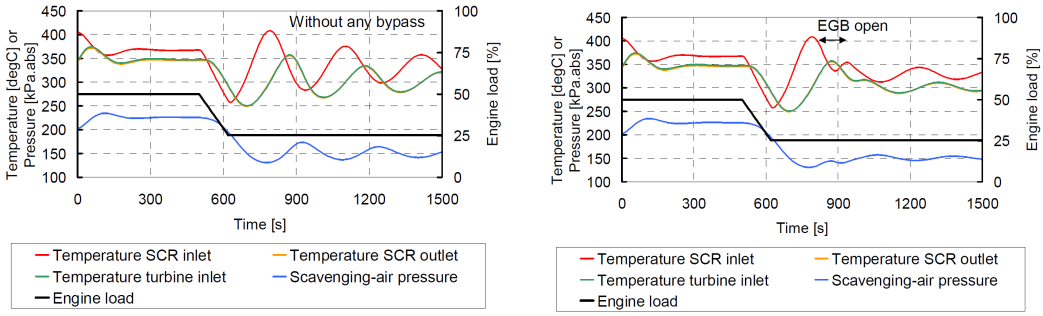

(a) without any bypass.

(b) Bypass of the turbocharger.

Figure 1.11: Simulation of how the turbocharger will fluctuated due to the heat capacity of the SCR reactor in the event of a load decrease and how the fluctuation can be minimized by bypassing the turbocharger through the EGB valve or bypassing the SCR reactor through V1. It should be noted that the curve "temperature turbine inlet" (green) and the curve "temperature SCR outlet" (orange) are equal as long as V1 is closed and hence the orange curve is not visible[70].

In the event of an increase of load, the problem with the turbine is the same, however, this time the SCR reactor is too cold and hence opening the EGB valve will not help. In that case V1 must be used to control the heating of the SCR reactor in a slow manner, based on a maximum temperature difference between T1 and T2 of 50 K[75].

Figure 1.10(b) also shows a cylinder & SCR bypass valve (CBV), this is used to increase the exhaust gas temperature out of the cylinder, by decreasing the amount of air into the combustion chamber, however, keeping the fuel addition constant, and hence decrease the heat capacity inside the combustion chamber. By means of this control structure the problems with too low exhaust gas temperatures at low load, as shown in Figure 1.8, is managed. An important consideration of using the CBV valve is that the cold air that is bypassed is mixed with the warm exhaust gas before the turbine and hence no loss of efficiency or fluctuation is observed when using the valve, however, it is at the expense of the specific fuel oil consumption (SFOC).
Fujibayashi et al.[70] also measured general engine parameters such as temperatures, pressure and turbocharger speed both when bypassing the SCR reactor and while the SCR reactor was operating and found the parameters to be almost identical as shown in Appendix A.

1.3.3 Downstream Negative Effects of an SCR Reactor

The main negative effects of implementing an SCR reactor in the high sulfur atmosphere is the formation of ABS and AS downstream of the SCR reactor, also adding to the particulate matter. Another part is controlling the ammonia slip which could be regulated in the future.

Jayaram et al.[80] measured how the installation of an SCR reactor at a 3.5 MW 4-stroke marine diesel engine changed the amount and content of particulate matter. Jayaram et al. measured a decrease of 77-91% in organic carbon and 17-61% in

elemental carbon across the SCR catalyst in different engine tests, however, they also measured an increase in the number of small particles $PM_{2.5}$ (Radius $< 2.5\mu m$) with a facotr of 1.5-3.8 mostly due to the oxidation of SO_2 into SO_3 which reacted with NH_3 or H_2O and formed sulfates or H_2SO_4 aerosols as shown in Figure 1.12.

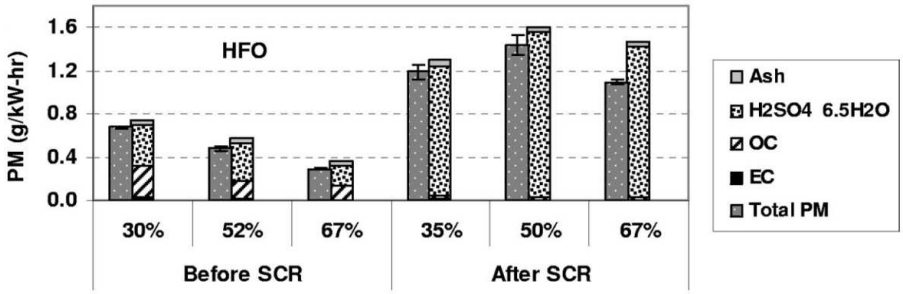

Figure 1.12: Effect of installing an SCR reactor on PM. Measurement performed before and after the SCR reactor as a function of Engine load. Measurement performed at 3.5 MW 4-stroke marine diesel engine using a V-SCR catalyst[80].

The sulfates are a large problem for downstream cold surfaces such as boilers at which they will condense and create a sticky surface which will catch additional PM, as shown in Figure 1.13, and will reduce the heat transfer substantially and hence the efficiency of the boiler. Soot blowers could be installed to keep the boiler surfaces clean, however, with the sticky sulfates the soot blowers are inefficient and hence the sulfates should be avoided or at least be controlled towards the less sticky compound ammonium sulfate compared to the sticky ammonium bisulfate.

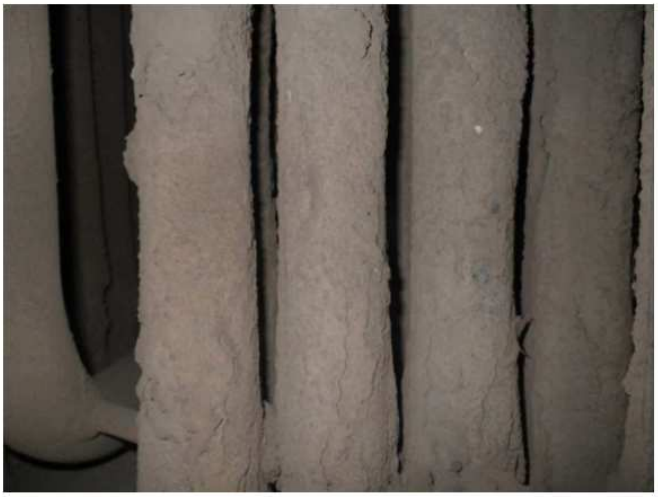

Figure 1.13: Condensation of sulfates at a boiler unit placed downstream of an SCR reactor. The SCR operation time and conditions are undisclosed[70].

1.4 Real Life Test of SCR on Ships

Reports have stated successful implementation of SCR reactors both before the turbocharger at 2-stroke engines and after the turbocharger at 4-stroke engines all

of which have been able to comply with Tier III regulation[70, 71, 74, 77, 78, 81].

Fujibayashi et al.[70] tested the preturbocharger SCR option on a 6.7 MW 2-stroke main engine at a 38000 DWT cargo ship. The preturbocharger SCR system was designed as already explained in Section 1.3.2.1. As part of the installation of the SCR reactor it was noted that the retrofitting of an SCR reactor does not seam easy due to the limited space in the engine room. Fujibayashi et al. had to relocate parts from the engine room in order to make room for the SCR reactor. After installation of the SCR reactor a sea-trial was performed. During the sea-trial the ship was maneuverable as before and the NO_x reduction complied with IMO Tier III as shown in Figure 1.14. The green line and circles shown in Figure 1.14 represent the load points which are part of the IMO E3 test cycle[82] which both state a minimum reduction and a not to exceed (NTE) emission limit.

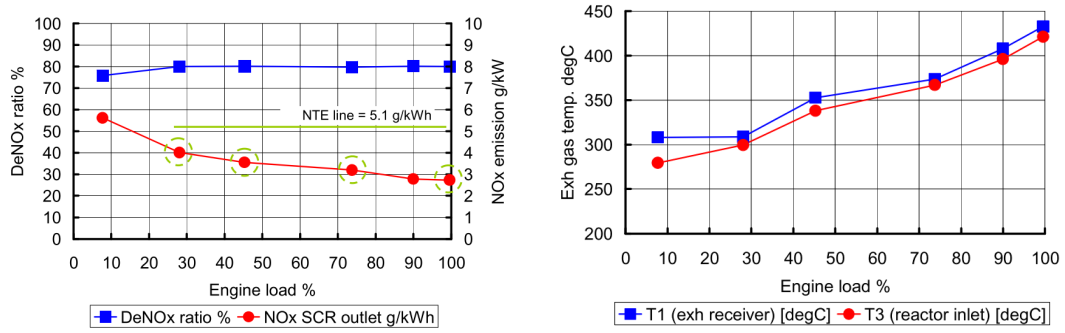

(a) SCR performance. The green line represent the Not to Exceed (NTE) emission limit, which is part of the IMO test cycle E3[82].

(b) Temperature profile. The temperature is controlled based on a minimum temperature of 310℃ at T1.

Figure 1.14: SCR performance during sea-trial at a 6.7 MW 2-stroke engine. The V-SCR catalyst is placed upstream the turbocharger, and catalyst temperature is controlled as explained in Section 1.3.2.1. The engine was tuned on a testbed to give 14.8 g/kWh NO_x, and hence urea is added to achieve 80% NO_x reduction[70].

Based on the sea-trials performed by several authors the most important factors to ensure steady and optimal SCR operation are to ensure good mixing of urea, controlling the temperature into the SCR reactor and installing soot blowers. Part of controlling the temperature is also to control the warm up period of the SCR reactor, which takes from 30 min. to 50 min. depending on the size of the reactor and the fuel oil used as shown by the horizontal lines in Figure 1.8. The importance of soot blowers is to ensure that the catalyst surface is not covered with soot, ash or sulfates and are usually designed to blow air at a certain cycle, such as every second minute[11, 70, 74, 77].

The lifetime of a marine SCR catalyst is expected to be at least 20.000 hours of operation, and is especially depending on the temperature control, since with the correct temperature control sulfates and VOC will first condense downstream of the SCR if they are formed[74, 77]. The lifetime of the catalyst also depends on the fuel oil used. The longest operating marine SCR system has been operated for 14 years

using low sulfur fuel (0.2 wt.%), other ships have reached 40.000 hours of operation using HFO[74].

1.5 Literature Conclusion

SCR as a technology is very mature, and has been widely used in stationary applications. The catalytic mechanism has been widely investigated by multiple authors, and on this basis the NO_x reduction has been modeled for both lab scale and full scale experiments. The reductant, NH_3, can be added as a gas or through the decomposition of urea, the latter being of interest for mobile application such as vehicles or ships. The catalyst is usually based on V_2O_5, doped by WO_3, and washcoated on a carrier of anatase.

The $V_2O_5/WO_3/TiO_2$ catalyst has shown great stability with respect to hydrothermal ageing, hydrocarbon poisoning and sulfur poisoning. Hydrothermal ageing can be a problem if used at vehicles together with a non-catalytic diesel particulate filter (DPF) creating high exotherms during regeneration. The DPF technology is not applied for ships and the temperature before the catalyst will be below 500℃ at which the V-SCR is considered stable. Hydrocarbon poisoning can occur, however, the deactivation is reversible and less pronounced with V-SCR compared to zeolites. Sulfur poisoning occurs at low temperatures, usually around 250-300℃, however depends on the fuel sulfur content, NH_3 concentration and the specific catalyst. The low temperature deactivation happens due to condensation of AS and ABS at the catalysts surface and within the pore structure. The addition of surface sulfates can also promote the SCR activity by increasing the surface acidity.

SCR reactors have been installed on both 4-stroke and 2-stroke marine engines and have successfully achieved IMO Tier III NO_x reduction. When using SCR of NO_x while using a high sulfur fuel a temperature of 300-360℃ is needed depending on the sulfur concentration to ensure that sulfates does not condense and block the catalyst. For such high temperatures the SCR reactor should be placed before the turbocharger at 2-stroke engines. Man Diesel and Turbo[22] and Hitachi Zosen Cooperation have developed a preturbocharger Tier III complying system, which can also control the dynamic effects of placing an SCR reactor upstream of the turbocharger. The high pressure effects of placing the SCR reactor upstream of the turbocharger should be investigated both with respect to desired and undesired reactions.

Mixing of urea at the large geometries present within the maritime industry can be difficult and research and specific design should be made to ensure stable and efficient SCR of NO_x.

In general it can be concluded that the $V_2O_5/WO_3/TiO_2$ catalyst is suited for use on ships together with urea as a NO_x abatement technology, however, a thorough investigation must be conducted to ensure stable, efficient, and competitive SCR technology for ships.

2 High Pressure SCR

This chapter will investigate the potential performance of an SCR reactor installed upstream of a turbocharger, and therefore, at an increased pressure. The chapter will start with an overview of the scarce literature on possible kinetic effects of having an SCR reactor at increased pressure, followed by the experimental work carried out as part of this Ph.D. study. The experiments have mainly been conducted at DTU Chemical Engineering using granulated catalyst in a packed bed reactor (PBR). A single experimental campaign has also been conducted at Haldor Topsøe A/S, stationary DeNOx (Now Umicore Denmark ApS), with a monolith reactor to test the pressure effects on industrial sized catalyst. All measurements presented here are performed using synthetic gas without sulfur and particles.

2.1 Introduction

The majority (2013) of marine SCR reactors have been installed on 4-stroke marine diesel engines[11]. The temperature downstream of the 4-stroke engines turbocharger is higher, therefore, a SCR system similar to a stationary design can be placed at this location[72]. However, with the enforcement of IMO Tier III regulation 13, the required NECA reduction of 80% compared to the earlier IMO Tier II, is increasing the demand for an efficient and reliable NO_x reduction method. For the large 2-stroke engines, one option is to install an SCR reactor upstream of the turbocharger. As earlier shown in Figure 1.8, the temperature downstream the turbocharger of a 2-stroke engine is too low for reliable continues SCR operation. This is because of the condensation of sulfates within the catalytic reactor, reducing the catalyst activity. A potential alternative could be installation of the SCR reactor upstream of the turbocharger, where the temperature is higher[70, 75, 83–85], but pressures up to 4.5 bar may be experienced at full load[84]. At increased pressure, the volume flow of the exhaust gas is lower compared to the low pressure position downstream of the turbocharger, and therefore, the required volume of catalyst should also decrease[33, 70, 86]. Furthermore, at the decreased volumetric flow rate the pressure drop across the catalyst will also decrease, despite the increased density of the exhaust gas[87]. Lujan et al.[88] tested the influence of installing a diesel oxidation catalyst (DOC) and a diesel particulate filter (DPF) upstream and downstream of a turbocharger on a test engine, and found that at the high engine load, where the pressure drop was significant, the pressure drop across the two catalytic units could be reduced by 25% by installing them upstream of the turbocharger. Beside a lower pressure drop, increased temperature and a possible

saving of catalyst volume, the effects of pressure on the chemical reactions should also be investigated as is the focus of this chapter.

Kröcher et al.[83] investigated the effect of increased pressure on two SCR monoliths containing 1.7 wt% V_2O_5 with cell densities of 225 channels pr. square inch (cpsi) and 87 cpsi. Kröcher et al. performed experiments using 1000 ppm NO, excess of NH_3 at pressures of 1 bar, 2 bar, and 4 bar. At increased pressure, they kept the partial pressure of NO and NH_3 constant, and they decreased the catalyst amount, so the actual residence time was constant. At 200℃ they observed 32% NO_x conversion for the 225 cpsi, independent on the pressure, indicating first order dependency on NO. As the temperature was increased in steps of 50℃, the conversion of NO_x increased, however, a slower increase in NO_x conversion was observed for the 2 and 4 bar experiments. At 250℃ a NO_x conversion of 70%, 60%, and 52% was observed at 1 bar, 2 bar, and 4 bar respectively. The decrease in NO_x reduction at increased pressure, was explained by Kröcher et al. by increased diffusion limitations, due to the inverse proportionality of the diffusivity from the bulk gas phase to the catalyst surface, decreasing the overall rate of reaction.

Rammelt et al.[86] also investigated the effects of increased pressure using a 1.9 wt% V_2O_5/10 wt% WO_3 / TiO_2 catalyst with a channel density of 300 or 25 cpsi, and a total catalyst volume of 15 cm^3. Rammelt et al. kept the mass flow rate constant (i.e. changing volumetric flow rate with pressure), and therefore observed an increased NO_x conversion, at increased pressure due to an overall positive effect from increased residence time and a decrease in diffusivities. Rammelt et al. concluded that the increase of NO_x conversion was less pronounced for the 25 cpsi catalyst, and concluded that this was due to increased mass transfer limitation, which was more pronounced in the large diffusion pathways in the 25 cpsi catalyst compared to the 300 cpsi catalyst. Kröcher et al.[83] also tested the difference between a low and high cell density catalyst (87 vs. 225) and also concluded that the effects of diffusion control was higher for lower cell densities. To test the overall effect, Kröcher et al.[83] measured the NO_x reduction for a given catalyst, using a fixed mass flow rate and then measured the amount of catalyst needed at increased pressure to achieve the same amount of NO_x reduction. Theoretically, without any mass transfer limitations and using a perfect gas, the required catalyst volume should be reduced to 50% and 25% at 2 bar and 4 bar. For the 87 cpsi catalyst, they reported that the catalyst volume could be reduced to 80% at 2 bar and 68% at 4 bar, at a temperature of 300℃. For the 225 cpsi catalyst, the volume could be reduced to 71% at 2 bar and to 54% at 4 bar also at 300℃. Both results show the clear effect of diffusion limitations, and the fact that the 225 cpsi come closer to the theoretical values, indicates a reaction that is less controlled by diffusion. The overall conclusions so far are that besides a slower diffusion, the pressure does not affect the reaction.

Bank et al.[72] tested two washcoated vanadium based SCR catalysts, with an unspecified content of V_2O_5 and a cell density of 100 cpsi and 200 cpsi at a temperature of 215℃, a NO_x concentration of 500 ppm, and an ANR of 1.5. Bank et al. reported

that no difference between the two cell densities were observed at an increased pressure of up to 2 bar. At the low temperature, the reaction is not diffusion controlled, and it is therefore expected that they measured the same NO_x conversion. Bank et al.[72] also measured the NH_3 adsorption capacity of the catalyst at a temperature of 215℃, and as a function of pressure. Bank et al. found that the NH_3 adsorption capacity, on the 100 cpsi catalyst, increased by a factor of 1.5 and 1.7 at a pressure of 1.5 bar and 2 bar respectively. Bank et al. used the NH_3 adsorption and desorption model proposed by Tronconi and co-workers in the work of Chatterjee et al.[89], but, found that it was hard to fit the adsorption and desorption processes because a different set of parameters were found for each pressure. Rammelt et al.[86] used a similar kinetic model also proposed by Tronconi and co-workers[90], but found reasonable fits independent of the pressure for steady state SCR. Both models were based on the modified Temkin kinetics for the adsorption and desorption of NH_3 which takes into account a linear decrease in the activation energy as the catalyst is filled with NH_3. Modified Temkin kinetics were also used by Lietti et al.[91] to model transient NH_3 temperature programmed desorption (TPD) experiments, and found reasonable fits. However, all experiments by Lietti et al. were performed at 1 bar.

In this study pressurized SCR experiments are investigated, using both lab scale packed bed reactors and pilot scale monoliths to test the effect of pressure on SCR kinetics. Furthermore, the transient adsorption and desorption of NH_3 at increased pressures up to 4.5 bar is investigated. Based on the experiments both steady state SCR kinetics and dynamic adsorption and desorption processes are modeled.

2.2 Experimental

2.2.1 Packed Bed Reactor

2.2.1.1 Setup

The pressurized lab-scale experiments conducted at DTU Chemical Engineering were all conducted using the packed bed reactor setup shown schematically in Figure 2.1. Gas was added using four mass flow controllers from Brooks (SLA5850). Water was added by the use of a HPLC pump (Gilson 307), and carried together with air, nitrogen, and NH_3 into the homemade evaporator (H1), which consists of 0.5 meter 1/8 inch 316 steel tubes which have been coiled together with heat tracing (HSS from Lund & Sørensen) and operated at a temperature of 350℃. After the evaporator, all tubes are heat traced to 150℃ to ensure that water vapor does not condense. NO was added to the hot gas downstream of the evaporator, to ensure that the oxidation of NO into NO_2 was low, similar to diesel engine conditions (NO>90% NO_x[92]). The activation energy for the NO oxidation is negative, consequently addition of NO at room temperature would cause an increased amount of NO_2[93].

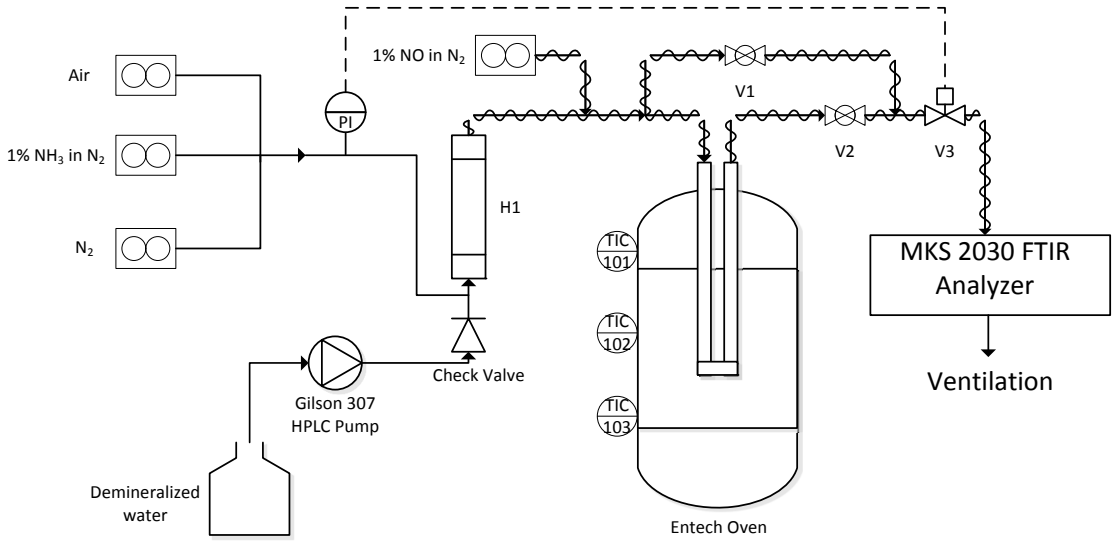

Figure 2.1: Packed bed reactor setup at DTU Chemical Engineering.

The synthetic gas mixture was passed through a packed bed reactor, contained within a U-type quartz reactor. The position of the catalytic bed was maintained by a quartz wool plug on both sides, and a constriction of the glass tube, beneath the catalyst bed. A thermocouple was place before the catalytic bed, to measure the temperature. After the reactor, pressure was reduced by two automatic back pressure valves (Fisher Fieldvue DVC 2000), and gas concentrations were measured at atmospheric pressure using an MKS 2030 FTIR gas analyzer.

2.2.1.2 Catalyst

SCR catalysts containing approximately 1 wt% V_2O_5/∼ 10wt% WO_3/TiO_2 (V-SCR) were supplied by Umicore Denmark ApS. The catalyst was produced as a monolith, from which the catalyst powder was produced by crushing and removal of visible fibers. The powder was pressed into self-supporting pellets, which were crushed and sieved into catalyst particles with a size fraction of 150-300 micron, and loaded in the reactor setup. The fraction of 150-300 micron was chosen to diminish diffusion limitations.

2.2.1.3 Steady State SCR - Experimental Methodology

Approximately 20 mg of catalyst was loaded in a U-type quartz reactor with an inner diameter of 3 mm as shown in Figure 2.3(a). The catalyst was degreened at 400℃ and 4.5 bar for 15 hours using a total volumetric flow rate of 1200 NmL/min containing 10 % O_2, 8% H_2O, 600 ppm NO_x, 720 ppm NH_3 (ANR=1.2) in N_2. After 15 hours of degreening, the SCR activity was measured at four different temperatures (200-350℃) before the temperature was raised to 400℃ again for an additional 5 hours, after which the SCR activity was measured again. Identical SCR activities was found before and after the last 5 hours of degreening, showing that the degreening process was completed.

After degreening, SCR experiments were carried out with typical gas concentrations of 10% O_2, 8% H_2O, 600 ppm NO_x, ANR = 0.8-1.2 in N_2. The pressure was varied in steps of 1.2 bar up to 4.8 bar. The volumetric flow rate was kept constant using a total flow rate of 300 NmL/min at 1.2 bar and a total flow rate of 1200 NmL/min at 4.8 bar. The gas outlet concentrations were continuously measured at the FTIR analyzer using 16 spectra's pr. sample resulting in gas concentration outputs every 16th second.

2.2.1.4 NH_3 TPD

For the NH_3 TPD experiments an SCR catalyst loading of 115 mg was used in a U-type quartz reactor with an inner diameter of 4 mm. The catalyst was degreened for 20 hours at 410℃ and 4.5 bar using a total volumetric flow rate of 600 NmL/min containing 9% O_2, 8% H_2O in N_2.

The TPD experiments consisted of 1 hour of NH_3 adsorption at a specific temperature (∼150℃, ∼200℃, ∼250℃ and ∼300℃) and pressure using a flow of 300 NmL/min containing 9% O_2, 8% H_2O, 600 ppm NH_3 in N_2. During NH_3 TPD the total flow rate was not changed proportional with the pressure, but instead a constant flow of 300 NmL/min was used. After 1 hour the catalyst was assumed to be saturated and the flow of NH_3 and H_2O was stopped. H_2O was stopped to remove pulsations from the pumping of H_2O, so the desorption curve was smooth. At 1 bar a total flow rate of 300 NmL/min was used, and in all other experiments a total flow rate of 276 NmL/min was used. The change was due to incorrect MFC settings, of the nitrogen flow. After flushing for 1 hour a temperature ramp (10 K/min) was performed from the saturation temperature and until 420℃. The temperature was maintained at 420℃ for 20 min before the reactor was cooled to the next adsorption temperature. The gas outlet concentrations were continuously measured at the FTIR analyzer using two spectra's pr. sample resulting in gas concentration outputs every 3rd second.

Blank experiments (i.e. no catalyst loaded) were performed. The first blank experiment was performed at 1.2 bar, including all four temperatures and a temperature ramp, however, since no change was observed between the different temperatures, the ramp was skipped and blank experiments without the ramp were performed to save time and only at a temperature of 145℃.

2.2.2 Monolith Setup

2.2.2.1 Setup

A measurement campaign at elevated pressure was also performed using the V-SCR catalyst in the form of a monolith. These experiments were conducted at Haldor Topsøe A/S using the setup schematically shown in Figure 2.2. Gases were added to the setup using Brooks smart flow controllers and water was added using Brooks liquid mass flow controller (model 5882). Air and nitrogen were passed through a preheater together with water, in which water was also evaporated. The preheated

gas was further heated in a second heater, and NH_3 and NO were added upstream of a static mixer from Sulzer and the hot mixed gas was sent to the monolith catalyst. The catalyst was contained within a square electrical heated furnace, and gas measurements were performed by a Gasmet FTIR analyzer (GASMET DX - 4000) by withdrawal of gas before and after the catalyst.

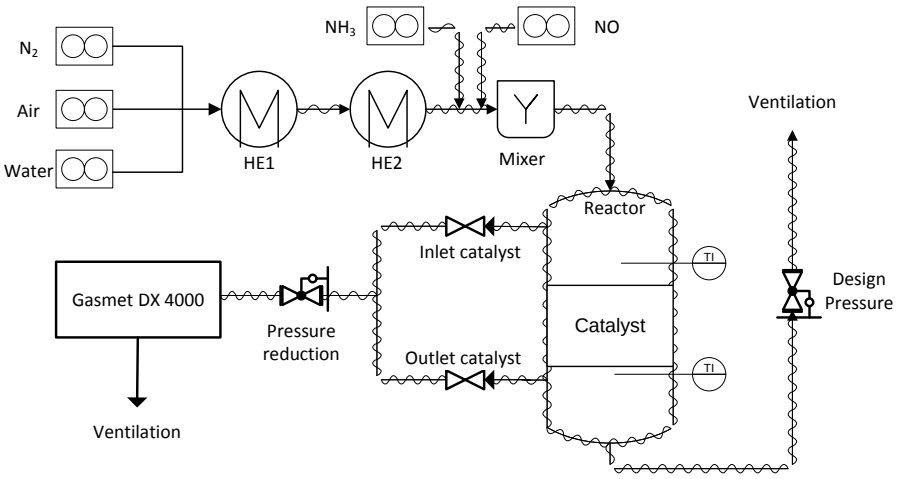

Figure 2.2: The monolith setup used at Haldor Topsøe A/S to measure pressurized SCR of NO_x. The same setup was used for pressurized SO_2 oxidation, as discussed in Chapter 3.

2.2.2.2 Catalyst

A V-SCR catalyst (∼1 wt% V_2O_5) was cut into a square cross sectional area (43.5mm) and a length of 99.1 mm and the sides were sealed with quartz wool. Furthermore, to reduce mass transfer limitations and the NO_x conversion, all but 9 channels of the monolith were sealed resulting in an open area of 223 mm^2, as also shown in Figure 2.3(b).

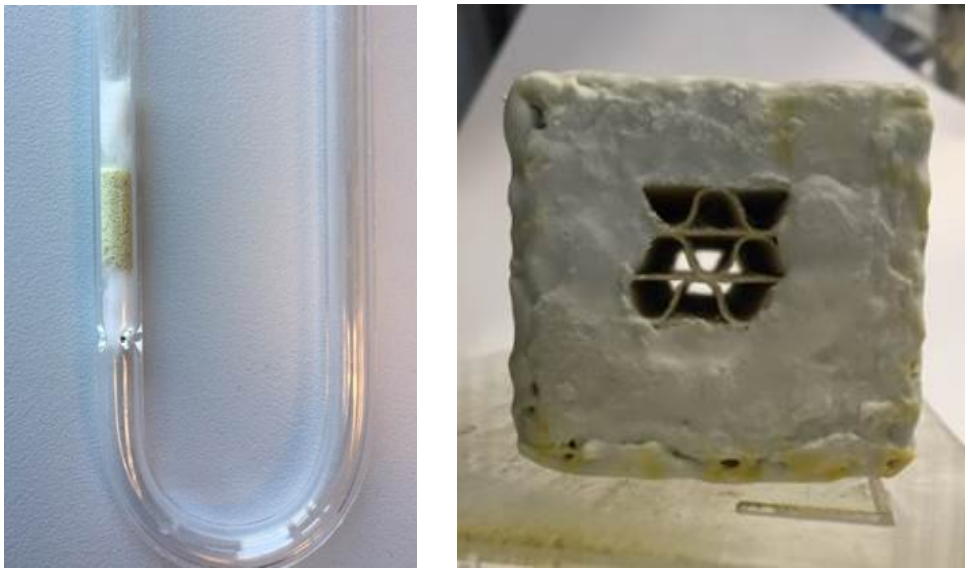

(a) PBR SCR Catalyst loaded in U-tube reactor with quartz wool around.

(b) Monolith SCR Catalyst with only 9 channels open.

Figure 2.3: Pictures of the catalysts used for steady state SCR experiments either as granulated particles in a packed bed reactor (PBR) (a) or as a monolith (b).

2.2.2.3 Steady State SCR

The monolith was loaded into the reactor setup, and the catalyst was degreened at 408℃ in a flow of air and 5% water for 15 hours. SCR was performed at 1 and 3 bar, while keeping the volumetric flow rate constant. At 1 bar a flow of 4.9 Nm^3/h was used containing 8% O_2, 5% H_2O, 720 ppm NO_x, ANR = 0.75 or 1.16 in N_2.

2.3 Results

First results related to NH_3 TPD will be discussed, including a transient kinetic model followed by steady state SCR experiments and modeling.

2.3.1 NH_3 TPD

2.3.1.1 Transient Results

The NH_3 TPD experiment was performed at 1.2, 2.4, 3.6 and 4.5 bar using a total volumetric flow rate during adsorption of 300 NmL/min containing 9% O_2, 8% H_2O, 600 ppm NH_3 in N_2. A typical result for the 1.2 bar and 4.5 bar experiments are shown in Figure 2.4.

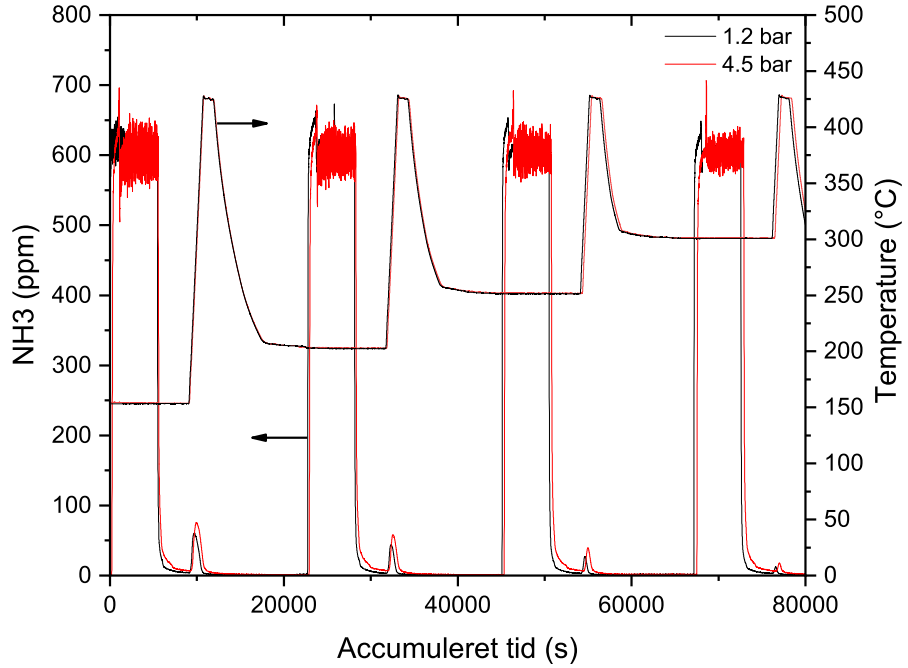

Figure 2.4: A comparison between the NH_3 TPD experiment conducted at 1.2 bar and at 4.5 bar. It should be noted that the total flow rate during desorption for the 1.2 bar is 300 Nml/min and 276 NmL/min for the 4.5 bar experiments.

Figure 2.4 shows a slight increase in the area under each of the desorption peaks for the 4.5 bar compared to the 1.2 bar experiment. This indicates that at increased pressure slightly more NH_3 is adsorbed on the surface of the catalyst, however, the increase of pressure almost by a factor four only increases the amount of NH_3 stored on the catalyst by 40% at a temperature of 150℃ as shown in Figure 2.6. This is a lot lower than the results reported by Bank et al.[72], who reported that for a washcoated monolith study, the integral ammonia storage for a 100 cpsi vanadium based SCR catalyst increased by approximately 70% by changing the pressure from 1 bar to 2 bar at 215℃. The reason for the difference between the results reported by Bank et al. and the results obtained here are unknown.

The 4.5 bar NH_3 TPD experiment with catalyst and two blank experiments without catalyst also performed at 4.5 bar are shown in Figure 2.5.

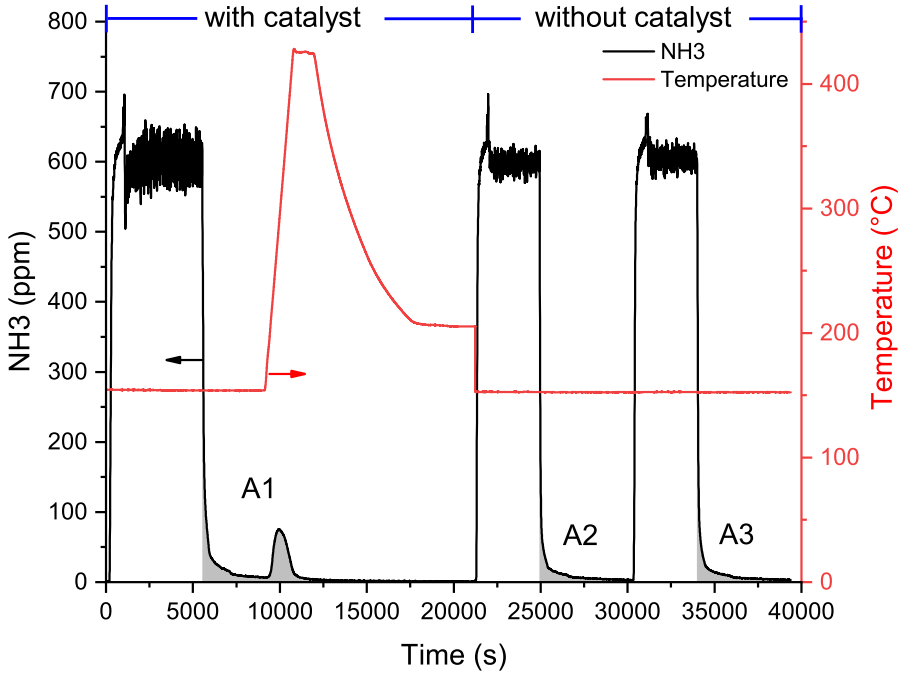

Figure 2.5: NH_3 TPD at a pressure of 4.5 bar, adsorption at 151℃, using a total flow rate during adsorption of 300 NmL/min containing 9% O_2, 8% H_2O, 600 ppm NH_3 in N_2 followed by two blank experiments using the same flow but without catalyst. The blank experiment and the experiment with catalyst was not performed the same day, the data has just been merged. Grey integrals under the curves of size: A1 = 362 μmol/g_{cat}, A2 = 152 μmol/g_{cat}, A3 = 171 μmol/g_{cat}.

Figure 2.5 shows three areas for which it should be noted that the length of the blank experiments only covered 5354 s. and the actual desorption experiment covers 6383 s. Therefore, the area for the blank experiments (A2 and A3) was increased by (1029 s.· 3 ppm NH_3=60μmol/g_{cat}). The 3 ppm NH_3 was chosen because this was the measured value at the end of the blank experiment. This value would slowly drop during the 1029 s. however, a value below 1.5 ppm NH_3 was never observed neither during the full blank TPD performed at 1.2 bar. The error caused by prolonging the experiment in this way was therefore, considered to be within 1-2% of the total blank experiment. In the same way, the other blank experiments were also prolonged, and two blank experiments were performed at each pressure as also shown in Figure 2.5, and the mean was used as the final blank result. The blank experiments resulted in backgrounds of 97, 150, 166 and 166 μmol/g_{cat} at 150℃ and at 1.2, 2.4, 3.6, and 4.5 bar respectively. The background measurements were measured to be between 1/3-2/3 of the full area measured, depending on the temperature. Based on the blank measurement, the final integration for each pressure and temperature could be calculated, and the results for both the full desorption curve and the desorption peak are shown in Figure 2.6.

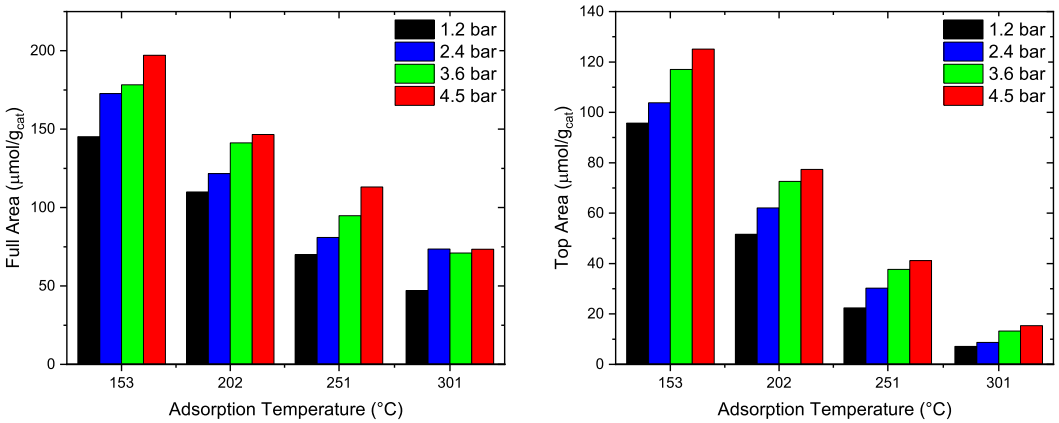

(a) Full integration (b) Integration of desorption peak

Figure 2.6: Calculation of the amount of NH_3 (μmol/g_{cat}) for the full desorption curve (a) and for the desorption peak during the ramp (b). It should be noted that the blank values have been subtracted and the results have been corrected so that all results are reported at a total flow of 300 NmL/min.

Figure 2.6 shows that in general the ammonia adsorption increases as the pressure increases, and that the ammonia adsorption decreases as the adsorption temperature increases. Figure 2.6(b) shows that as the temperature increases the amount of tightly bound ammonia (that in the peak) is reduced, and instead more NH_3 is desorbed during the 1-hour flush at the adsorption temperature.

2.3.1.2 Modeling of Transient Adsorption/Desorption Experiments

To model the transient adsorption/desorption experiments, a transient model was set up in order to obtain the kinetics describing the adsorption-desorption processes. The gas phase concentration of NH_3 was modeled similar to Lietti et al.[91] as plug flow, which was simplified in this study as a number of CSTR's in series. The gas phase concentration of NH_3 is therefore given as shown in Equation 2.1:

$$\frac{dC_N}{dt} = \frac{v_0}{\epsilon \cdot V_N} \cdot (C_{N-1} - C_N) + (r_d - r_a) \cdot \frac{1-\epsilon}{\epsilon} \Omega' \tag{2.1}$$

In which N is the CSTR number, C_N is the NH_3 concentration out of the N'th CSTR, C_{N-1} is the inlet concentration of NH_3, v_0 is the volumetric flow rate, V_N is the volume of the N'th CSTR, ϵ is the porosity of the reactor volume, Ω' is the NH_3 adsorption capacity and r_d and r_a is the rate of desorption and the rate of adsorption. The rate of adsorption and desorption for a given CSTR is given by Equation 2.2 and Equation 2.3 respectively.

$$r_{a,N} = k_a^0 \cdot \exp\left(\frac{-E_a}{R \cdot T}\right) C_N \cdot (1 - \theta_N) \tag{2.2}$$

$$r_{d,N} = k_d^0 \cdot \exp\left(\frac{-E_d^0 \cdot (1 - \alpha \cdot \theta_N)}{R \cdot T}\right) \cdot \theta_N \tag{2.3}$$

In which k_a^0 and E_a are the preexponential factor and the activation energy of the adsorption process, and k_d^0 and E_d^0 are the preexponential factor and the activation energy for the desorption process. θ_N is the surface coverage of NH_3, and α is a Temkin parameter. The Temkin desorption kinetics were reported by Lietti et al.[91] to provide a better fit compared to a regular Langmuir isotherm ($\alpha = 0$). The Temkin parameter takes into account a linear decrease in activation energy as the surface of the catalyst is filled ($\theta \to 1$). Lietti et al.[91] found that the rate of adsorption was represented by a non-activated ($E_a = 0$) process in line with the adsorption of an alkaline species such as NH_3 on the acidic surface of the catalyst, and this will also be used in this study. The rate of change of the NH_3 coverage on the catalyst is given by the difference between the rate of adsorption and desorption as shown in Equation 2.4.

$$\frac{d\theta_N}{dt} = r_{a,N} - r_{d,N} \tag{2.4}$$

2.3.1.3 Transient Model Fitting

The unknown adsorption and desorption kinetic parameters, i.e. k_a^0, k_d^0, E_d^0, α, and Ω' was fitted by the use of Matlab's "fmincon" function using 30 CSTR's in series. According to Levenspiel[94] the number of CSTR's that should be used to closely approximate plug flow for a simulation of a fixed bed is given by:

$$N_{tanks} \sim n_{particles} \tag{2.5}$$

and with a height of 12 mm and a particle diameter of 150-300 μm this results in 40-80 tanks in series. The number of 30 CSTR's in series was chosen to ensure fast simulation, and the final fitting was verified against a run with 80 tanks in series which did not change the fitting results. The fitting procedure minimizes the function given by Equation 2.6

$$F(x) = \sum \left(\frac{|y_{meas} - y_{model}|}{y_{meas}} \cdot \text{weight} \right) \tag{2.6}$$

In which y_{meas} and y_{model} are vectors containing the measured and modeled gas phase NH_3 concentration as a function of time. "Weight" is also a vector with the same length as y_{meas} containing zeros and ones to ensure that only the desired data is used for fitting. As shown in Figure 2.5 the blank experiment gives a substantial addition to the first part of the desorption curve and because it was not found possible to subtract the background at each specific time from the measured value, it was decided to only fit the NH_3 peak during the ramp of temperature. Furthermore, the NH_3 capacity of the catalyst (Ω') which must be highest at the lowest temperature and the highest pressure, as also observed from Figure 2.6, was

calculated based on the integration shown in Figure 2.5.

$$\Omega' = \left(\int_{\text{Full desorption}} C_{NH3,exp}(t) - \int_{\text{Full desorption}} C_{NH3,blank}(t) \right) \cdot \frac{v_0}{V_m \cdot w_{cat}} \cdot \rho \quad (2.7)$$

$$\Omega' = 103912 \cdot 10^{-6} \cdot \text{s} \cdot \frac{0.276 \text{ Nl/min}}{22.4 \text{ Nl/mol} \cdot 60 \text{ s/min} \cdot 115.6 \cdot 10^{-6} \text{kg}} \cdot 1236 \text{ kg/m}^3 \quad (2.8)$$

$$\Omega' = 228 \frac{\text{mol NH}_3}{\text{m}^3 \text{ particle}} \quad (2.9)$$

It should be noted that this calculation is performed under the assumption that the surface of the catalyst is completely filled with NH_3 ($\theta = 1$) at a pressure of 4.5 bar and at a temperature of 150℃. In case the model predicts a non saturated surface, a new NH_3 capacity should be calculated and a new fitting performed hence the calculation would be iterative. As shown in Figure 2.8, the surface coverage is found to be 0.98 and considered close enough to 1.

The NH_3 capacity reported by Lietti et al.[91] is 270 mol $NH_3/m^3_{\text{reactor}}$ for a ternary 1.47 wt% V_2O_5-9 wt% WO_3-TiO_2 catalyst. As a comparison, the NH_3 capacity found in this study can be translated into the same units to give 372 mol $NH_3/m^3_{\text{reactor}}$ based upon the bed porosity. The bed porosity was calculated based on the empirical formula presented by Pushnov[95] as shown in Equation 2.10 for spherical particles. Pushnov reported an average deviation of the formula of ±5.26% for spherical particles, and is therefore, considered applicable. Hence, it is assumed that the catalyst particles can be approximate as spherical particles.

$$\epsilon = \frac{1}{(D_{\text{reactor}}/d_{\text{particle}})^2} + 0.375 = 0.38 \quad (2.10)$$

$$\Omega = \Omega' \cdot \frac{1-\epsilon}{\epsilon} = 372 \frac{\text{mol}}{\text{m}^3_{\text{reactor}}} \quad (2.11)$$

The calculated NH_3 capacity in the case of the pressurized experiments reported here is, therefore, higher than the one reported by Lietti et al.[91]. However, with the increased pressure and the fact that the catalysts are different makes the result seem reasonable. Lietti et al.[91] also reported the NH_3 capacity for a binary catalyst (V_2O_5-TiO_2) for which they found an NH_3 capacity of 209 mol/m^3 and explained the difference due to changes in surface area, i.e., 46 m^2/g for the binary catalyst vs. 80 m^2/g for the ternary catalyst. For the catalyst used in this study a surface area of 75 m^2/g has been found by N_2 adsorption calculations (BET method). The surface areas of the ternary catalyst used by Lietti et al. and the one used here, is thus comparable, and the difference in NH_3 capacity, cannot be explained by different surface areas.

With the NH_3 capacity fixed at 372 mol $NH_3/m^3_{\text{reactor}}$, the four last fitting parameters (k_a^0, k_d^0, E_d^0 and α) were fitted using using 30 CSTR's in series, only fitting the NH_3 peaks, however, using the combined data with all pressures and temperatures. Based upon different initial guesses it was found that the model was able to find different solutions that all fitted the data equally good, however, using different values

of the fitted parameters. Therefore, the quality of an individual fit was evaluated based on how well the NH_3 adsorption and desorption kinetics were able to predict the steady state NO conversion which will be presented in the next section. The final fitting parameters are shown in Table 2.1 in which the values reported in the article by Lietti et al.[91] also are shown.

Table 2.1: The fitted adsorption-desorption kinetics parameters including the parameters fitted by Lietti et al.[91] for a Ternary $V_2O_5/WO_3/TiO_2$ catalyst. Ω is in this study calculated based upon the amount of NH_3 adsorbed at 150℃ and 4.5 bar, as shown in Equation 2.9 and Equation 2.11. E_a^0 is assumed to be zero in both studies.

Parameters	k_a^0	E_a^0	k_d^0	E_d^0	α	Ω
Units	$\frac{m^3}{mol \cdot s}$	$\frac{kJ}{mol}$	$\frac{1}{s}$	$\frac{kJ}{mol}$	-	$\frac{mol}{m^3_{reactor}}$
This Study	6.8	0	$11 \cdot 10^5$	92.8	0.299	372
Lietti et al.[91]	0.487	0	$2.68 \cdot 10^5$	95.8	0.405	270

Most of the fitted values in this study are found rather close to those reported by Lietti et al.[91], the difference being the rate of adsorption, which is found more than ten times larger than that reported by Lietti et al. and the Temkin surface coverage dependency parameter (α) is found to be 3/4 of the one Lietti et al. reported. The increased rate of adsorption could be related to a more acidic catalyst, which is also in line with the higher NH_3 capacity. A plot of how well the model predicts the measured data is shown in Figure 2.7 and Figure 2.8 for 1.2 bar and 4.5 bar respectively. In Appendix B a graph for each pressure measured (1.2 bar, 2.4 bar, 3.6 bar, and 4.5 bar) is shown together with a zoom of the NH_3 peaks.

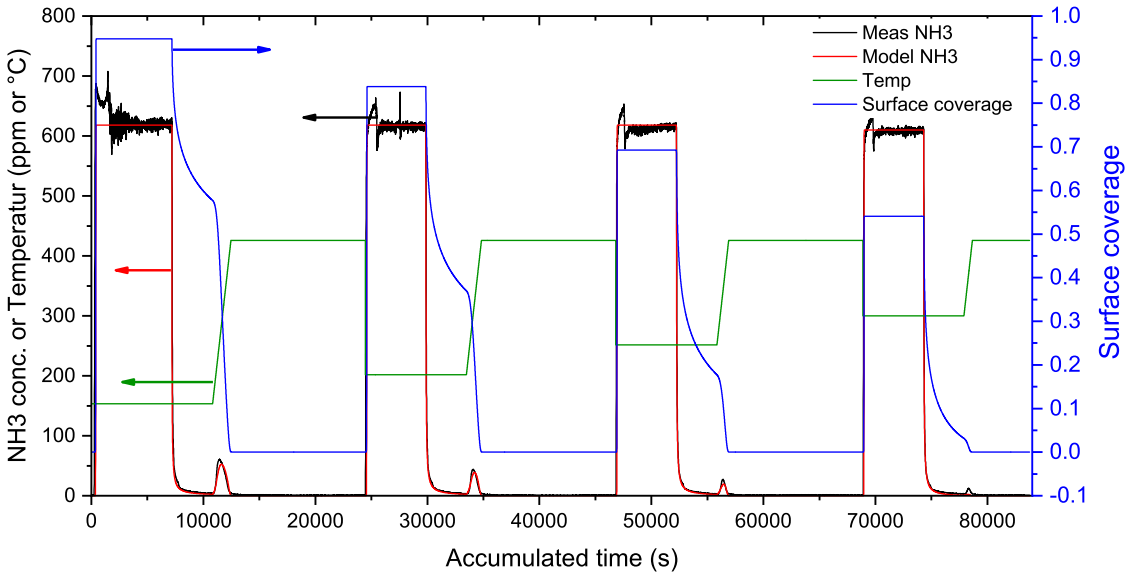

Figure 2.7: Measured and predicted NH_3 adsorption and desorption at 1.2 bar, using an NH_3 concentration of 610 ppm, at four different temperatures (150, 200, 250, and 300℃). The model is based on the fitted parameters shown in Table 2.1.

From Figure 2.7 (and Figure B.2) it is observed that the model does not predict

the desorption at 300℃ and 1.2 bar that well, since most of the NH_3 is predicted to desorp during the 1 hour flush. At 4.5 bar (Figure 2.8 and Figure B.8), however, the high temperature peak at 300℃ is well fitted. Furthermore, from Figure 2.8 it is observed that at a temperature of 150℃ the model predicts a surface coverage of 0.98 which is assumed so close to 1, that the used Ω of 372 mol $NH_3/m^3_{reactor}$ is kept.

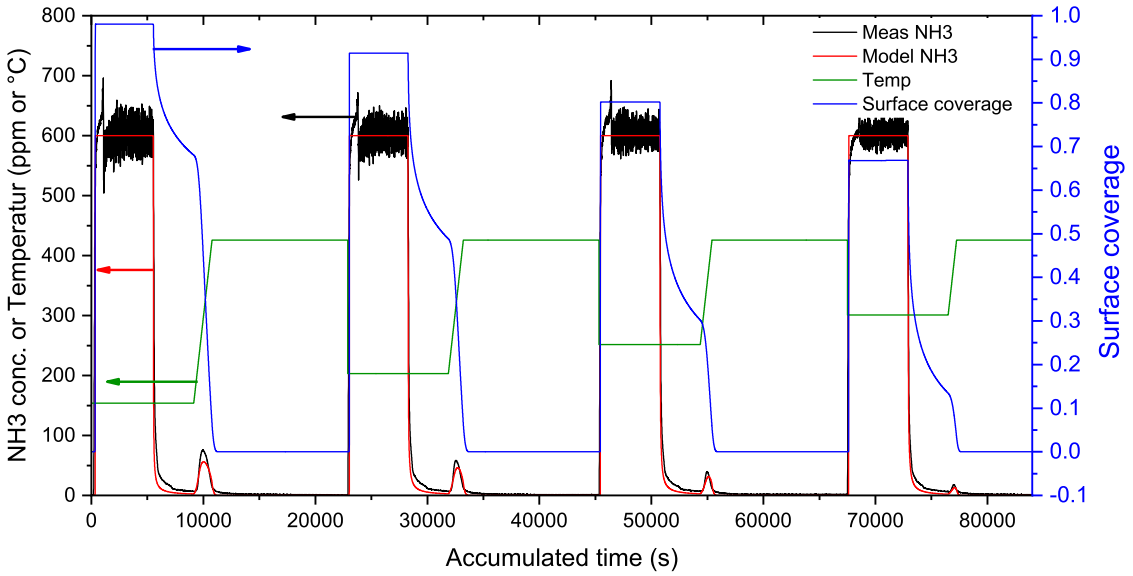

Figure 2.8: Measured and predicted NH_3 adsorption and desorption at 4.5 bar, using an NH_3 concentration of 610 ppm, at four different temperatures (150, 200, 250, and 300℃). The model is based on the fitted parameters shown in Table 2.1

2.3.2 Steady State SCR

2.3.2.1 Experimental Results

Pressurized SCR experiments were carried out at steady state condition in a temperature range of 200-400℃, and a pressure range of 1.2-4.8 bar in the lab-scale reactor. A flow of 300 NmL/min at 1.2 bar was used and the volumetric flow rate was kept constant by increasing the total flow rate proportional to the increase of pressure. Typical concentrations were 10% O_2, 8% H_2O, 600 ppm NO_x, ANR = 0.8 or ANR = 1.2 in N_2. The measured NO_x conversion as a function of temperature is shown for ANR = 1.2 and ANR = 0.8 in Figure 2.9.

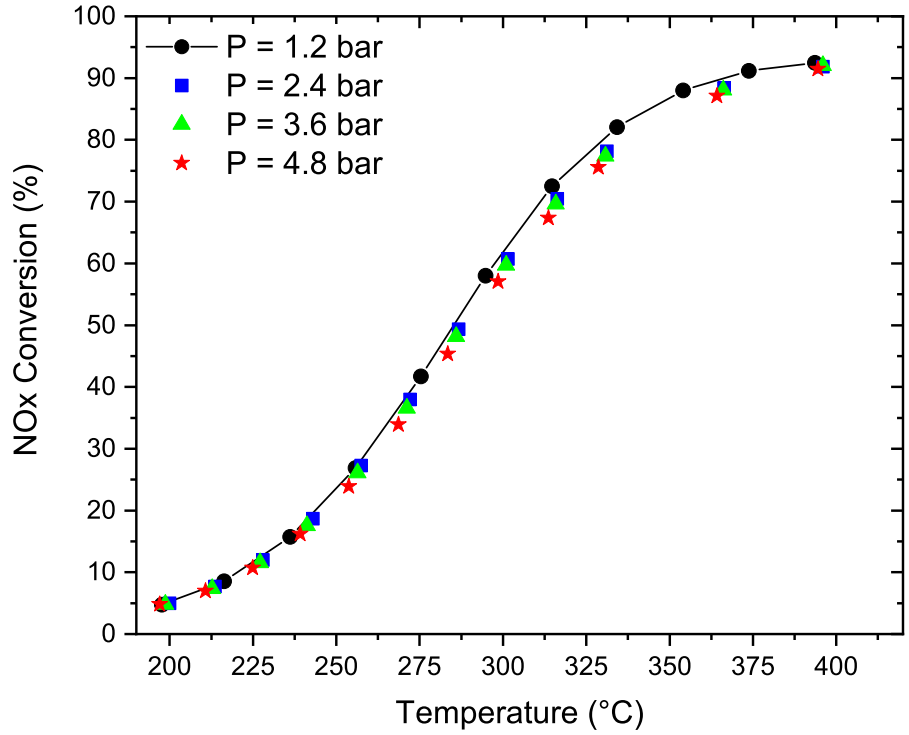

(a) ANR = 1.2

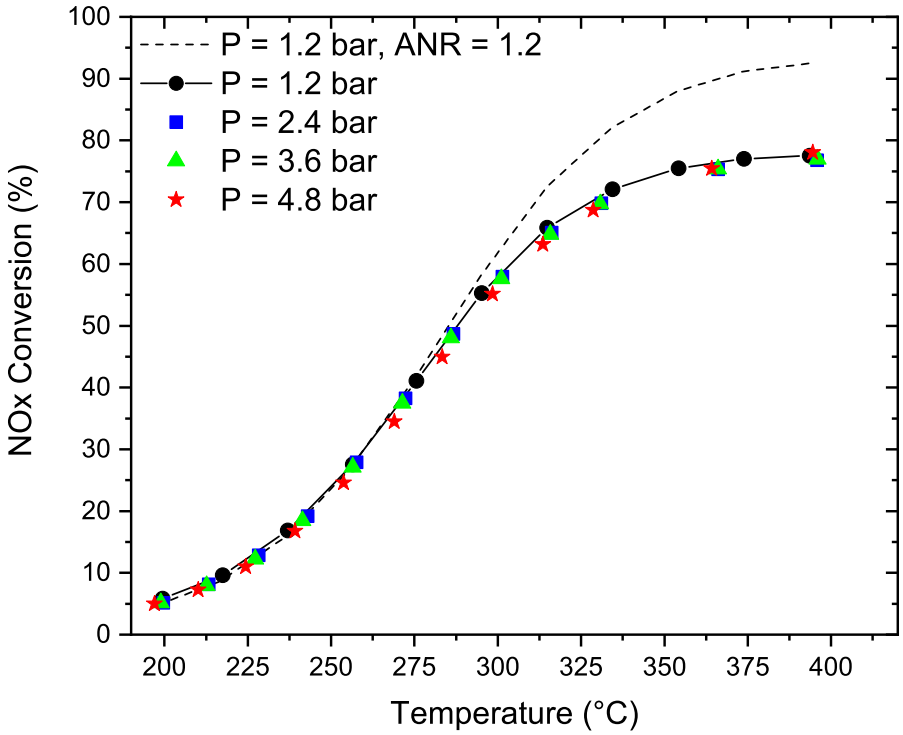

(b) ANR = 0.8

Figure 2.9: Steady state SCR using 20.8 mg 1.2 wt% V-SCR catalyst and a flow of 300 NmL/min at 1.2 bar containing 10% O_2, 8% H_2O, 600 ppm NO_x, ANR = 1.2 (a) or ANR = 0.8 (b) in N_2. The actual flow rate is kept constant by increasing the total flow rate proportional to the pressure increase.

Figure 2.9 shows that the NO_x conversion is independent of the pressure when the residence time within the catalyst is constant. This shows that the rate still follows a first order dependency of NO at all pressures. The small fluctuations observed are believed to be within uncertainty. Furthermore, Figure 2.9(b) shows that when NH_3 becomes the limiting reactant the conversion of NO_x at high temperature levels off at a NO_x conversion close to the ANR value, as also typically reported for atmospheric pressures where a kinetic expression taking into account the NH_3 surface coverage is usually used[26, 44, 51, 55], either in more complicated forms of Temkin parameters as presented above or the simplified Eley-Rideal-type[51] as given in Equation 2.12.

$$R_{NO} = k_{NO} \cdot C_{NO} \cdot \frac{K_{NH3} \cdot C_{NH3}}{1 + K_{NH3} \cdot C_{NH3}} \tag{2.12}$$

Because no changes in NO conversion was observed at increased pressure using either an ANR 0.8 or 1.2 it was decided not to investigate at even lower ANR. The addition of NO to the hot gas ensured that the maximum content of NO_2 that was observed was 40 ppm NO_2 out of a total NO_x concentration of 600 ppm, and hence the reaction can be modeled taking only the standard SCR reaction into account, i.e. considering all NO_x as NO. The highest NO_2 concentration of 40 ppm was observed during the 4.8 bar experiment. Formation of other byproducts such as N_2O from NH_3 oxidation was not observed neither at low or high pressure, as expected for a system which has water present, which limits the NH_3 oxidation through competitive adsorption[44, 63].

A new reactor loading was made with the same catalyst as above and approximately the same amount as above (20.5 mg vs. 20.8 mg). To test the NO reaction order the inlet NO concentration was varied between 300, 600, and 900 ppm NO_x, still with a constant residence time and using an ANR of 0.8 or 1.2 as shown in Figure 2.10.

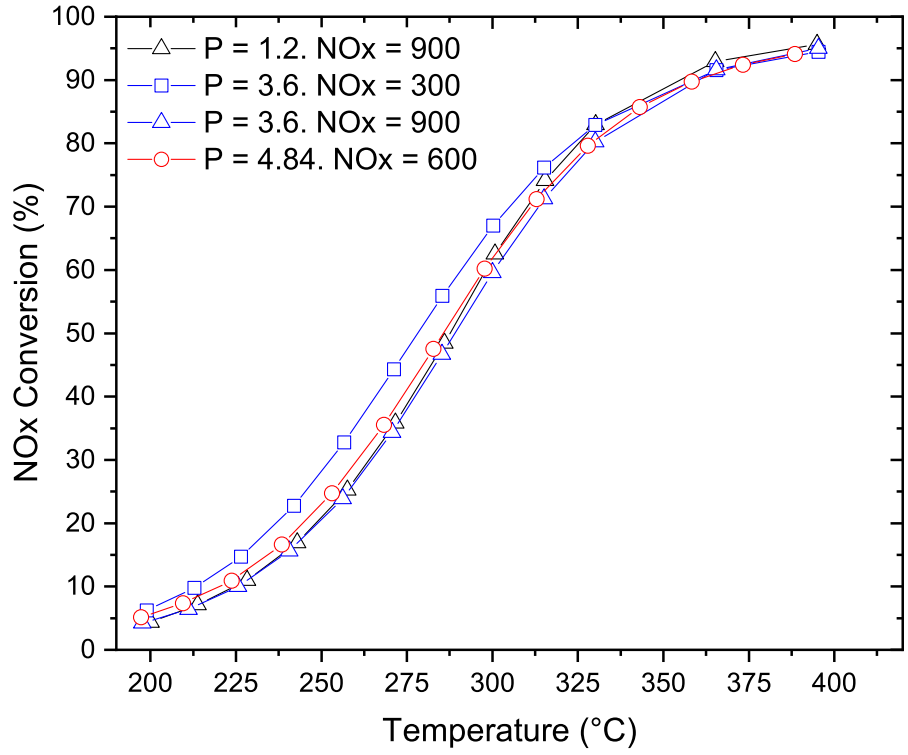

(a) ANR = 1.2

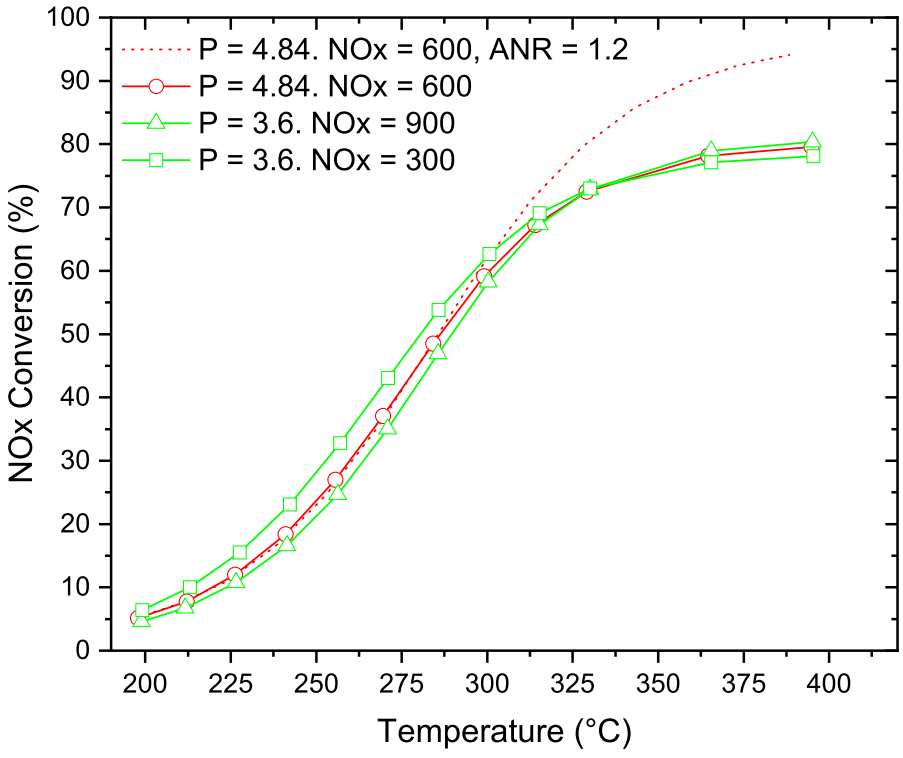

(b) ANR = 0.8

Figure 2.10: Steady state SCR using 20.5 mg of 1.2 wt% V-SCR catalyst and a flow rate of 300 NmL/min at 1.2 bar containing 10% O_2, 5% H_2O, 300, 600, or 900 ppm NO_x, ANR = 0.8 or ANR = 1.2 in N_2. The actual flow rate is kept constant by increasing the total flow rate proportional to the pressure increase.

Figure 2.10 shows that varying the inlet NO_x concentration from 600 ppm to 900 ppm of NO_x did not make any changes to the NO_x conversion as expected for a reaction that is first order in NO. The NO_2 content was increased to 50 ppm when 900 ppm NO was added at 3.6 bar i.e. 94% of NO_x is NO and the assumption of only standard SCR is still applicable. When the inlet concentration was lowered to 300 ppm the NO_x conversion was increased at the lower temperature range which was unexpected. 300 ppm of NO_x is well within normal SCR operation[44, 49], however, measured at atmospheric pressure. At increased pressure the expected effects are increased NH_3 adsorption, decreased diffusivity, and the possibility of increased formation of NO_2. The increased NH_3 adsorption was already shown by NH_3 TPD, however, in an experiment with ANR = 1.2 the rate of NO_x disapparence is not affected by increased NH_3 adsorption, and if it was, this tendency should have been visible independently of the NO_x inlet concentration. A decrease in diffusivity would lower the NO_x conversion, and is first observed in diffusion controlled operation, such as a monolith, and again should be visible independently of the NO_x inlet concentration. Lastly, increased formation of NO_2 at increased pressure was observed, however, newer exceeding 6% of the total NO_x and the effect is more pronounced at higher inlet NO_x concentration due a second order reaction dependency in NO for the NO oxidation[93]. Therefore, the change in conversion observed with an inlet concentration of 300 ppm NO_x at an ANR of 1.2 or 0.8 is most likely due to an unintended lower total flow rate, resulting in an increased residence time.

2.3.2.2 Steady State Modeling

The fitted NH_3 adsorption and desorption kinetics (see Table 2.1), that now can be used to describes how NH_3 is adsorbed and desorbed on the surface of the catalyst was used to model the steady state SCR reaction observed in Figure 2.9. The gas phase concentration of NH_3 calculated for an isothermal plug flow reactor can be written as given by Equation 2.13.

$$\frac{dC_{NH3}}{dW} = (r_d - r_a) \cdot \frac{\Omega \cdot \epsilon}{v_0 \cdot \rho \cdot (1 - \epsilon)} \tag{2.13}$$

The gas phase concentration of NO, also for an isothermal plug flow reactor can be written as Equation 2.14

$$\frac{dC_{NO}}{dW} = -r_{NO} \cdot \frac{\Omega \cdot \epsilon}{v_0 \cdot \rho \cdot (1 - \epsilon)} \tag{2.14}$$

in which the rate of NO reduction is given by Equation 2.15[91].

$$r_{NO} = k_{NO} \cdot C_{NO} \cdot \theta^*_{NH3} \cdot \left(1 - \exp\left(\frac{-\theta_{NH3}}{\theta^*_{NH3}}\right)\right) \tag{2.15}$$

The rate given by equation 2.15 takes into account that above a critical NH_3 surface coverage (θ^*_{NH3}) the rate of NO disapperence is practically independent on the NH_3 surface coverage. This critical surface coverage has a value between 0 and 1 and should be fitted to the experimental data. The NO rate constant is assumed to

follow a regular Arrhenius expression but the fitting is performed using a modified version of the Arrhenius equation as shown in Equation 2.16.

$$k(T) = k(T_{ref}) \cdot \exp\left(\frac{-E_{A,NO}}{R} \cdot \left(\frac{1}{T} - \frac{1}{T_{ref}}\right)\right) \tag{2.16}$$

When the Arrhenius equation is modified as shown in Equation 2.16, in which $k(T_{ref})$ and $E_{A,NO}$ are fitted, the parameters correlates less[96]. T_{ref} was chosen as 230℃.

The concentration of NH_3 on the surface of the catalyst is now also a function of the NO reaction rate due to equimolar consumption of NH_3 on the surface of the catalyst by NO, as given in Equation 2.17

$$\frac{d\theta_{NH3}}{dt} = 0 = r_a - r_d - r_{NO} \tag{2.17}$$

Calculations in Appendix C.1, shows that the effectiveness factor is above 0.9 for all pressures and for temperatures below 380℃, and hence no diffusion limitations are present. Furthermore, in Appendix C.2 the axial and radial dispersion is calculated, showing that the assumption of plug flow is valid. For comparison the results will also be fitted using an Eley-Rideal expression as already given in Equation 2.12, and also assuming plug flow as shown in Equation 2.18.

$$\frac{dC_{NO}}{dW} = \frac{-k'_{NO} \cdot C_{NO}}{v_0} \cdot \frac{K_{NH3} \cdot C_{NH3}}{1 + K_{NH3} \cdot C_{NH3}} \tag{2.18}$$

Here k'_{NO} is still fitted by the modified Arrhenius expression given in Equation 2.16 also using a T_{ref} of 230℃. The NH_3 adsorption equilibriums constant (K_{NH3}) is calculated based on the Arrhenius expression as given Equation 2.19

$$K_{NH3} = K_{NH3,0} \cdot \exp\left(\frac{-\Delta H_{ad}}{R \cdot T}\right) \tag{2.19}$$

2.3.2.3 Steady State Model Fitting

Based on the NH_3 desorption and adsorption kinetics presented in Table 2.1, the three unknown SCR related parameters i.e. $k(T_{ref})$, $E_{A,NO}$, and θ^*_{NH3} were fitted using Matlab's function "lsqcurvefit" which minimizes on the residual sum of squares (RSS) as given in Equation 2.20.

$$RSS = \sum (y_{model} - y_{meas})^2 \tag{2.20}$$

The fitted results are shown in Table 2.2 together with the parameters fitted by Lietti et al.[91] at atmospheric pressure.

Table 2.2: The fitted SCR parameters using the Temkin NH_3 adsorption and desorption parameters given in Table 2.1. The rate fitted by Lietti et al.[91] is based on a normal Arrhenius expression, the displayed rate constant is calculated based on the reported activation energy (59.4 kJ/mol) and preexponential factor ($7.19 \cdot 10^5$ m^3/s/mol).

Parameters	This Study	Lietti et al.[91]
k(230℃) - m^3/s/mol	2.208	0.48
$E_{A,NO}$ - kJ/mol	64.6	59.4
θ^*_{NH3}	0.1407	0.121

The fitted kinetics, as shown in Table 2.2, are similar to those reported by Lietti et al.[91] and similar activation energies can be found for the SCR reaction in the literature, i.e. 55 kJ/mol[86] and 67 kJ/mol[97], however, higher activation energies are also reported i.e. 80 kJ/mol[52], and 94 kJ/mol[51]. Furthermore, from Table 2.2 it is observed that the critical surface coverage of NH_3 is found low (0.14 and 0.12) in both this study and the study by Lietti et al.[91]. The low critical NH_3 dependency means that the rate of NO disappearance will quickly be independent on the amount of NH_3 present on the surface of the catalyst. This explains why the increased NH_3 storage on the surface of the catalyst at increased pressure (See Figure 2.6) does not result in an increased NO_x reduction as observed from the steady state SCR experiments shown in Figure 2.9.

Figure 2.11 shows how well the model fits the measured data in a parity plot.

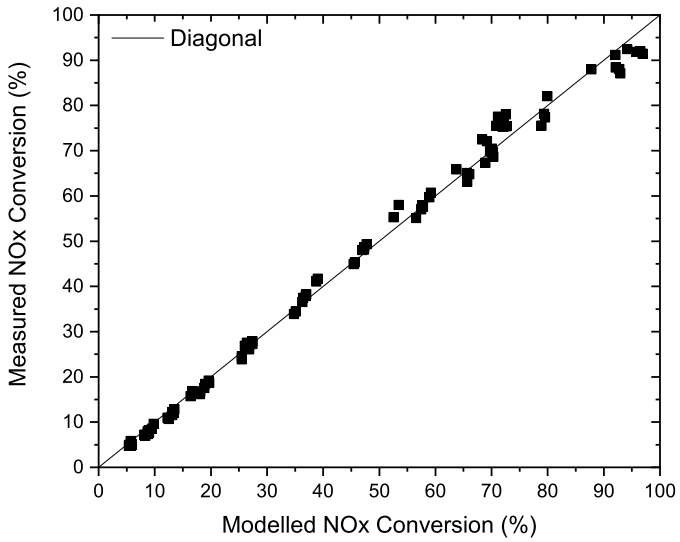

Figure 2.11: The measured NO_x conversion as given in Figure 2.9 vs. the calculated NO_x conversion using the kinetics shown in Table 2.1 and Table 2.2.

As shown by the parity plot given in Figure 2.11 the model predicts the conversion fairly well across all pressures, but at the full conversion i.e. high temperature, the model is predicting a bit lower NO_x conversion than what is measured due to lack of NH_3 on the surface.

For comparison the Eley-Rideal expression was also fitted using the steady state SCR data to fit both NO reduction and NH_3 coverage (using simple Langmuir isotherm). The fitting was done using lsqcurvefit in Matlab® and the fitted parameters are shown in Table 2.3 together with those reported by Koebel and Elsener[36].

Table 2.3: The fitted Eley-Rideal parameters using the data presented in Figure 2.9.

Parameters	This Study	Koebel & Elsener[36]
$k(T_{230°C})$ - m3/s/kg	0.0588	
$E_{A,NO}$ - kJ/mol	62.5	74.7
$K_{NH3,0}$ - Pa^{-1}	$24.08 \cdot 10^{-12}$	$3 \cdot 10^{-12}$
H_{ad} - kJ/mol	-114.6	-137

2.3.2.4 Comparison of Kinetics

An experiment with a constant flow rate of 600 NmL/min containing 10% O_2, 8% H_2O, 600 ppm NO_x, ANR = 0.8 in N_2 was performed and the pressure was changed from 1.4 bar to 4.4 bar, without changing the total flow rate. All four experiments were modeled using both the Eley-Rideal expression (Table 2.3) and the Temkin parameters (Table 2.1 and Table 2.2) to test how well they fit the experimental data. The results are shown in Figure 2.12.

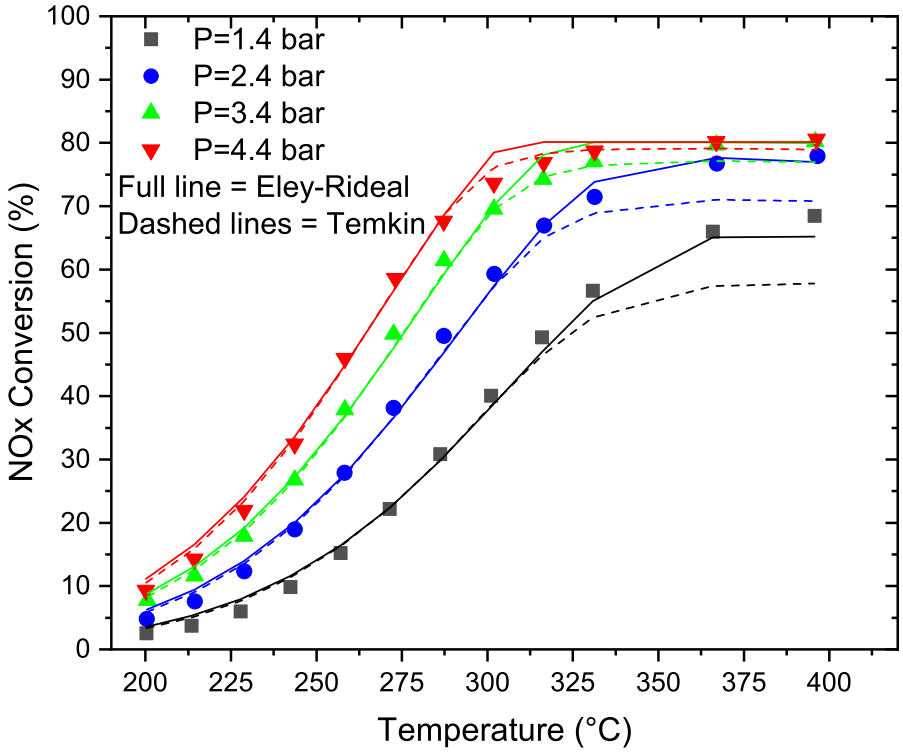

Figure 2.12: Experiments carried out with 20.5 mg 1.2 wt% SCR catalyst using a total flow rate of 600 NmL/min containing 10% O_2, 8% H_2O, 600 ppm NO_x, ANR = 0.8 in N_2 and changing the pressure without changing the flow. Full lines are model prediction by Eley-Rideal parameters according to Table 2.3. Dashed lines are based on Temkin parameters according to Table 2.1 and Table 2.2.

Figure 2.12 shows that at temperatures below 300℃, the two models estimates the same amount of NO_x conversion, which is due to a low conversion of NO_x which results in a rate that is not dependent on the NH_3 concentration, i.e. $\theta > \theta^* = 0.14$. At temperatures above 300℃ the model with Temkin kinetics does not fit the measured NO_x conversion well at the 1.2 bar experiment. This was also observed from the fitted TPD kinetics as shown in Figure 2.7 in which the model did not fully describe the high temperature desorption peak. At higher pressures the Temkin model predicts the NO_x conversion a little bit better than the Eley-Rideal, however, since the Eley-Rideal model in general is found to fit the experimental data well, this model will be used to fit the monolith experiment presented in the next section.

It should be noted that the Temkin model was found to have multiple solutions depending on the initial guess, and therefore, it cannot be ruled out that a better fit could be found. Furthermore, it should be noted that the NH_3 adsorption/desorption kinetics, were fitted using the independent NH_3 TPD experiments, and hence the overall fit is believed to be quite good. An optimization that could be done, before performing more NH_3 TPD experiments is to reducing the empty space, before and after the catalyst, as also stated by Lietti et al.[91] so the area for the blank experiments becomes negligible. With the present data in hand, as presented in this study, it is recommended to use the simplified model of Eley-Rideal kinetics also at increased pressure.

2.3.3 Full Monolith Experiment

Pressurized SCR experiments were carried out using a V-SCR catalyst (∼1 wt% V_2O_5), in the form of a monolith with an open inlet area of 223 mm^2. A total volumetric flow rate of 4.9 Nm^3/h was used at 1 bar containing 8% O_2, 5% H_2O, 720 ppm NO_x, ANR = 0.75 or 1.16 in N_2. The experiment was also carried out at an increased pressure of 3.1 bar using a total volumetric flow rate of 14.5 Nm^3/h, hence the actual residence time was similar at the two different pressures. The NO_x reduction measured across the monolith as a function of temperature for the two pressures and two ANR's are shown in Figure 2.13.

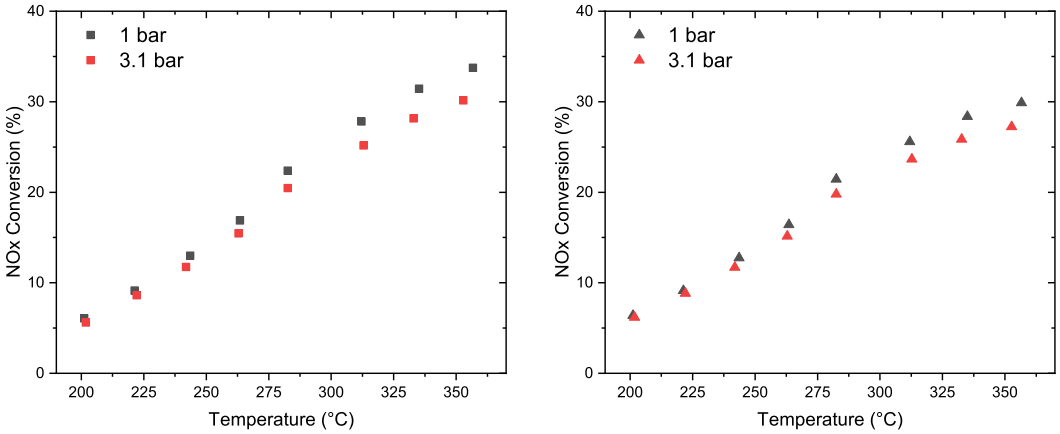

(a) ANR = 1.16 (b) ANR = 0.75

Figure 2.13: Monolith experiments using a total volumetric flow rate of 4.9 Nm^3/h at 1 bar containing 8% O_2, 5% H_2O, 720 ppm NO_x, ANR = 1.16 (a) or ANR = 0.75 (b) in N_2. At 3.1 bar a total volumetric flow rate of 14.5 Nm^3/h, was used, and hence the actual residence time is similar at the two pressures.

Figure 2.13 shows that at the low temperature of 200°C, similar NO_x conversions are observed independent on the pressure, when the residence time is constant. As the temperature is increased a decrease in NO_x conversion is observed for the 3.1 bar experiment, which was not observed for the packed bed reactor system. The lower NO_x conversion at elevated pressures becomes visible around 250°C and more pronounced as the temperature is increased. At a temperature of approximately 250°C the SCR reaction within a monolith starts to become controlled by external and internal diffusion limitations and as the temperature is increased the limitations becomes more pronounced[44]. Because the diffusivity is inversed proportional with the pressure the reaction will become increasingly diffusion limited as the pressure is increased, which will limit the SCR reaction. The same trends were reported by Kröcher et al.[83] for a monolith experiment.

The increased diffusion limitations observed at increased pressure were modeled using the single channel monolith model developed in our group by Olsen[98]. The model is a 2D single channel monolith model, which calculates the concentration of NH_3 and NO both in the radial and axial direction under the following assumptions:

- Only standard SCR takes place (i.e. NO_x = NO)
- The reaction follows an Eley-Rideal mechanism (Equation 2.12)
- Complete mixing of NO and NH_3 with the flue gas at the inlet to the channel
- Film diffusion resistance is present at the boundary layer between the bulk gas flow and the catalyst surface
- The pore structure of the catalyst can be considered to be a bimodal pore structure

When the flow passes down the length of the monolith channel a developing laminar flow will be approached. Based on the work of Shah et al.[99] and London et al.[100], Tronconi et al.[51, 101] proposed the correlation shown in Equation 2.21 for the calculation of the Sherwood number for a developing laminar flow down the length of a monolith catalyst.

$$Sh = Sh_{\infty} + 8.827 \cdot (1000 \cdot Z^*)^{-0.545} \cdot \exp(-48.2 \cdot Z^*) \tag{2.21}$$

$$Z^* = \frac{z \cdot D_{AB}}{U \cdot d_h^2} \tag{2.22}$$

In which Sh_{∞} is the asymptotic Sherwood number, which for triangular channel shapes is 2.494. Z^* is the dimensionless axial coordinate, z is the axial coordinate, U is the linear velocity, and d_h is the hydraulic diameter. Based on the Eley-Rideal kinetics found using the granulated catalyst (Table 2.3), and a catalyst density of 1800 kg/m^3, the experiment was modeled as shown in Figure 2.14.

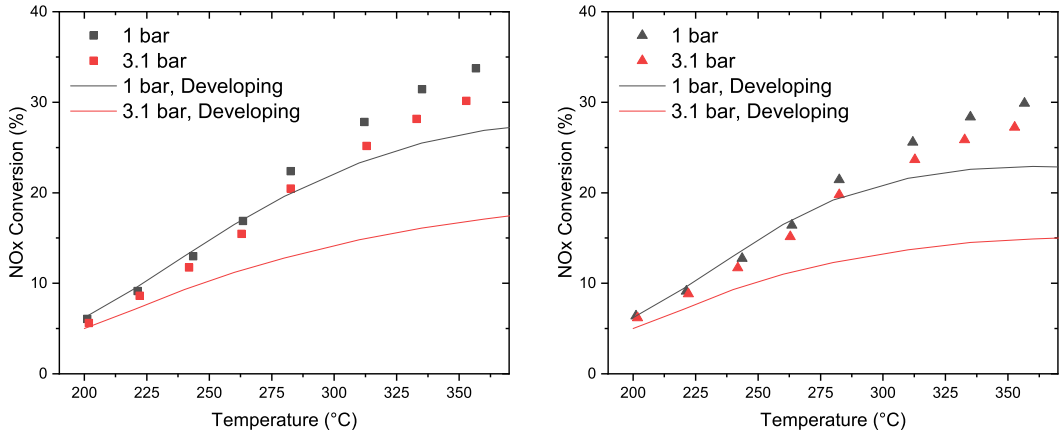

(a) ANR = 1.16 (b) ANR = 0.75

Figure 2.14: Monolith experiments using a total volumetric flow rate of 4.9 Nm^3/h at 1 bar containing 8% O_2, 5% H_2O, 720 ppm NO_x, ANR = 1.16 (a) or ANR = 0.75 (b) in N_2. At 3.1 bar a total volumetric flow rate of 14.5 Nm^3/h, was used, and hence the actual residence time is similar at the two pressures. The model developed by Olsen[98] was used to predict the experimental data, using the PBR kinetics shown in Table 2.3

Figure 2.14 shows that the model prediction, does not fit the experimental data that well. It is observed that at the increased pressure, the model predicts a decrease in NO_x conversion of almost 10% points. The decreased NO_x conversion was found to be due to a decreased mass transfer coefficient. It was therefore considered that the assumption of a developing laminar flow was not applicable for this experiment using a short monolith (10 cm) and a high flow rate. Reynolds number within the monolith channel was found to be approximately 1000 at 1 bar and 3000 at 3 bar, the increase due to an increased density. Therefore, the mass transfer coefficient was instead calculated based upon a laminar flow in tubes, as given by the Graetz number (Equation 2.23[94]) at 1 bar and both the laminar and turbulent (Equation

2.24[94]) flow in tubes was tried at the high pressure.

$$Sh = 1.86 \cdot Gz^{1/3} = 1.86 \cdot \left(Re \cdot Sc \cdot \frac{d_h}{L} \right)^{1/3} \tag{2.23}$$

$$Sh = 0.023 \cdot Re^{0.8} \cdot Sc^{1/3} \tag{2.24}$$

In which Re is Reynolds number, Sc is Schmidts number, d_h is the hydraulic diameter, and L is the length of the monolith. The model prediction using these expressions for external mass transfer limitations are shown in Figure 2.15

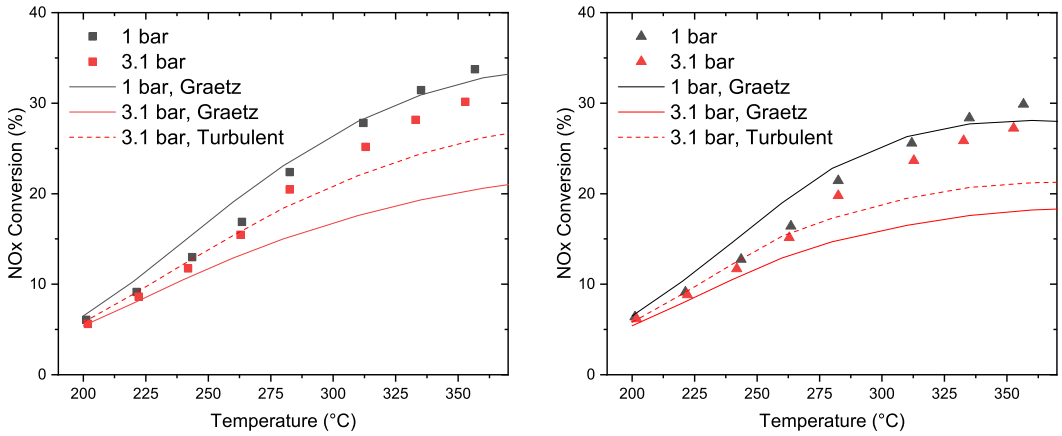

(a) ANR = 1.16 (b) ANR = 0.76

Figure 2.15: Monolith experiments using a total flow of 4.9 Nm^3/h at 1 bar containing 8% O_2, 5% H_2O, 720 ppm NO_x, ANR = 1.16 (a) or ANR = 0.75 (b) in N_2. The actual residence time was kept constant by increasing the total flow rate proportional to the pressure. The model developed by Olsen[98] was used to predict the experimental data, using the PBR kinetics shown in Table 2.3. The external mass transfer was modeled as pure laminar flow at 1 bar, and at 3 bar as both laminar (Equation 2.23 and turbulent flow (Equation 2.24).

Figure 2.15 shows that using the laminar flow for the 1 bar experiment gives a quite good fit to the experimental data. At 3 bar, where Reynolds number is calculated at around 3000, which is in the intermediate zone between pure laminar and pure turbulent flow, the turbulent model is found to give the best model prediction. Only 9 channels of the monolith was open to flow, so the square sectional area available for the gas, is reduced by 88% when the gas enters the monolith, which results in turbulence, so the fact that the turbulent model predicts the experimental data best in this case can be explained. Figure 2.15(b), shows that when NH_3 becomes limited at the high temperature, the model predicts a 5% points too low NO_x conversion. Regular length, full open monoliths should be tested in another study, to see how well the developing laminar flow predicts the external mass transfer at increased pressure. From this study it is concluded that at increase pressure, when the residence time is kept constant a decrease in NO_x reduction efficiency is observed, due to increase external and internal mass transfer limitations, as also shown by Kröcher et al.[83].

It should be noted that the drop in NO_x reduction is only observed due to the constant residence time. If an SCR reactor was installed on a real ship this would

not be the case and the total effect of increasing pressure is positive as also reported by Kröcher et al.[83]. Kröcher et al.[83] stated that to achieve 70% NO_x reduction at 350℃ and having an NH_3 slip of 10 ppm, the volume of a 87 cpsi catalyst could be reduced from 100% at 1 bar, to 80% at 2 bar and 70% at 4 bar, which shows that in total a positive effect is present. If no diffusion limitation had been present the catalyst volume could have been reduced to 50% and 25% at 2 and 4 bar respectively.

2.4 Conclusion

Selective catalytic reduction of NO_x was investigated at increased pressures of up to 4.8 bar, to study the possible effects on reaction kinetics by positioning an SCR reactor upstream of a turbocharger at a large two-stroke diesel engine.

NH_3 adsorption and desorption processes were investigated using a ∼1 wt% V-SCR catalyst in a packed bed reactor. The experiments were carried out at four different adsorption temperatures (150℃, 200℃, 250℃, and 300℃) and at four different pressures (1.2 bar, 2.4 bar, 3.6 bar and 4.5 bar). The NH_3 capacity of the catalyst, i.e., the amount of NH_3 bound to the surface of the catalyst, was found to increase with increasing pressure and decrease with increasing temperature. For example at 4.5 bar and 150℃ the NH_3 adsorption was increased with 36% compared to the 1.2 bar experiment also conducted at a temperature of 150℃.

Based on the work of Lietti et al.[91] a transient model was established based upon a non activated adsorption of NH_3 ($E_A^0 = 0$), and a Temkin desorption model of NH_3 and was implemented in Matlab®. The maximum NH_3 capacity of the catalyst was fixed based upon the experiment conducted at 4.5 bar, and 150℃ and was calculated to 372 $mol/m^3_{reactor}$. The four remaining kinetic parameters (k_a^0, k_d^0, E_d^0 and α) were fitted using the Matlab® function "fmincon". During the fitting procedure multiple solutions were found based on different initial guesses, and therefore, the final solution was chosen based on also being apple to model the steady-state SCR also performed at increased pressure.

Steady-state SCR was performed across a packed bed reactor using a constant residence time also at increased pressure, by increasing the total flow rate proportional to the pressure increase. The experiments were conducted using a total flow rate of 300 NmL/min at 1.2 bar containing 10% O_2, 8% H_2O, 600 ppm NO_x, ANR of 0.8 or 1.2 in N_2. The measured NO_x conversion was found independent on the pressure when the residence time was kept constant. This indicated that the reaction followed the same kinetics, independent of the pressure. Experiments were also conducted with 300 and 900 ppm of NO_x indicating the same trend. The experiment using 300 ppm NO_x showed an increased NO_x conversion, which was concluded to be due to an increased residence time.

For comparison, a steady state model using the simplified Eley-Rideal type of NH_3 coverage was also implemented in Matlab®. The rate of NO disappearance was

fitted for both of the models using the steady state data made with constant residence time. The two models were then used to predict the NO_x conversion using an ANR of 0.8 for an experiment with a constant flow rate, and therefore not constant residence time when the pressure was increased. The results were compared to experimental data, and the two models calculated identical NO_x conversion at low temperature, where the high NH_3 surface coverage resulted in a rate of NO consumption that was first order in NO and zero order in NH_3. At temperatures above 300℃, the Temkin model predicted a too low NO_x conversion at pressures of 1.4 and 2.4 bar, but gave good results at 3.4 bar and 4.4 bar. The Eley-Rideal model, in general, was better at predicting the NO_x conversion, however, at the high pressure of 3.4 and 4.4 bar, the model predicted full conversion of NH_3 before it was observed in the experiment. It was concluded that with the fitted parameters the Eley-Rideal kinetics gave the best results. It should be noted that the Temkin parameters for the NH_3 adsorption/desorption, were also fitted to the independent NH_3 TPD experiments, while the Langmuir isotherm, part of the Eley-Rideal expression, was fitted together with the NO rate constant using the steady state dataset. A better fit to the experimental data by the Eley-Rideal kinetics were expected, however, it does show the important conclusion, that the simple Eley-Rideal expression, also can be used at increased pressure.

The last experimental campaign was performed at Haldor Topsøe A/S, at which steady-state SCR was performed across a monolith SCR catalyst, again using a constant residence time. The full monolith experiments showed that when the residence time in the catalyst was kept constant, the amount of NO_x reduction was decreased at increasing pressure, due to a decreased diffusivity of NH_3 and NO, resulting in increased internal and external mass transfer limitations, as also proposed by Kröcher et al.[83]. The monolith experiment was modeled using the single channel monolith model developed by Olsen[98]. The use of a developing laminar flow for the calculation of external mass transfer limitation, was found inadequate, because a too low mass transfer was calculated , resulting in a too low NO_x reduction compared to the experimental data. The experimental data was found to be better predicted calculating Sherwoods number for a laminar flow at 1 bar, and at increase pressure, where Reynolds number was also increase a turbulent model was used.

3 Pressurized SO_2 Oxidation across V-Based SCR Catalyst - Article

The following chapter is a copy of the published article "SO_2 Oxidation across Marine V_2O_5-WO_3-TiO_2 SCR Catalysts – A Study at Elevated Pressure for Preturbine SCR Configuration" published in Emission Control Science and Technology, after being accepted 12th of June 2018 and available online the 5th of July.

The article is available online here: http://link.springer.com/10.1007/s40825-018-0092-8 and the citation is given below, for which it should be noted that in the moment of written the article was only available online, and hence no volume number is given[102]:

S. R. Christensen, B.B. Hansen, K. Johansen, K. H. Pedersen, J. R. Thøgersen and A. D. Jensen (2018) "SO_2 Oxidation across Marine V_2O_5-WO_3-TiO_2 SCR Catalysts – A Study at Elevated Pressure for Preturbine SCR Configuration", *Emission Control Science and Technology*, DOI: 10.1007/s40825-018-0092-8

The article published is given below.

SO_2 Oxidation across Marine V_2O_5-WO_3-TiO_2 SCR Catalysts – A Study at Elevated Pressure for Preturbine SCR Configuration

Authors: Steen R. Christensen[a], Brian B. Hansen[a], Keld Johansen[b], Kim H. Pedersen[c], Joakim R. Thøgersen[c], and Anker Degn Jensen[a,*].

[a] *Department of Chemical and Biochemical Engineering, Technical University of Denmark, Søltofts Plads B229, 2800 Kgs Lyngby, Denmark*
[b] *Haldor Topsoe A/S, Haldor Topsøes Allé 1, 2800 Kgs. Lyngby, Denmark*
[c] *Umicore Denmark ApS, Nøjsomhedsvej 20, DK-2800 Kgs. Lyngby, Denmark*
[*] Corresponding author: aj@kt.dtu.dk , +45 4525 2841,
OrCID: 0000-0002-7341-4859

3.1 Abstract

The undesired oxidation of SO2 was studied experimentally at elevated pressures of up to 4.5 bar across two commercial vanadium (1.2wt% and 3 wt% V_2O_5) based Selective Catalytic Reduction (SCR) catalysts. This pressure range, is of interest for preturbine SCR reactor configuration for NO_x reduction on ships. The residence time in the catalyst was kept constant, independent on pressure, by adjusting the total flow rate. The conversion of SO_2 was of the order 0.2-3 % at temperatures of 300-400℃ and was independent of the pressure. Based on the measured conversion of SO_2, the kinetics were fitted using a n'th order rate expression. The reaction order of SO_2 was found close to one, and the reaction order of SO_3 was found close to zero, also at increased pressures of up to 4.5 bar. The rate of SO_2 oxidation was clearly promoted by the presence of 1000 ppm NO_x at elevated pressure, however, at atmospheric pressure the effect was within experimental uncertainty. The promoting effect is explained by a catalyzed redox reaction between SO_2 and NO_2, and since more NO_2 is formed at elevated pressure, a higher degree of promotion by NO_x is observed at elevated pressures.

Keywords:

SO_2 oxidation; Pressurized SO_2 oxidation; preturbo SCR configuration; SCR of NO_x on Ships; SO_3 formation;

3.2 Introduction

In today's shipping industry, more than 90% of oceangoing vessels are powered by diesel engines burning fossil fuels[10]. Emissions, such as nitrogen oxides (NO_x) and sulfur oxides (SO_x) contributes to the acidification of the sea and land and also reduced air quality in harbor cities[15]. Around 70% of the emissions from

ships are produced within 400 km. of land, and the shipping industry contributes to approximately 15% of the global anthropogenic NO_x and 5-8% of the global SO_x emissions[12, 103]. Consequently, limitations of NO_x and SO_x emissions are targeted through the introduction of Marpol 73/78 Annex VI Tier III regulation 13 and 14[17].

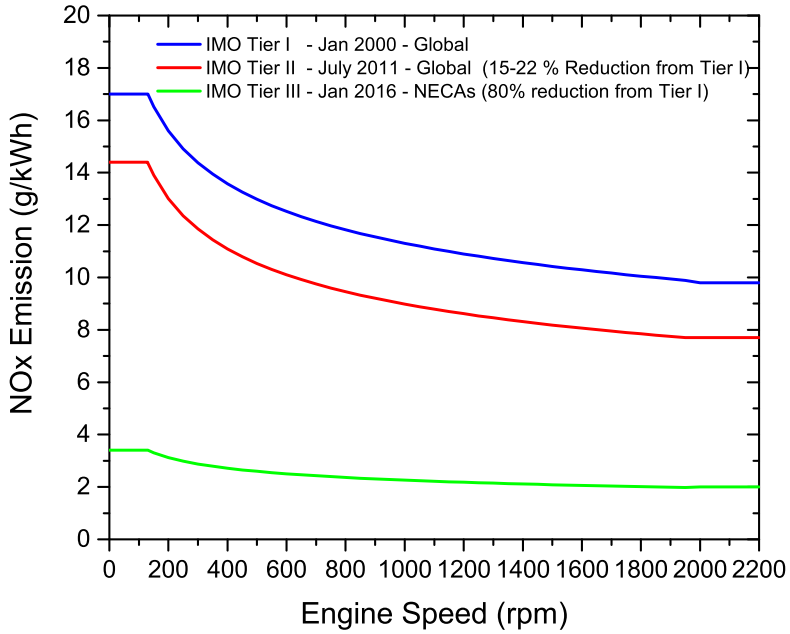

Figure 3.1: Allowed NO_x emissions as a function of engine speed according to Marpol 73/78 Annex VI Regulation 13[17].

The NO_x compliance to IMO Tier III is expected to be achieved through either Exhaust Gas Recirculation (EGR), use of dual-fuel engines, or by the implementation of Selective Catalytic Reduction (SCR) of NO_x[68]. EGR is a primary NO_x reduction method, in which the production of NO_x from the engine is reduced by lowering the combustion temperature and oxygen content through recirculation of exhaust gas (increased H_2O and CO_2 inside the combustion chamber)[10]. SCR, on the other hand, is a secondary NO_x reduction method, in which the NO_x emissions are reduced downstream of the engine, by introducing a catalytic reactor in the exhaust gas aftertreatment system.

SCR of NO_x is a well-known technology, which has been used on both stationary and mobile sources to reduce NO_x emissions since the 1980s[25–27]. NO_x emissions from mobile units, such as ships, are reduced across a catalyst by introducing a 30-40 wt% aqueous solution of urea usually sprayed into the exhaust gas as small droplets upstream of the catalyst[30]. The droplets evaporate and decompose into ammonia and CO_2 according to Reaction 3.1. Ammonia then reacts with oxygen and NO_x across the catalyst forming harmless nitrogen and water, according to Reaction 3.2 resulting in a NO_x reduction of usually 80-95 % at temperatures of

300-450 ℃[30].

$$NH_2{-}CO{-}NH_2 + H_2O \longrightarrow 2NH_3 + CO_2 \tag{3.1}$$
$$4NH_3 + 4NO + O_2 \longrightarrow 4N_2 + 6H_2O \tag{3.2}$$

The catalyst used for SCR of NO_x on ships is usually the ternary vanadium based (V-SCR) catalyst, doped with tungsten on a carrier of titanium dioxide (V_2O_5/ WO_3/ TiO_2)[14, 72, 77]. The V-SCR catalysts are well known for not being deactivated by the high SO_2 concentrations, up to 1000 ppm, present in marine diesel exhaust gas[31, 64, 65]. The oxidation of SO_2 according to Reaction 3.3, is also slightly activated by a V-SCR catalyst, usually resulting in an SO_2 oxidation of 1-3% under SCR operating conditions[104]. This reaction is critical to study because the produced SO_3 readily reacts with water forming sulfuric acid causing corrosion, or it can further react with ammonia forming ammonium bisulfate (ABS) or ammonium sulfate (AS) according to Reaction 3.4 and 3.5 respectively[1, 105, 106].

$$SO_2 + \frac{1}{2}O_2 \longrightarrow SO_3 \tag{3.3}$$
$$SO_3 + H_2O + NH_3 \longrightarrow NH_4HSO_4 \tag{3.4}$$
$$SO_3 + H_2O + 2NH_3 \longrightarrow (NH_4)_2SO_4 \tag{3.5}$$

The formed sulfates may condense when the exhaust gas temperature decreases. The condensation of sulfates within the catalyst pore system is a particular problem, since capillary forces result in a higher dew point temperature than in the bulk, and therefore a higher temperature is needed to ensure that the catalyst is not deactivated[1, 107]. The specific dew point temperature depends on both the concentrations of NH_3, H_2SO_4, and the pore sizes[107]. With a high sulfur fuel (e.g., 3.5 wt% sulfur) the catalyst must, therefore, be placed at temperatures above 330-340℃[72, 83]. However, if a low sulfur fuel is used instead (e.g., 0.1 wt% of sulfur) a lower temperature of 260℃ can be used, without deactivating the catalyst[83]. In two-stroke marine diesel engines such high temperatures are only continuously achievable by installing the catalytic reactor upstream of the turbocharger, where a pressure of up to 4.5 bar is present[72]. The higher pressure will increase the condensation temperature[84] and could affect the oxidation of SO_2.

Earlier studies of SO_2 oxidation[108–110] have reported that the rate of SO_2 oxidation has a zero order oxygen dependency at concentrations above 1-2 vol%, which is the case for marine diesel engines exhaust gas ($O_2 > 10$ vol%[10, 63]). Water has been reported to inhibit the rate of SO_2 oxidation[109], however, at practical water concentrations (5-15%) the rate is found to be independent of the water concentration. The reaction is commonly reported to be first order in SO_2[52, 66, 111], while the reported SO_3 orders range from negative first order[108] to a zero order dependency[52, 66, 111]. Earlier studies have all been carried out at atmospheric pressure. Therefore this study will expand upon the current knowledge of catalytic SO_2 oxidation to high pressure marine conditions, using two commercial V_2O_5/ WO_3/ TiO_2 catalysts supplied by Haldor Topsøe A/S. The effect of temperature, pressure, SO_2 concentration, and NO_x concentration is presented.

3.3 Experimental Methods

3.3.1 Apparatus

The setup used for measurements of pressurized SO_2 oxidation is shown schematically in Figure 3.2. Nitrogen, air, and liquid water were added to the first heater (HE1) using Brooks Smart Mass Flow Controllers (MFC's) for gas addition and Brooks liquid mass Flow model 5882 for addition of water. Water was evaporated in the first heater, a second heater (HE2) was used to control the reaction temperature in the range of 290-420℃, and heating elements around the reactor helped to maintain the reaction temperature. A manual backpressure valve was used to control the reaction pressure to between 1-4.5 bar. Gaseous SO_2 was added to the hot gas and passed through a static mixer from Sulzer, before reaching the reactor. The standard experimental conditions were: 5% H_2O, 8-10% O_2, and approximately 1000 ppm of SO_2 in N_2 as shown in Table 3.1, and in some experiments, 1000-1500 ppm of NO_x was also added to the flue gas before the mixer, as with SO_2. Isothermal conditions were verified by K-type thermocouples placed before and after the catalyst.

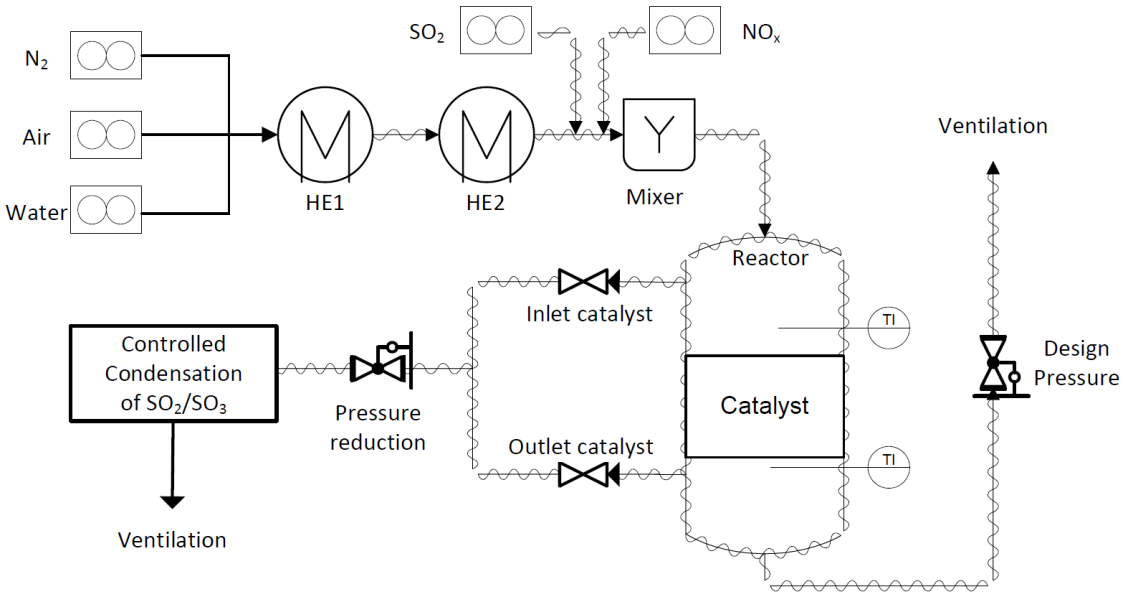

Figure 3.2: Monolith reactor setup at Haldor Topsøe A/S.

To reach steady state conditions, a conditioning period of 15-20 hours must be used when measuring the oxidation of SO_2. The long conditioning time is due to sulfating of the catalyst and is part of the mechanism behind SO_2 oxidation, involving adsorption of SO_2, oxidation of SO_2 to SO_3 on the surface of the catalyst, and lastly the desorption of SO_3[66, 104, 109]. To ensure sufficient conditioning time, the catalyst was left overnight after a change in temperature, species concentration, or pressure was introduced. Sufficient conditioning time was assumed when two measurements, with approximately 2-4 hours between each measurement, using the same conditions showed the same conversion of SO_2. If this was not the case, the

catalyst was left an additional day, and measurements were repeated.

Table 3.1 gives an overview of the performed experiments covering 2 different commercial maritime SCR catalysts. To clarify the direct pressure effects on reaction kinetics, similar residence times in the catalyst were imposed by increasing the total flow rate proportionally to the pressure. The residence time for the different conditions is indicated by the linear velocity through the channels or by the weight based residence time (W/Q), where W is the mass of the catalyst element and Q is the total volumetric flow rate (1 bar, 0℃), as shown in Table 3.1. As shown in Table 3.1 there were minor changes in the SO_2 inlet concentration when the pressure was varied, indicating offset in the actual total flow compared to the expected total flow. The total flow rate as shown in Table 3.1, was therefore calculated from the measured outlet SO_x concentrations and the flow rate of SO_2 added to the flue gas.

Table 3.1: The total flow rate and the linear velocity through the catalyst channels (at reaction pressure and 0℃). The measured mean inlet concentration and the standard deviation based upon all measurements are also shown.

Catalyst	Pressure	Total Flow rate	Linear Velocity	Mean SO_2 Inlet Conc.	Weight Based Residence Time
	Bar	m^3/h @ 0℃, 1 atm	ppm, dry	$kg_{cat}{\cdot}s/m^3$	
0.66 L Low V-SCR	1	4.5	0.85	930±15	119.1
0.66 L Low V-SCR	3	14.4	0.94	860±15	107.3
0.66 L Low V-SCR	4.5	21.9	0.95	850±15	106.0
0.34 L High V-SCR	1	2.6	0.48	1120±15	97.5
0.34 L High V-SCR	2.9	8.5	0.55	980±15	84.5

The outlet concentrations of SO_2 and SO_3 were measured using the controlled condensation method as described by the Topsøe method 1305[112], which is a modification of the ASTM D-3226-73T standard method. The Topsøe method is based on controlled condensation of sulfuric acid at a temperature of 70℃ and subsequent titration of sulfate ions. At a temperature of 70℃ only sulfuric acid will condense, and since SO_2 has a very low solubility in sulfuric acid, SO_2 will be unaffected by the condensation. SO_2 is then subsequently collected in a 6% aqueous solution of H_2O_2 (converted into sulfuric acid). The collected samples are titrated with 0.005 M barium perchlorate as titrant and thorin as an indicator, using a Metrohm 862 compact titrosampler.

3.3.2 Catalysts

The conversion of SO_2 into SO_3 was measured for two ternary (1.2 wt% or 3 wt% V_2O_5 / ∼10% WO_3 / TiO_2) marine SCR catalyst (V-SCR) with a honeycomb structure supplied by Haldor Topsøe A/S. Both catalysts were cut into a square cross-sectional surface area (43.5 mm) to fit into the reactor and sealed with quartz wool as shown in Figure 3.3.

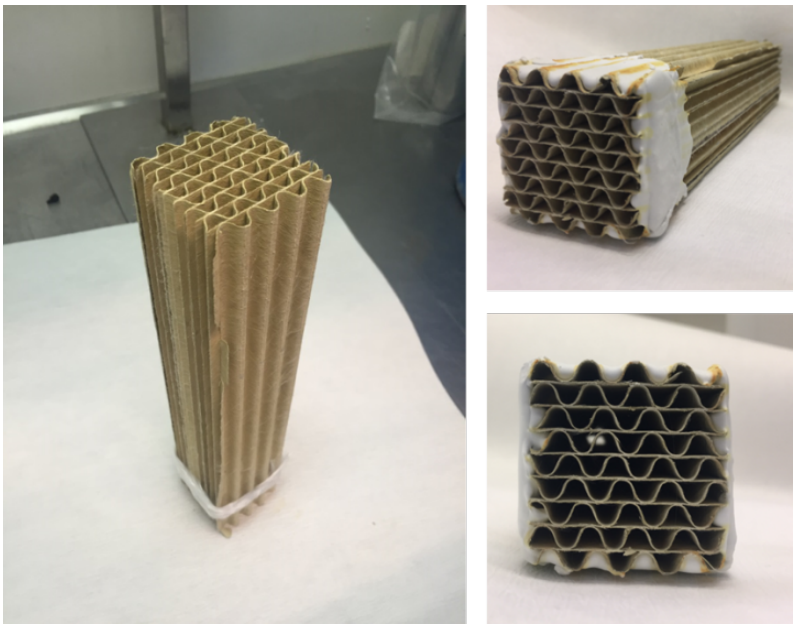

Figure 3.3: Pictures of the high vanadia content SCR catalyst, with quartz wool in one end. It should be noted that the catalyst was fixed using quartz wool in both ends before loading.

The catalyst was forced to fit into the reactor to ensure that no gas would bypass the catalyst. Further information on the catalyst properties can be found in Table 3.2. A roughly twice as large volume of catalyst was used for the low V-SCR catalyst to get a reasonable amount of SO_2 oxidation also at the lowest temperature of 300℃.

Table 3.2: Characteristics of the tested catalysts.

	Low V-SCR	High V-SCR
V_2O_5 Content - wt%	1.2	3
Width or Length - mm	43.6	43.5
Height - mm	460	231
Weight - g	145.7	69
# of open Channels	59	61
Hydraulic diameter - mm	4.3	4.3
Void - %	80	80

3.4 Results and Discussion

3.4.1 Pressurized SO_2 Oxidation

A background measurement was performed at 390℃, 1000 ppm SO_2, and 1 bar, by measuring the conversion of SO_2 at the inlet to the catalyst, which yielded a negligible SO_2 oxidation (0.07%). Consequently, the conversion of SO_2 into SO_3 could be measured by simultaneously measuring the SO_2 and SO_3 concentration out of the reactor. The sum of SO_2 and SO_3 out of the reactor was assumed to

correspond to the inlet concentration of SO_2. The conversion of SO_2 was calculated based on the measured SO_3 concentration and the inlet concentration of SO_2.

The conversion of SO_2 was measured across a low V-SCR and a high V-SCR catalyst at temperatures and pressures relevant for marine SCR, i.e., 300-400°C and 1-4.5 bar and the results are shown in Figure 3.4. The mean conversion of SO_2 is shown by the symbols in Figure 3.4 and is based upon two measurements. The two measurements used to calculate the mean are shown as the top and bottom point of the bar in each symbol.

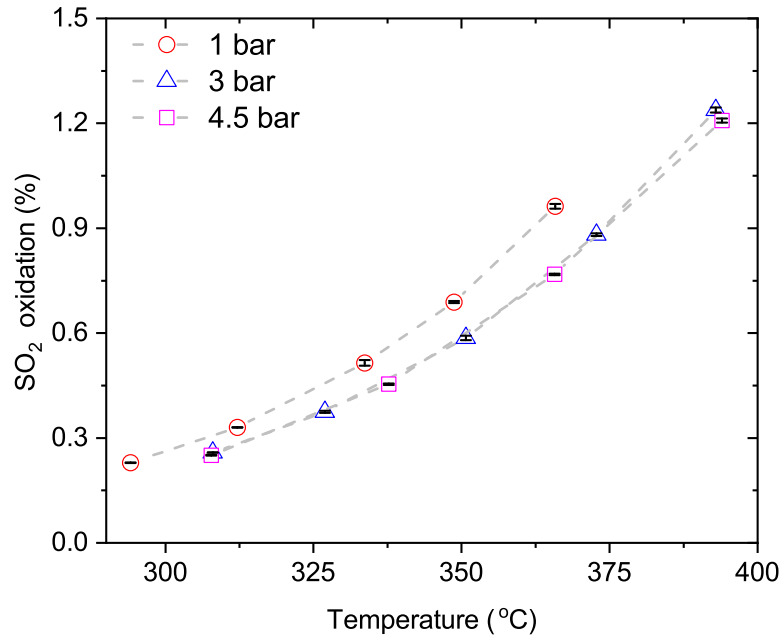

(a) Conversion of SO_2 for the low V-SCR catalyst.

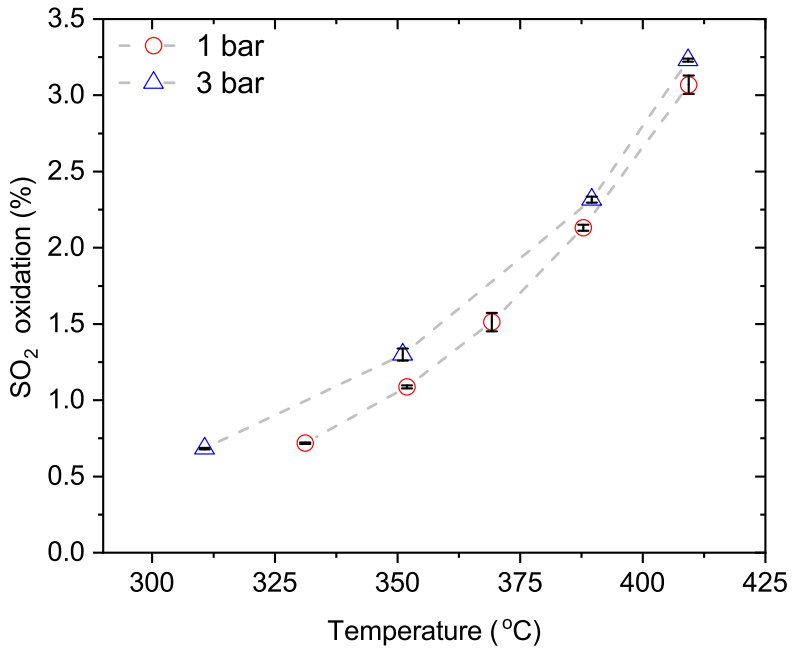

(b) Conversion of SO_2 for the high V-SCR catalyst.

Figure 3.4: The mean steady state SO_2 oxidation measured across two marine type commercial V-SCR catalysts. Symbols shows the mean, top and bottom of bar is the two measurements used to calculate the mean, and dashed lines connects each measurement. General test conditions were 5% H_2O, 8-10% O_2, SO_2 according to Table 3.1 and balance N_2. It should be noted that the 3 bar test for the high V-SCR was performed with 2% H_2O as discussed in Section 3.4.2

Figure 3.4 shows that when the residence time is kept constant, as is the case for 3 and 4.5 bar for the low V-SCR catalyst, according to Table 3.1, the measured conversion of SO_2 is identical, independent of the change in pressure, indicating

pressure independent kinetics. Figure 3.4 shows that in general a higher conversion of SO_2 is found for the high V-SCR catalyst compared to the low V-SCR catalyst as has also been found in literature[108, 111]. The highest measured conversion of SO_2 is below approximately 1.2% for the low V-SCR catalyst (Figure 3.4(a)) and 3.2% for the high V-SCR catalyst (Figure 3.4(b)). For the high V-SCR catalyst the maximum value corresponds to an SO_3 concentration of around 30 ppm at a pressure of 3 bar. It should be noted that these levels of SO_2 conversion are far below the equilibrium conversion predicted by HSC chemistry 9.0® (X_e (300-400℃)>95%) and therefore, the measured kinetics are not influenced by the reverse reaction. A similar conversion of SO_2 has also been reported by other authors in studies at atmospheric pressure[26, 104, 113]. The two measurements performed at each steady state, as indicated by the top and bottom of the bars in each symbol shows that the double determination gave very similar results for the low V-SCR catalyst, indicating steady state conditions and good repeatability. For the high V-SCR catalyst (Figure 3.4(b)) a higher uncertainty, compared to the low V-SCR catalyst, is observed. The measured conversion of SO_2 at the high V-SCR catalyst is higher at 3 bar, even though the residence time in the catalyst is lower (by 12%) than the residence time at 1 bar, as also shown in Table 1, which is unexpected and must be due to uncertainties in the calculated/measured flow. The observed uncertainty is not considered prohibitively large and the results are useful and trustworthy.

3.4.2 SO_2 Oxidation and H_2O

Addition of water significantly decreases the SO_2 oxidation, but at practical water concentrations (≤5 vol% at atmospheric pressure) the rate of SO_2 oxidation is known to be independent of the water concentration[26, 109]. Therefore, experiments were in general performed with 5 vol% of water in the gas, however, MFC limitations during the 3 bar high V-SCR experiment yielded only 2 vol% of water. A repetition was, therefore, performed at 390℃ and 3 bar, both with 2 vol% of water and 5 vol% of water in the gas to ensure that the results obtained with 2 vol% of water at 3 bar could be compared to the results using 5 vol% of water at 1 bar. Figure 3.5 shows the measured conversion of SO_2.

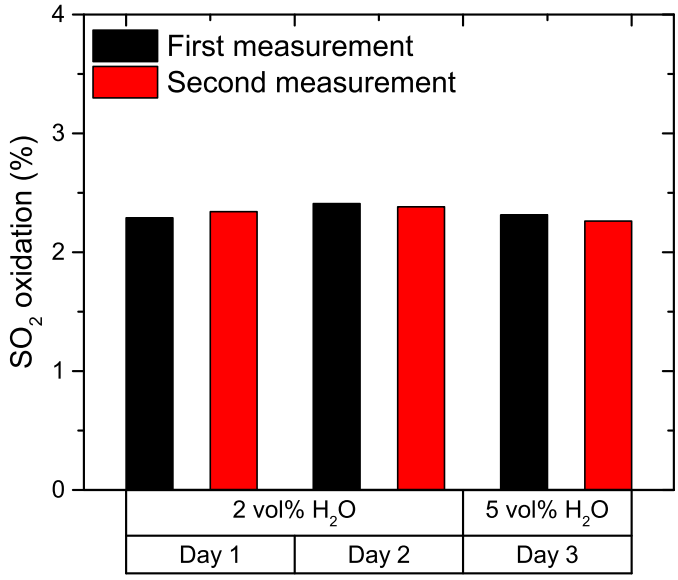

Figure 3.5: Repetition of SO_2 oxidation at 390°C and 3 bar across the high V-SCR with 2 vol% and 5 vol% of H_2O.

Figure 3.5 shows that at a temperature of 390°C and a pressure of 3 bar, the measured conversion of SO_2 is independent of the water concentration when changing from 2 vol% of water to 5 vol% of water. Svachula et al.[109] also tested the inhibiting effect of water on SO_2 oxidation at atmospheric pressure and stated that the conversion of SO_2 is independent of water at concentrations above 5 vol% of water. The experiments presented here, are well in line with the results of Svachula et al., since the concentration of 2 vol% water at 3 bar corresponds to the same partial pressure as 6 vol% at 1 bar. Therefore, based on Figure 3.5 the results obtained using 2 vol% of water at 3 bar and the results obtained using 5 vol% of water at 1 bar are considered comparable.

3.4.3 SO_2 Inlet Concentration

The conversion of SO_2 was measured as a function of the inlet concentration of SO_2 at a temperature of 350°C at 1 and 3 bar for the low-V SCR catalyst. The inlet concentration of SO_2 was changed from the standard concentration of approximately 900 ppm to 1400 ppm of SO_2 at 1 bar and at 3 bar. At 3 bar an additional experiment was also performed with 400 ppm of SO_2. The conversion of SO_2 using the different inlet concentrations is shown in Figure 3.6.

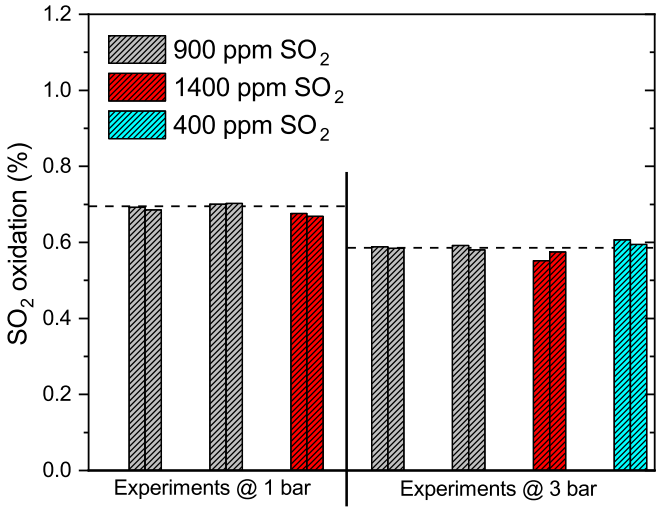

Figure 3.6: The conversion of SO_2 with varying SO_2 inlet concentrations measured at 350°C at 1 and 3 bar. The dashed lines indicate the mean of the standard experiment using 900 ppm of SO_2.

Figure 3.6 shows that the conversion of SO_2 is independent of the SO_2 inlet concentration, indicating a first order reaction as discussed further below. It should be noted that the difference in the conversion of SO_2 observed at 1 bar and 3 bar, is due to a higher residence time at 1 bar, as already discussed and shown in Table 3.1, and hence the conversion of SO_2 should not be compared across pressure in Figure 3.6.

3.4.4 SO_2 Kinetic Model

The extent of external and internal mass transfer limitation is estimated from the Carberry number, and the internal effectiveness factor, See Appendix D. On this basis the SO_2 oxidation was found to be kinetically controlled, as also reported by other authors[52, 104, 109, 113] and therefore, the reaction will take place in the full monolith wall. A reactor model assuming plug flow of gas through the channels, no transport limitations and an n'th order rate expression was applied when fitting the kinetic parameters, as shown in Equation 3.6. The rate expression on the right hand side of Equation 3.6 assumes a zero reaction order in oxygen which has been reported by other authors under conditions where the oxygen concentration is above 2 vol%[109], which is the case for all experiments presented here and typical ship engine out concentrations[63].

$$F_{SO_2,0} \cdot \frac{dX}{dW} = -r_{SO_2} = k \cdot p_{SO_2}^{\alpha} \cdot p_{SO_3}^{\beta} \tag{3.6}$$

In Equation 3.6 $F_{SO_2,0}$ is the molar feed rate of SO_2, W is the mass of catalyst and X is the conversion of SO_2. The rate constant was fitted using a modified Arrhenius equation, as shown in Equation 3.7.

$$k(T) = k(T_{ref}) \cdot \exp\left(\frac{-E_a}{R} \cdot \left(\frac{1}{T} - \frac{1}{T_{ref}}\right)\right) \tag{3.7}$$

In which $k(T_{ref})$ is the rate constant at a reference temperature, which was chosen at 350℃, a midpoint in the investigated temperature interval. This way of formulating the rate constant minimizes the correlation between the pre-exponential factor and the activation energy[96]. The four variables, $k(T_{ref})$, E_a, α, and β were fitted by minimization of the residual sum of square (RSS), as given in Equation 3.8, using the function "lsqcurvefit" in Matlab®.

$$RSS = \sum \left(y_{calc} - y_{exp}\right)^2 \tag{3.8}$$

The goodness of a fitting result is evaluated based on the residual mean square error (RMSE) which is the RSS value divided by the number of data points.

3.4.5 Fitting Results

The first fitting was done for the low V-SCR catalyst where changes in the inlet SO_2 concentration were performed at 1 bar and 3 bar, which made it possible to fit both rate constant, activation energy and the reaction orders at each pressure as shown in Table 3.3.

Table 3.3: The results of fitting at individual pressures across the low V-SCR catalyst, where changes in the inlet SO_2 concentration was performed, see Section 3.4.3

Pressure bar	k(350℃) mol/(kg·s·Pa^n)	E_a kJ/mol	α	β	RMSE
1 bar	$0.092 \cdot 10^{-6}$	53.2	0.77	0.14	$3.45 \cdot 10^{-5}$
3 bar	$0.092 \cdot 10^{-6}$	50.3	0.78	0.18	$6.13 \cdot 10^{-5}$

The low RMSE values in Table 3.3 indicate a good fit. However, the fitting solutions depended on the initial guess, due to too few data points. The solutions shown in Table 3.4, were the ones giving the lowest RMSE while still keeping similar reference rate constants and activation energies at the two pressures. The results shown in Table 3.3 show that the reaction rate parameters did not significantly change when changing the pressure, and therefore, the datasets were merged into one dataset for each catalyst and refitted as shown in Table 3.4.

Table 3.4: Results of fitting the merged data for each catalyst. Bold entries are forced and therefore not fitted.

Low V-SCR Catalyst					High V-SCR Catalyst				
k(350℃) mol/(kg·s·Pa^n)	E_a kJ/mol	α	β	RMSE	k(350℃) mol/(kg·s·Pa^n)	E_a kJ/mol	α	β	RMSE
$0.092 \cdot 10^{-6}$	50.7	0.78	0.16	$1.05 \cdot 10^{-4}$	$0.040 \cdot 10^{-6}$	49.7	1.08	0.16	$4.28 \cdot 10^{-3}$
$0.040 \cdot 10^{-6}$	60.5	0.91	**0**	$1.28 \cdot 10^{-4}$	$0.016 \cdot 10^{-6}$	59.2	1.25	**0**	$4.41 \cdot 10^{-3}$
$0.025 \cdot 10^{-6}$	57.2	**1**	**0**	$1.07 \cdot 10^{-3}$	$0.053 \cdot 10^{-6}$	63.4	**1**	**0**	$0.545 \cdot 10^{-1}$

The fitting of the merged dataset for the low V-SCR catalyst resulted in solutions that were independent of the initial guess, and as expected the goodness of the fit

was poorer as shown by the RMSE values in Table 3.4 compared to Table 3.3. Table 3.4 also shows fitting results for the merged dataset for the high V-SCR catalyst. Entry 1, in Table 3.4, shows that when all four parameters were fitted, it resulted in a slightly positive value for the reaction order of SO_3 (β) for both catalysts. Dunn et al.[108] tested a series of binary catalysts (1-7 wt% V_2O_5/TiO_2) and found that the reaction order of SO_2 could only be fitted as a first order when a negative first order was assumed for SO_3. Dunn et al. observed as high as 10% SO_2 conversion, resulting in an SO_3 concentration of around 100 ppm. However, since Dunn et al. performed atmospheric experiments, the partial pressure of SO_3 corresponds to about the same value as obtained at elevated pressure in the experiments presented here. A negative first order dependency of SO_3 was not found in this work, but rather a value close to zero. Since the reaction order of SO_3 was found close to zero it was assumed to be zero and the other three parameters refitted.

Based on a zero order dependency of SO_3 ($\beta = 0$), the fitted reaction order of SO_2 (α) was close to 1 for the low V-SCR as shown in Table 3.4 entry 2. Experiments with variation in inlet SO_2 concentration was only performed using the low V-SCR catalyst, making that dataset better suited for fitting of reaction orders. The small positive reaction order of $\alpha = 1.25$, found for the high V-SCR catalyst is considered close to one, since the fractional higher order does not seem physical. Based on these fitting results, the reaction order of SO_2 is in general found close to 1, and hence for practical purposes, a first order dependency can be used, also for increased pressures of up to 4.5 bar. A practical first order dependency was also proposed by Svachula et al.[109] for atmospheric pressures.

The proposed first order dependency of SO_2, and a zero order dependency on SO_3, resulted in an activation energy of 57.2 kJ/mol and a reference rate constant at 350℃ of $0.025 \cdot 10^{-6}$ mol/(kg·s·Pa) for the low V-SCR catalyst and 63.4 kJ/mol and a reference rate constant at 350℃ of $0.053 \cdot 10^{-6}$ mol/(kg·s·Pa) for the high V-SCR catalyst. The reference rate constant for the high V-SCR is 2.1 times higher than that for the low V-SCR catalyst. This indicates that the rate of SO_2 oxidation scales roughly linearly with the V-content since the high V-SCR catalyst contains 2.5 times more active material (3 wt% vs. 1.2 wt%). Similar activation energies have also been reported by other authors[66, 111], however, higher activation energies have also been reported, i.e., Beeckman et al.[52] with an activation energy of 110 kJ/mol.

In Figure 3.7 the measured conversion of SO_2 is plotted against that calculated based upon the kinetics assuming first order in SO_2 and zero order in SO_3 as shown in Table 3.4.

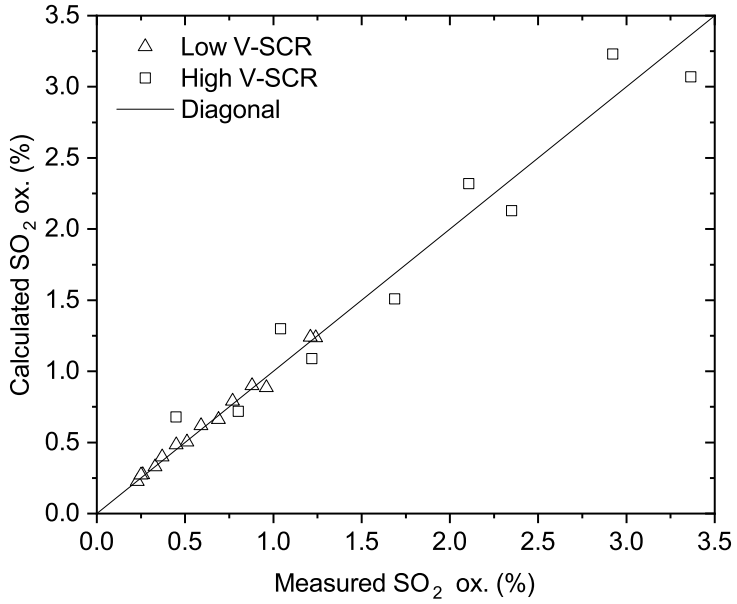

Figure 3.7: A parity plot, showing how well the final kinetics fits the measured data. A good fit is indicated by points on the diagonal

Figure 3.7 shows that there is a good agreement between the fitted and measured data for the low V-SCR catalyst. For the high V-SCR catalyst a poorer agreement is observed which was also expected, based on the uncertainty observed in the dataset.

3.4.6 Fitted Kinetics Compared to Literature Values

SO_2 oxidation kinetics have been found in the literature, and for comparison, the natural logarithm of the rate of reaction is shown in Figure 3.8 together with the kinetics found in this study. Full kinetic expressions are sparse in the literature, so the data shown in Figure 3.8 are based on rate plots found in the literature, which were read off as [X,Y] points by use of "plot digitizer"[114] and transformed into the same units i.e., mol/(m^3_{cat}·s). For instance in Beeckman et al.[52] the first order rate constant is found in units of cm/s, which are changed based on the supplied catalyst volume specific surface area, SS=$1.23 \cdot 10^6 cm^2/cm^3$[52], and using first order in SO_2 with an initial concentration of 1000 ppm SO_2.

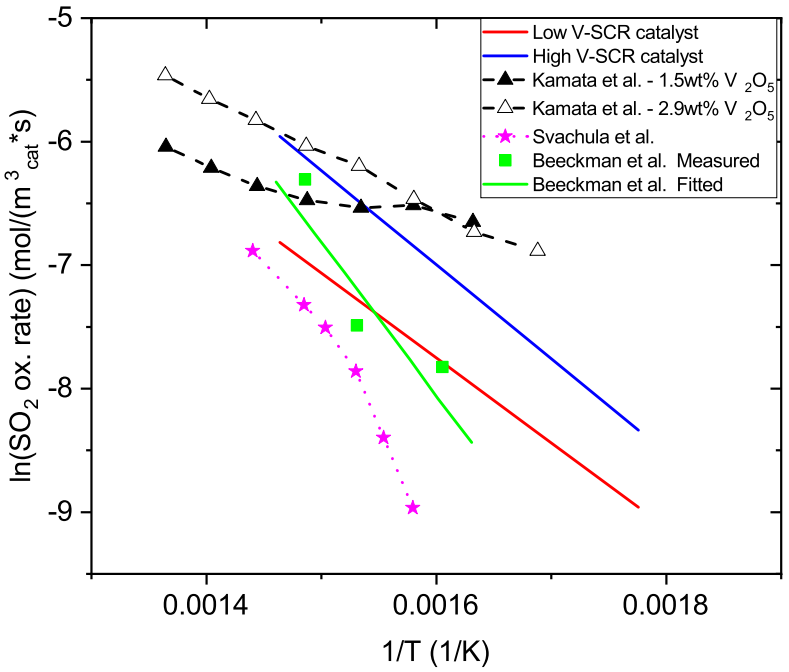

Figure 3.8: The rate of SO_2 oxidation, based on kinetics fitted to first order in SO_2 and zero order in SO_3 at 1000 ppm SO_2 and compared to kinetics found in the literature by Kamata et al.[111], Svachula et al.[109], and Beeckman et al.[52].

Figure 3.8 shows that the kinetics found in this study are similar to those found in the literature[52, 109, 111]. Kamata et al.[111] studied SO_2 oxidation on grounded binary catalysts with various loading of V_2O_5 on TiO_2 in an atmosphere of 500 ppm SO_2, 7500 ppm O_2, and balance N_2. The fact that no WO_3 was present in the catalyst and no water in the gas phase compared to the results presented here, would be expected to result in a higher rate, although this is not apparent from Fig. 8. A possible reason could be that Kamata et al. did experiments with a low oxygen concentration, where the rate can be limited by the lack of oxygen (O_2 <2%[109]). Kamata et al. observed similar rates at temperatures lower than 600 K for catalysts with 1.5wt% or 2.9wt% V_2O_5, which is likely due to difficulties in measuring the very low rate, especially because, Kamata et al. measured the conversion of SO_2 by evaluating the consumption of SO_2, and not the formation of SO_3 directly.

Beeckman et al.[52] tested a commercial catalyst, with 0.4 wt% V_2O_5 on TiO_2 in an atmosphere of 400 ppm NO, 400 ppm NH_3, 1000 ppm SO_2, 4% O_2 and 10% H_2O. Beeckman et al. do not state whether WO_3 is part of the catalyst. However, one could speculate that WO_3 (or MoO_3) is present since it is commonly added to commercial vanadium based SCR catalyst, to suppress the SO_2 oxidation[115] and suppress the transformation of TiO_2, from the high surface area form of anatase to rutile[44]. With the presence of both NO and NH_3 and the possible lack of WO_3 and less V_2O_5 in the catalyst makes it hard to speculate on whether or not a similar rate should be expected. Ammonia in the gas is reported to decrease the rate of SO_2 oxidation[109, 113] and is kinetically modelled as a competitive adsorption on the surface of the catalyst. However, none of the studies comment on the sulfate formation which happens when NH_3 and SO_3 is present in the gas. Formation of

sulfates could decrease the measured conversion of SO_2, but not necessarily the SO_2 oxidation itself. For instance, Orsenigo et al.[104] reported a decrease in measured SO_3 when ammonia was added to the exhaust gas, however, they also detected a maximum concentration of SO_3 after ammonia was should off again, after which the SO_3 levels then returned to its original values in a matter of 8 hours. The maximum could be due to decomposition of sulfates. Studies including NH_3 and taking into account sulfate formation should be performed.

The rate of SO_2 oxidation reported by Svachula et al.[109] was measured using 1000 ppm SO_2, 2% O_2, 10% H_2O and balance N_2 on commercial V-SCR catalyst. As with Beeckman et al. the presence of WO_3 in the commercial catalyst is not stated, and the V_2O_5 concentration is stated to be low, within a possible range of 0.3-2 wt% V_2O_5 that Svachula et al. investigated. The low V_2O_5 concentration, should result in a lower rate of SO_2 oxidation compared to the results from this study, which is clear in Figure 3.8. Svachula et al. reported a change in activation energy within the investigated temperature interval (T=360-420℃), and compared it to those typically found for vanadium based sulfuric acid catalyst. However, vanadium present in sulfuric acid catalysts are known to be in the liquid molten state[116] which is not the case for the vanadium based SCR catalyst, hence the break is unexpected, and not observed for the catalyst used here.

3.4.7 SO_2 Oxidation in the presence of NO_x

SO_2 oxidation was also studied across the low V-SCR catalyst with 1000 ppm of NO_x present in the gas at 1 and 3 bar and an additional experiment was performed with 1000 ppm NO, and 400 ppm NO_2 at 3 bar. NO_x was added as pure NO, however, small amounts of the NO can be oxidized to NO_2 before and within the catalyst especially at increased pressure (not measured), and the term "NO_x addition" is therefore used. When both NO and NO_2 were added, a NO_2 generator was used, in which NO and air were mixed using an over-stoichiometric ratio of oxygen and allowed to react at room temperature in a long Teflon tube. The NO_2 generator is known from previous tests by Haldor Topsøe A/S to result in conversions above 95% of NO to NO_2. When 400 ppm of NO_2 was added, it is under the assumption of 100% NO conversion in the NO_2 generator. NO, and NO_2 are added separately to the hot gas, and subsequently mixed. In SCR experiments not reported here with a similar residence time 1-2 ppm of NO_2 was present at atmospheric pressure and 6-8 ppm of NO_2 at 3 bar. The oxidation of NO is believed to follow a second order dependency in NO, hence increasing the NO concentration (by increasing the pressure from 1 to 3 bar), more than doubles the NO_2 concentration[93].

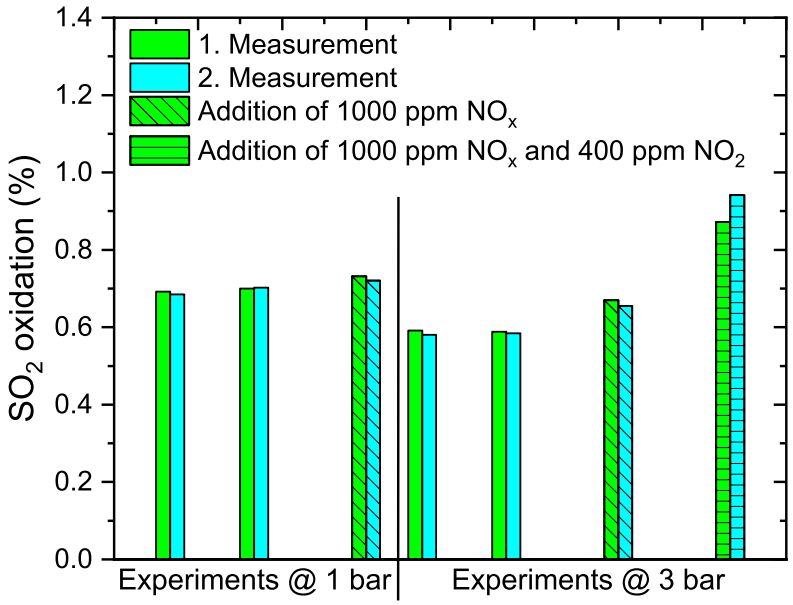

Figure 3.9: SO_2 oxidation measured at 350℃ at 1 and 3 bar across the low V-SCR catalyst without NO_x, with 1000 ppm NO_x, and with 400 ppm NO_2 and 1000 ppm NO_x. Beside NO_x standard conditions as shown in Table 3.1 was used.

Figure 3.9 shows a small increase of 4.5% in the conversion of SO_2 when 1000 ppm of NO_x was added to the gas mixture at 1 bar indicating a small promoting effect of NO_x. However, the small relative increase of 4.5% compared to the 1.8% of difference between the two repetitions is considered too small to give a definite conclusion. At 3 bar and when 1000 ppm of NO_x was added, the conversion of SO_2 increased from 0.59% to 0.66% SO_2 oxidation, i.e., an increase by 12%, which is expected to be due to a catalyzed reaction between SO_2 and NO_2 according to Reaction 3.9. To further investigate if the increased oxidation was due to a reaction with NO_2, an additional amount of 400 ppm of NO_2 was added, which increased the conversion of SO_2 with 54% compared to without NO_x, from 0.59% to a mean of 0.91% SO_2 oxidation.

$$NO_2 + SO_2 \longrightarrow NO + SO_3 \tag{3.9}$$

Measurements performed by Orsenigo et al.[104], showed that the promoting effect of NO_x on the conversion of SO_2 was only observed when a catalyst was present, indicating that the gas phase reaction is negligible. The lack of gas phase reaction was also confirmed by calculations using a detailed chemical kinetic model of the gas phase reactions[117] at 400℃, 1 bar, 1000 ppm NO_2 and 3000 ppm SO_2. Orsenico et al.[104] suggested that the promoting effect could be explained by an over oxidation of the V-SCR catalyst, however, in this study it is explained by Reaction 3.9 being catalyzed by the V-SCR catalyst, since this reaction thermodynamically should be possible ($\Delta G^o = -35$kJ/mol[118]). Earlier studies[104, 109, 113] have all reported a promoting effect of NO_x measured at atmospheric pressures. However, in these studies, NO_x and air were mixed at room temperature and subsequently heated together which can cause an increased formation of NO_2 since the NO oxidation in air has a negative activation energy ($E_a/R = -530 \pm 400K$[93]) and therefore will

be limited at increased temperature. This also explains why the addition of NO_x at 1 bar in the experiments presented in this paper only gives a small promoting effect because NO is added directly to the hot (300-400℃) feed gas, and hence, only at elevated pressure a substantial amount of NO_2 is expected.

3.5 Conclusion

The following conclusions can be drawn from this study of SO_2 oxidation at pressures up to 4.5 bar across two commercial marine V-SCR catalysts with either 'low' or 'high' vanadium content:

- The oxidation of SO_2 is found to be kinetically limited in the temperature interval relevant for SCR operation (300-425℃).
- The measured conversion of SO_2 into SO_3 across the commercial catalysts is of the order 0.2-3%, with no influence of pressure when the residence time was constant. This shows that the kinetics is independent on the pressure in the investigated range.
- The catalyst with the higher vanadium content was more active for SO_2 oxidation.
- The kinetics of the reaction was fitted, and the reaction orders were found to be close to one for SO_2 and zero for SO_3. For practical purposes, it is therefore proposed that the reaction order is approximated by a first order dependency in SO_2 and a zero order dependency in SO_3 also at pressures up to 4.5 bar.
- The rate of SO_2 oxidation was found independent of water concentrations above 2 vol% at 3 bar, in correspondence with previous findings that the rate is independent of the water concentration above 5 vol% at 1 bar.
- The fitted kinetics are well in line with those found in the literature measured at atmospheric pressure.
- The rate of SO_2 oxidation was clearly promoted by the presence of NO_x at increased pressure, however, at 1 bar the promoting effect was within experimental uncertainty. The promoting effect is explained by a catalyzed redox reaction between SO_2 and NO_2.

Acknowledgement

This work is part of the Danish societal partnership, Blue INNOship and partly funded by Innovation Fund Denmark (IFD) under File No: 155-2014-10 and the Danish Maritime Fund. SRC gratefully acknowledge the funding support and the help received from the team at Topsøe A/S while running the experiments at their facilities.

Conflict of Interest

On behalf of all authors, the corresponding author states that there is no conflict of interest.

4 Ammonium Sulfates

One solution for complying with NO_x regulation 13 of IMO Tier III, is to use an SCR reactor, and one configuration is to install the reactor upstream of the turbocharger to ensure high enough temperature, at which increased pressure of up to 4.5 bar also will be present. From Chapter 2 it has been realized that the known first order reaction dependency of NO for SCR kinetics (at excess NH_3) does not change when the pressure is increased, and that the formation of NO_2 is still limited. At ANR<1 the surface coverage of NH_3 can be described by Langmuir surface coverage or Temkin kinetics. Furthermore, from Chapter 3 it was realized that SO_2 present in the exhaust gas will be oxidized into SO_3 across the SCR catalyst, however, still following a first order reaction dependency for SO_2 at the increased pressure. The sulfur oxidation across the SCR catalyst will typically be below 3% SO_2 conversion[104], however, part of the SO_2 is also oxidized into SO_3 in the combustion chamber, prior to the SCR reactor. The engine out SO_2 oxidation depends on the engine tuning, fuel type etc. and can be as high as 10% of the total SO_x[4]. Ammonia and possibly urea byproducts added to the exhaust gas for operation of the SCR catalyst and SO_3 already present in the exhaust gas or produced across the catalyst can react in the gas phase and create ammonium sulfates. These sulfates can condense and deposits on steel surfaces or within the catalyst increasing maintenance burdens[61, 119, 120]. Therefore, this chapter will elaborate on the formation and deposition of ammonium sulfates both theoretically and experimentally. The bench scale experiments have been carried out at DTU Chemical Engineering and full scale measurement at Alfa Laval's test and training center in Aalborg Denmark. Urea is only used as reactant at Alfa Laval, while in all bench scale experiments pure ammonia is used. Therefore, byproducts produced from insufficient urea decomposition or from urea impurities will not be observed during bench scale experiments.

4.1 Introduction

Since the first ship was installed with an SCR catalyst in 1989 in Japan[69], formation of sulfates within and downstream of the SCR catalyst has caused operational problems, such as deactivation of the catalyst and corrosion of marine boilers and turbochargers due to condensation of sulfates. The formation of sulfates originate from reactions between NH_3, SO_3, and H_2O, producing ammonium bisulfate (ABS) or ammonium sulfate (AS) according to reaction 4.1 and reaction

4.2 respectively[35, 105, 121].

$$\text{ABS:} \quad NH_3 + SO_3 + H_2O \rightleftharpoons NH_4HSO_4 \tag{4.1}$$

$$\text{AS:} \quad 2\,NH_3 + SO_3 + H_2O \rightleftharpoons (NH_4)_2SO_4 \tag{4.2}$$

The formation of either sulfate will result in solid residues when the exhaust gas is cooled below the dew point temperature of the species.

AS is known to be a corrosive white solid powder, which can be removed by the use of soot blowers[121]. AS does not melt, but decomposes into ABS according to reaction 4.3 at temperatures above 230℃ based on Nam et al.[122], above 238℃ based on Kijlstra et al.[61], and Matsuda et al.[106] noted that ABS was the only observed condensed species at temperatures above 240℃.

$$(NH_4)_2SO_4 \rightleftharpoons NH_4HSO_4 + NH_3 \tag{4.3}$$

Based upon a thermodynamic study performed by Burke et al.[105], the principal product from a gas cooled to below 240℃ containing NH_3 (10, 30, 50 or 100 ppm), SO_3 (5, 10, or 50 ppm) and 10% H_2O was at all times AS, therefore, AS is concluded to be the thermodynamically stable product. However, Burke et al.[105] obtained experimental data, in which only ABS was observed and Reaction 4.2 was therefore concluded to be kinetically hindered. Only in experiments with high ammonia to SO_3 ratios (ASR =NH_3/SO_3>2[105, 121]) and at temperatures below 240℃ AS was the observed condensed product.

At typical marine engine SCR conditions urea is added to achieve NH_3/NO_x ratios of typically 0.8 to comply with IMO Tier III. This will typically lead to NH_3 slip of $\leq$ 10 ppm NH_3[28] and SO_3 will typically be present in concentrations above 10 ppm and as high as 60 ppm [4]. Therefore, the observed product will be ABS, due to an almost complete consumption of NH_3. ABS exist both as a solid (T<147℃[61, 121, 122]), and as a melt and is reported to decompose at 350℃[61, 107, 122] or in the range of 350-450℃[105] according to the backwards of Reaction 4.1.

The formation of ABS, is on the contrary to AS a fast reaction, and follows equilibrium calculations[105]. ABS as a liquid is corrosive, hygroscopic, and sticky, which causes problems because particulate matter (PM) or fly ash in the exhaust gas sticks to ABS and increases the pressure drop across boilers and the SCR catalyst, as well as decreasing the heat transfer rate in the boiler. To investigate the pressure build up, Burke et al.[105] performed an experiment in which a slip stream (9000 Nm^3/hr) from a coal fired power plant, containing 10 g/Nm^3 PM, 1-20 ppm SO_3 was withdrawn at a temperature of 290℃. The exhaust gas was mixed with NH_3 to a concentration of 50 ppm and cooled across a Ljungstrom air preheater to 140℃. During a test period of 3240 hours the pressure drop increased from 1.2 kPa to 1.67 kPa, after which an electrostatic precipitator was installed to remove soot upstream of the air preheater. The removal of soot caused the rate of deposition (probably of ABS) to increase, instead of decline, indicating that PM had a cleaning effect. The change in pressure drop increase, due to soot removal was not disclosed. The cleaning effect of PM is probably because PM acted as a condensation nuclei, and

therefore, prevented ABS to stick to the surface of the air preheater as noted by Burke et al.[105].

At Funomachi Works, an SCR pilot was operated to treat an exhaust gas of 6000 Nm^3/hr from an iron-ore sintering furnace. The exhaust gas contained 130-200 ppm NO_x, 100-180 ppm SO_x (10-20 ppm SO_3) and 0.11-0.27 g/Nm^3 of PM. The NH_3 slip after the SCR reactor was not measured but estimated to be around 5 ppm. The exhaust gas was cooled from 280-350℃ to 180-230℃ downstream of the SCR reactor by the use of a Ljungstrom air preheater. The air preheater was operated for 4000 hours, and during the first 1800 hours soot blowing was employed and the gas side pressure drop of the air preheater remained nearly constant at 0.55 kPa. The final 2200 hours was operated without soot blowing during which the pressure drop increased from 0.55 kPa to 0.82 kPa[105].

Similar facilities reported the need for continuous soot blowing and possible water wash of air preheaters every second month to ensure reliable operation[105]. Therefore it is very important to correctly estimate dew point temperatures of ABS depending on specific operating conditions and also to understand the effects of having soot in the exhaust gas. The bulk dew point temperature of ABS is calculated on the basis of a Clausius-Clapeyron Expression. Formation temperatures have also been estimated by minimization of the total Gibbs free energy for a system of reactions, however, in that case it is very important to also take the equilibrium of SO_3, H_2O and sulfuric acid (H_2SO_4) into account (See Reaction 4.4). At typical AS/ABS formation temperatures, most of the SO_3 will be present as H_2SO_4 in the exhaust gas as also shown by the equilibrium given in Figure 4.1, and the formation of ABS and AS will therefore proceed through Reaction 4.5 and 4.6 respectively.

$$SO_3 + H_2O \rightleftharpoons H_2SO_4 \tag{4.4}$$

$$NH_3 + H_2SO_4 \rightleftharpoons NH_4HSO_4 \tag{4.5}$$

$$2\,NH_3 + H_2SO_4 \rightleftharpoons (NH_4)_2SO_4 \tag{4.6}$$

As noted by Burke et al.[105] the calculated condensation temperature of ABS based upon thermodynamics will be too high if the sulfuric acid equilibrium is not included, i.e. if only Reaction 4.1 and Reaction 4.2 is taken into account.

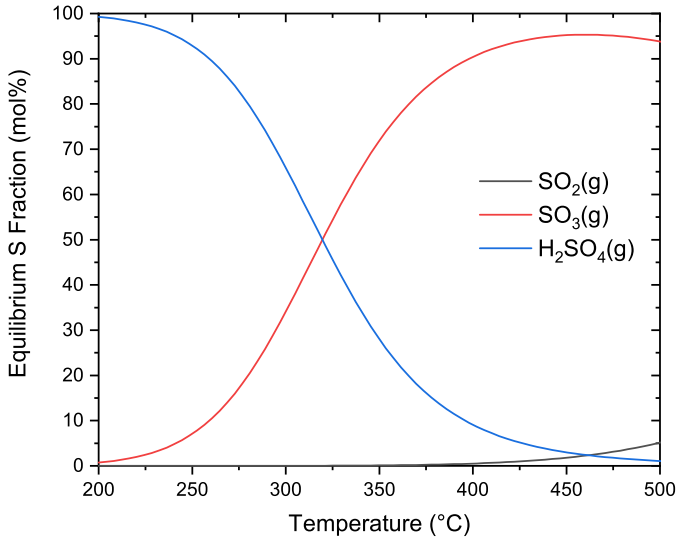

Figure 4.1: Chemical equilibrium between gaseous SO_2, SO_3, and H_2SO_4. Calculated for a flue gas containing an initial amount of 10% H_2O, 10% O_2, 1000 ppm SO_2 in N_2 with the use of HSC Chemistry 9.0®

Matsuda et al.[106], included the formation of sulfuric acid in their analysis, and used that the enthalpy of formation of Reaction 4.5 to form liquid ABS is ΔH^o_{298} =-222 kJ/mol, and used this as a fixed value for the heat of vaporization when determining the preexponential factor of the Clausius-Clapeyron expression, as shown in Equation 4.7. Thøgersen et al.[107] used the bulk dew point expression as presented by Matsuda et al.[106] to calculate dew points of ABS for an SCR catalyst, and found that the proposed equation fitted well. For comparison Thøgersen et al.[107] also reported the bulk dew point equation calculated based upon the data made by Ando et al.[123], as shown in Equation 4.8. Lastly Muzio et al.[1] combined the experiments by Wei et al.[124] and Menasha et al.[125] to achieve a single broad Clausius- equation, as given by Equation 4.9

$$\text{Matsuda et al.} : P_{ABS} = P_{NH3} \cdot P_{SO4} = 1.41 \cdot 10^{12} \cdot \exp\left(\frac{-222\frac{kJ}{mol}}{R \cdot T}\right) \tag{4.7}$$

$$\text{Ando et al.} : P_{ABS} = P_{NH3} \cdot P_{SO4} = 1.17 \cdot 10^{18} \cdot \exp\left(\frac{-257\frac{kJ}{mol}}{R \cdot T}\right) \tag{4.8}$$

$$\text{Muzio et al.} : P_{ABS} = P_{NH3} \cdot P_{SO4} = 2.97 \cdot 10^{13} \cdot \exp\left(\frac{-230\frac{kJ}{mol}}{R \cdot T}\right) \tag{4.9}$$

Here P_{NH3} is the partial pressure of NH_3 given in atm, P_{SO4} is the partial pressure of both SO_3 and H_2SO_4 also in atm., P_{ABS} is the product of P_{NH3} and P_{SO4} and is referred to as the ABS potential, R is the gas constant, and T is the bulk dew point temperature in Kelvin at a given ABS potential. The above bulk dew point equations, can be used to estimate at which temperature ABS will start to condense at a given ABS potential, however, since the three expressions give different dew point temperatures, they should be tested against experimental data to see which

one fits best. The three equations will be compared to each other during the catalyst test in Section 4.5.3.

Beside the bulk dew point temperature, the pore system of a catalyst needs to be taken into account to ensure that the catalyst stays active. The dew point temperature of gases within narrow pores are known to be higher than the dew point temperature in the bulk gas phase due to van der Waals forces. The condensation of a gas within a pore can be described by Thompson's theory of capillary condensation, through the Kelvin equation as given in Equation 4.10.

$$ln\left(\frac{P_{pore}}{P_{bulk}}\right) = -\frac{2 \cdot \sigma \cdot M}{\rho \cdot \gamma \cdot R \cdot T} = \frac{-2.33 \cdot 10^{-4}}{\gamma \cdot T}(cm^{-1}K^{-1}) \tag{4.10}$$

In which P_{pore} is the partial pressure of the ABS potential within the pores, P_{bulk} is the partial pressure of the ABS in the bulk (i.e. Equation 4.7, 4.8, or 4.9), σ is the surface tension of ABS (150 dyn/cm[106]), M is the molar mass of ABS (115 g/mol), ρ is the density of ABS (1.78 g/cm^3[106]), R is the gas constant, and γ is the pore radius which for the last part of Equation 4.10 should be given in units of centimeters, and T is the temperature in Kelvin.

The design specification that can be used from the above equations, is that when the ABS potential at a specific temperature is higher than the calculated bulk pressure ($P_{ABS} = P_{NH3} \cdot P_{SO4} > P_{bulk}$) ABS will condense in the bulk phase, on the surface of boiler or the catalyst, and eventually all catalyst activity will be lost. When the ABS potential is lower than the calculated bulk ABS pressure at a specific temperature, the deactivation of the catalyst depends on the pore size distribution of the single catalyst. At a specific ABS potential all pores with a radius that fulfill ($P(T,\gamma)_{pore} \geq P(T)_{bulk}$) will eventually be filled with ABS and loss of catalyst activity will be observed. Thøgersen et al.[107] stated that loss of catalyst activity (for the specific catalyst used) was typically first observed 28 K above the expected bulk dew point and the loss increased as the dew point was approached.

Therefore, studies on how, and when sulfates are formed and possible solutions to reduce the loss of catalyst activity or the need for boiler/turbocharger wash are important for the success of marine SCR reactors.

4.2 Full Scale Measurements at Alfa Laval Aalborg

This experimental campaign was carried out at Alfa Laval's test and training center in Aalborg, at which they have an SCR reactor installed after a 1.98 MW 4-stroke diesel engine. The main idea was to condense and collect material after the SCR reactor to identify what type of lab scale experiments were needed in order to expand the knowledge base within the use of marine SCR reactors.

4.2.1 Experimental Facility

Alfa Laval's test and training center is comprised of a 1.98 MW 4-stroke marine diesel engine (MAN 9L28/32), followed by heaters that ensure a minimum temperature of 330℃, before a 40wt% aqueous urea solution is sprayed into the exhaust gas upstream of a marine SCR reactor for NO_x reduction. The SCR reactor reduces the NO_x concentration to Tier III compliance, according to 2.39 g NO_x/kWh for 750 rpm[24]. After the SCR reactor, a marine boiler is installed, for waste heat recovery and finally a wet SO_x scrubber for removal of SO_2 and SO_3 is installed. The scrubber reduces the measured SO_2 concentration to below 10 ppm at a CO_2 concentration of 5.5%, which correspond to a fuel sulfur equivalent of 0.04%[126] (see Equation 4.11), i.e. 60% below Tier III SECA compliance (0.1%[127]).

$$\text{Fuel S Eq. } [\%\ \text{w/w}] = \frac{\frac{SO_2[\text{ppm, dry}]}{CO_2[\%, \text{dry}]}}{43.3} \tag{4.11}$$

The setup is shown in Figure 4.2 and more info can be found in the paper by Hansen et al.[24].

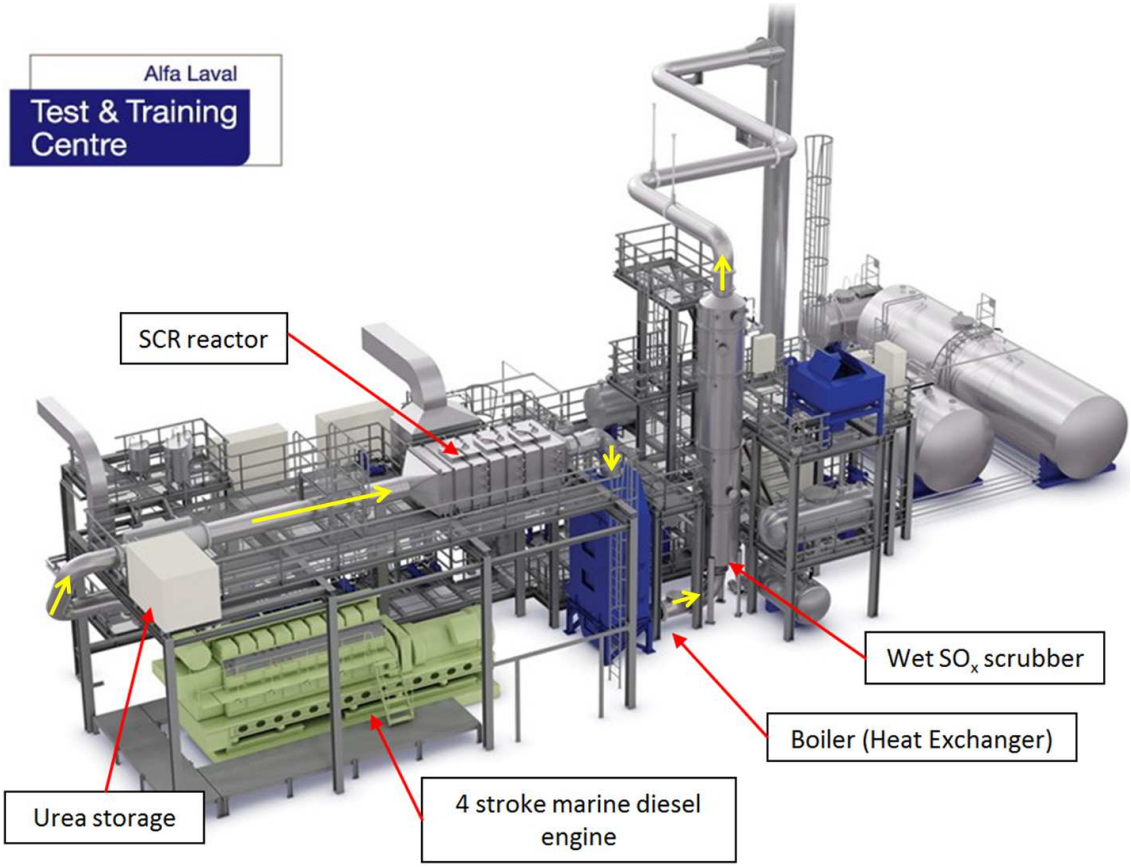

Figure 4.2: Alfa Laval's test and training center in Aalborg, Denmark. The setup consists of a 1.98 MW 4-stroke diesel engine (MAN 9L28/32), an SCR reactor, a boiler unit, and a wet SO_x scrubber. The exhaust gas direction is indicated by yellow arrows. Adapted from Hansen et al.[24].

The engine is capable of using both heavy fuel oil (HFO) ($\sim$ 2.4wt% sulfur) and marine diesel oil (MDO) ($\sim$ 0.1wt% sulfur), however, MDO is at all times use

for starting and stopping the facility to clean the fuel line for HFO. Furthermore, the engine is connected to the public electrical grid and is therefore operated as a generator with a fixed rotation speed of 750 rpm to deliver power with a frequency of 50 Hz. Typical exhaust gas emissions out of the engine are 14% O_2, 10% H_2O, 5% CO_2, 450 ppm NO_x, 500 ppm SO_2 and approximately 30 ppm SO_3[24].

Collection of condensed materials were previously performed by withdrawal of deposits from the surface of the boiler tubes after close down of the engine. In order to withdraw material during operation, a water cooled condensation probe was designed. The probe has an outer diameter of 1 inch and a length of 1.77 meters, corresponding to the width of the SCR reactor. The probe was designed as a tube in a tube as shown in Figure 4.3. The probe was connected to a cooling bath (HETO CBN 8-30) combined with a thermostat (HETO HMT 200), which enabled the possibility to heat the probe above the dew point of water in the exhaust gas (approximately 10 vol% H_2O and hence a T_{dew} ~44℃) and below the boiling point of the cooling water i.e. 100℃. During the experiment, the cooling capacity of the cooling bath was found insufficient. Therefore, to keep the temperature below 100℃, hot water was withdrawn, and cold water added once every hour, resulting in a cooling bath temperature of 50-90℃, and a temperature gradient between inlet and outlet water from the probe at a constant value of 6℃.

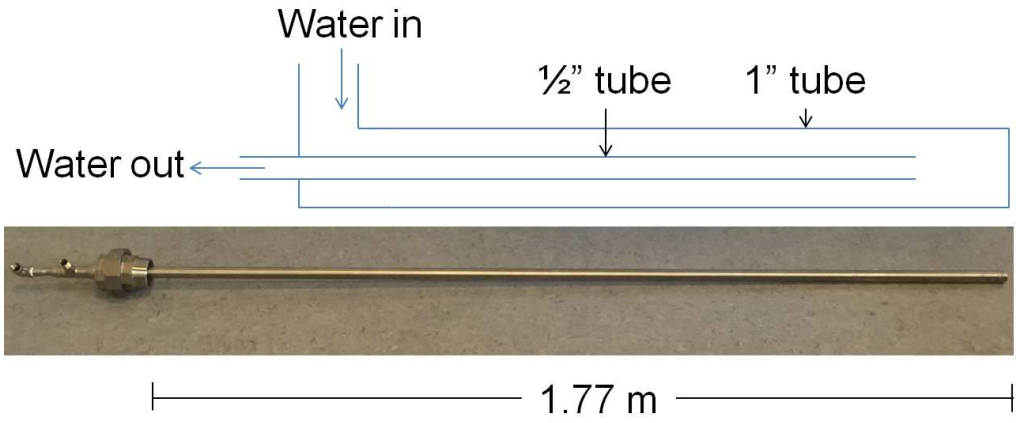

Figure 4.3: Dimensions of the water cooled condensation probe, and a picture of the actual probe.

4.2.2 Method

Collection of condensed materials were done by installing the water cooled condensation probe just after the SCR reactor. After a minimum of 1 hour, the probe was withdrawn, and condensed material was scraped off into a container. The container was stored in a desiccator for a couple of days before the samples were analyzed for ammonium, sulfate and soot content at Haldor Topsøe A/S.

The ammonium concentration was analyzed by utilizing that ammonium, hypochlorit ions, and salicyl ions react at pH>12.6 and form the colored product indophenol

blue. The concentration of indophenol blue was measured with a DR2800 HACH spectrometer.
The sulfate concentration was analyzed using an ion chromatograph (DIONEX DX-120 or DIONEX DX-100), with an IonPac AS4A or AS4A-SC column and a mobile phase of aqueous sodium carbonate and sodium hydrogen carbonate to separate and determine the concentration of sulfate ions.
FTIR measurements were also tried, in which 1 mg of sample and 100 mg KBr was pressed into a self-supporting pellet and an IR spectrum was measured using a Bio-Rad FTS575c spectrometer (ATR-FTIR). However, the quantification of AS and ABS was complicated due to the presence of soot, darkening the sample yielding a lower transmission. ATR-FTIR was therefore not used for samples containing high amounts of soot.

To test if soot also affect the determination of sulfate and ammonium, three samples were mixed in the lab using pure AS, pure ABS and printex U as a soot substitute. The three samples were analyzed by Haldor Topsøe A/S and as shown in Table 4.1 the measured and expected amount falls well in line.

Table 4.1: Testing of the determination of ammonium and sulfate concentration of pure samples also when mixed with printex U.

NH_4^+	SO_4^{2-}	sum	$\frac{n(NH_4^+)}{n(SO_4^{2-})}$	Expected	Deviation
wt%	wt%	wt%		$n(NH_4^+)/n(SO4)$	%
21.40	75.40	96.80	1.51	1.46	3.18
20.00	77.00	97.00	1.38	1.37	1.00
14.40	55.40	69.80	1.38	1.43	-2.88

4.2.3 Results

The first condensation test was done by inserting the probe after the SCR reactor, before starting the engine and keeping the probe within the exhaust gas until after the engine was closed down again. The engine was operated for 6 hours, out of which 5 hours and 20 min was operated on HFO. During the 6 hours experiment, different engine loads were tested. After the 6 hours experiment, the pilot plant was cooled for 1 hour before the condensation probe was withdrawn and condensed material scrapped of. The condensed material was collected as one sample for every approximately 20 cm of the probe, to test whether the condensed material in one side of the reactor was different to the other. Table 4.2 shows that no difference was observed across the probe and furthermore that the condensed material had an ammonia to sulfate ratio close to 1 (mean of 1.03), which indicate almost pure ABS and soot.

Table 4.2: Analysis of condensed materials after the SCR reactor at Alfa Laval's test and training center. The condensed materials were condensed on the surface of a steel water cooled probe and analyzed at Haldor Topsøe A/S. Sample 1.2 and 1.6, were used for unsuccessful ATR-FTIR analysis.

#	NH_4^+	SO_4^{2-}	sum	$\frac{n(NH_4^+)}{n(SO_4^{2-})}$
	wt%	wt%	wt%	
1.1	9.30	48.30	57.60	1.03
1.3	9.80	49.90	59.70	1.05
1.4	10.60	51.70	62.30	1.09
1.5	10.10	50.10	60.20	1.07
1.7	8.80	51.30	60.10	0.91

The second experiment, was also performed while the engine was operated on HFO, however, this time at a constant load of 1.2 MW for 150 hours. Therefore the probe was inserted and withdrawn while the engine was running. Because the previous test showed that no difference was observed across the probe sampling area, this time the full length of the probe was collected as a single sample. The condensed material was analyzed at Haldor Topsøe A/S and the results are shown in Table 4.3.

Table 4.3: The collected samples on the condensation probe after the SCR reactor at Alfa Laval's test and training center. Analysis of ammonium, sulfate and carbon are measured by Haldor Topsøe A/S.

Sample	Day	Mass	Total Time	NH_4^+	SO_4^{2-}	Carbon	$\frac{n(NH_4^+)}{n(SO_4^{2-})}$
#	-	mg	min	wt%	wt%	wt%	
2.1	Day 1	952	160	4.6	46.5	24.9	1.90
2.2	Day 1	665	160	4.7	48.8	21.0	1.95
2.3	Day 2	382	60	4.0	45.4	22.9	2.13
2.4	Day 2	304	65	4.3	47.5	21.5	2.07
2.5	Day 2	747	105	4.5	45.7	24.2	1.91

Table 4.3 shows that all the condensed material collected and withdrawn while the engine was running was mainly AS and not ABS. AS should only be produced at NH_3/SO_4 ratios larger than 2 which was not expected after the SCR reactor[105, 121]. At the end of the 150 hours experiment, three deposits were also scrapped of from the boiler after cool down and sent for analysis as shown in Table 4.4.

Table 4.4: Three condensed samples from the boiler at Alfa Laval Aalborg. The collection of samples were done after 150 hours of experiment, with the engine running on HFO (2.4 wt% sulfur) at a constant load on 1.2 MW.

Sample #	NH_4^+ wt%	SO_4^+ wt%	Carbon wt%	Molar (NH_4^+/SO_4^+) -
AL1	9.8	55.8	19.8	0.94
AL2	11.6	62.6	18.3	0.99
AL3	10.8	59.5	17.9	0.97

Table 4.4 shows that the condensed material is ABS in approximately 18.7 wt% soot. ABS and soot accounts for ∼90 wt% of the collected phase, the last 10 wt% are a mixture of moisture and trace metals based on ICP analysis such as chromium and titanium, probably originating from the fuel oil or lubrication oil. Interestingly both results observed after close down of the engine indicate ABS as the primary sulfate specie, however, the measurement performed during operation indicate AS. The difference could be because AS decomposes into ABS when the setup is shut down, and no NH_3 is present in the exhaust gas. The exhaust gas, which is controlled above 330℃ is above the decomposition temperature of AS (240℃), therefore, further studies on when AS or ABS is produced should be performed, as performed in section 4.3.

Beside the different trends on the formation of AS and ABS, it was observed that all materials collected, both on the condensation probe and on the surface of the boiler was quite easy to remove, as loose dust, and not the sticky ABS as expected from the literature[70, 121]. One explanation could be that the high soot fraction (∼ 20 wt%) acts as a sponge and therefore, prevent the presence of sticky ABS on the surface of the soot particles and hence also on the surface of the probe/boiler. This is further investigated in section 4.4.

Lastly, it was noted that the marine SCR catalyst installed at the facility was at all time heated to temperatures above 330℃ before urea was added which prevented the deactivation of the catalyst due to ABS condensation. The high temperatures cannot be reduced due to local legislation, preventing such a large engine to be used without satisfactory removal of NO_x. Therefore, another smaller facility should be established at which the temperature can be lowered, and the deactivation of the SCR catalyst could be studied as a function of temperature and partial pressures of NH_3 and H_2SO_4 as shown in section 4.5.

4.2.4 Conclusion

Full-scale measurements at Alfa Laval's test and training facility have been performed, on the formation of condensible materials after an SCR reactor installed on a 1.98 MW marine diesel engine operated at HFO (2.4 wt% sulfur). The condensible materials have been collected by the use of a water cooled steel probe, installed after the SCR reactor. Collected materials have been analyzed for ammonium, sulfate and soot content at Haldor Topsøe A/S.

It was observed that condensed material collected after the setup was shut down indicated the presence of ABS, however, the test at which the probe was withdrawn during engine experiment showed that the condensible material was AS. Whether this difference was due to decomposition of AS into ABS during close down or if it was due to change in the gaseous content of NH_3 and H_2SO_4 should be further investigated at well controlled conditions in a smaller scale. Furthermore, it was observed that all materials collected were quite easy to remove from the probe or boiler surfaces also when ABS was the collected material. It is therefore hypothesized that soot can act as a sponge and prevent the presence of the sticky ABS on the surface of the soot particles. If this is the case, this is of high industrial relevance, because the amount of soot present, can then be an important design variable.

4.3 Formation of AS and ABS

At the full-scale facility at Alfa Laval's test and training center, the formation of ABS and AS were found to change based upon whether the measurement was performed after or before close down of the engine. Therefore, it was decided to use a setup at which the formation of AS and ABS on the surface of cooled metal surface could be studied as a function of partial pressures of NH_3 and H_2SO_4. The experiments were performed at DTU Chemical Engineering.

4.3.1 Experimental Facility

The formation of AS and ABS were studied in a bench-scale setup as shown in Figure 4.4. The setup consists of a natural gas burner consuming 62 L natural gas/min (∼37 kW), a water cooled injection probe, a heat exchanger for controlling the temperature in the reactor and a steel cabinet reactor for full-length monoliths (50 cm). For simplicity, the reactor was left empty for the AS/ABS experiments, and instead, an aqueous solution of 0.15 M sulfuric acid was sprayed into the setup to achieve H_2SO_4 concentrations of approximately 45 ppm, similar to those expected after a marine diesel engine operated on HFO . The ammonia to sulfuric acid ratio was varied between 0.5 and 4.5 by changing the feed of NH_3.

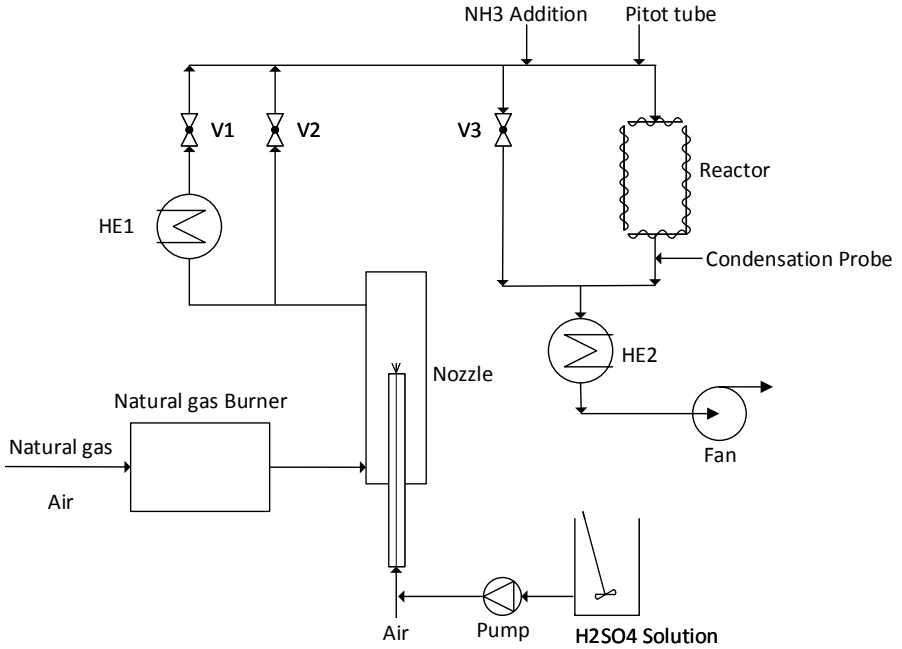

Figure 4.4: The setup used to measure the formation of AS and ABS as a function of partial pressures of NH_3 and H_2SO_4.

A small-scale replication of the condensation probe used at Alfa Laval's test facility was produced with a length of 20 cm and an outer diameter of 1 inch. The condensation probe was connected to an oil bath (Julabo FP40 + Julabo HE V2), with a maximum operating temperature of 200℃.

The flue gas H_2SO_4 concentration was measured using controlled condensation of SO_2/SO_3 and subsequent titration with $BaCl_2O_8$ and thorin as indicator as described by Nielsen et al.[112]. The sampling of flue gas H_2SO_4 was performed at selected times at the pitot tube's placement (see Figure 4.4). After the H_2SO_4 concentration was determined, NH_3 was added to achieve ammonia to sulfuric acid ratio's (ASR) of 0.5-4. The NH_3 concentration was continuously measured using an MKS multigas 2030 FTIR. The condensible materials were collected using an oil bath temperature of 80-170℃. 80℃ is similar to the experiments performed at Alfa Laval, and 170℃ is the expected surface temperature of a marine boiler using a water pressure of 7-8 bar. At Alfa Laval a temperature gradient of 6℃ was observed between inlet and outlet water from the probe. The probe used here is 10 times shorter and the fluid flow is similar, therefore, the gradient is assumed negligible.

4.3.2 Method

The 0.15 M aqueous solution of sulfuric acid was sprayed into the gas after the burner at temperatures of approximately 800℃. By closing valve V1 and opening V2 the heat exchanger, HE1, was bypassed to minimize the loss of H_2SO_4, which resulted in temperatures after the empty reactor at around 300-340℃, similar to the operation conditions of a marine SCR catalyst. The total flow rate through the reactor can be controlled by opening/closing valve V3, and was controlled to approximately 42 Nm^3/h. The temperature of the probe was controlled at 80℃, 110℃, 140℃, 155℃ and 170℃, by the use of the oil bath.

The materials collected on the probe were scraped off, and due to the lack of soot in the system, the collected materials were white powders such as that shown in Figure 4.5, which could be analyzed at DTU using attenuated total reflection (ATR) FTIR and compared with the ATR-FTIR spectra of pure AS and ABS. From the ATR-FTIR spectra, only qualitative information about the formed sulfates was obtained, therefore, in the cases where both sulfates were formed, it is considered a mixture of the two.

Figure 4.5: A picture of the condensed material on the surface of the oil cooled steel tube using an oil temperature of 170℃ and an ASR = 2.5. Approximately 41 mg of condensed materials were collected and later analyzed to be AS.

4.3.3 Results

The probe was typically inserted into the setup for 30 min to 1 hour to collect between 30-100 mg of sulfates. The ATR-FTIR spectra was measured, and as shown in Figure 4.6 the difference between AS and ABS could be observed.

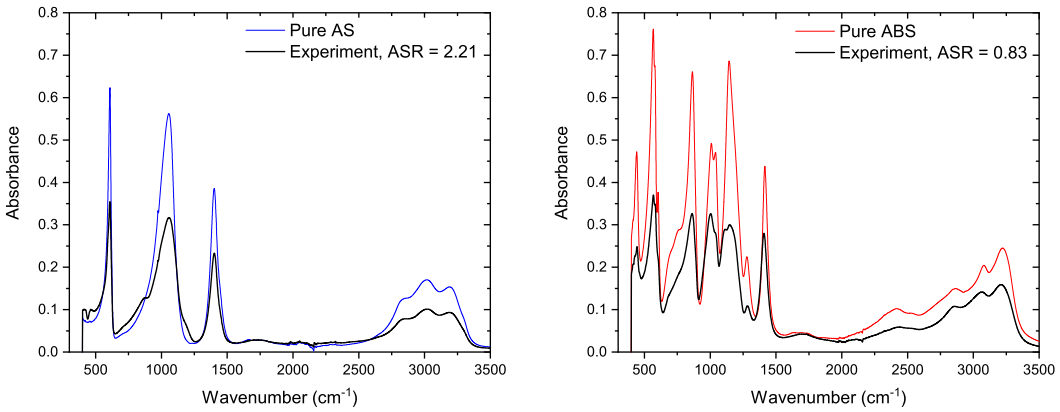

(a) ASR = 2.21 (b) ASR = 0.83

Figure 4.6: ATR-FTIR spectra of pure AS and pure ABS and compared to two different experiment in which the pure substance and the collected specie is considered identical. The probe temperature was in both cases 170℃, however, the ASR was different.

In a similar fashion, experiments were conducted using different ASR by changing the NH_3 concentration, when approximately 45 ppm of H_2SO_4 was added. Different probe temperatures were also used as shown by the combined results in Figure 4.7

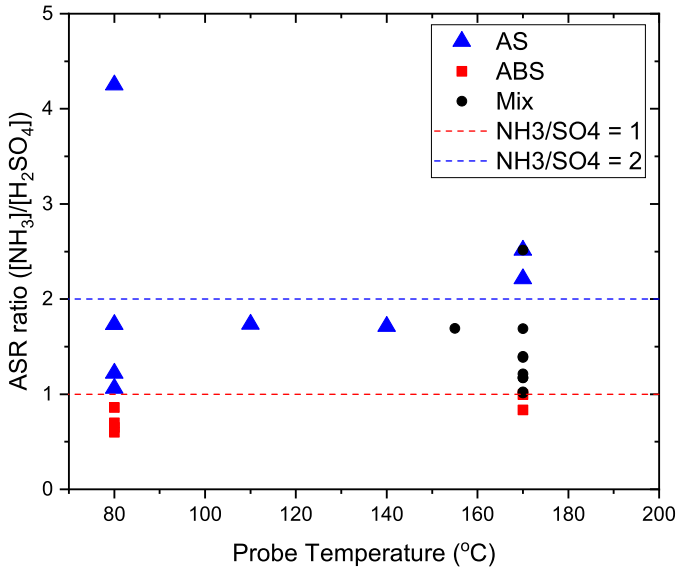

Figure 4.7: The results from ATR-FTIR of condensible materials at different ammonia to sulfate ratios (ASR) and surface temperatures on the condensation probe.

Figure 4.7 shows that at temperatures below 140℃ AS is the measured product, when the ASR is above 1, although a mixture would be expected. When increasing

the probe temperature above 155℃ a mixture of ABS and AS is observed, as long as the ASR is between 1 and 2. This could be due to sulfuric acid condensation, which has a dew point temperature of 155℃ at the operation conditions based upon the dew point temperature equation given by Verhoff et al.[128]. Another factor is that above 147℃, the produced ABS will be a melt and not a solid which also could affect the further reaction to AS. Perhaps the formation of AS from liquid sulfuric acid is not kinetically limited. Independent on the reason for this tendency, the experiment show the importance of having the correct probe temperature if the sulfate formation on the surface of a marine boiler is of interest.

A single measurement at 170℃ showed the presence of ABS in the FTIR spectra even though the expected product was AS, at the applied ASR of 2.4. Since calibration was not performed only qualitative information is received from the FTIR, so the amount of ABS could be small, but is unknown.

To ensure that the observed change from AS to a mixture between AS and ABS as a function of temperature, was not due to the decomposition of AS into ABS an in-situ ATR-FTIR measurement was performed at Haldor Topsøe A/S. Pure AS was put on top of the ATR crystal and spectra were continuously measured while the sample was heated from 40℃ to 300℃. In Figure 4.8, the temperature is measured a couple of mm from the sample, and hence shows a lower temperature, but the actual temperature has been calibrated to be 300℃±15℃ at the end of the temperature ramp. A multicomponent analysis program (PEAXACT) was used to calculate the eigenspectra which coincided with AS initially and after a prolonged period at 300℃ (> 150 min.) coincided with ABS. The calculation was obtained by normalizing the concentration to 1, which means that the intensity increase during the temperature ramp, due to better contact with the crystal and removal of physiosorbed water, and the intensity loss due to loss of sample is ignored, the result is shown in Figure 4.8.

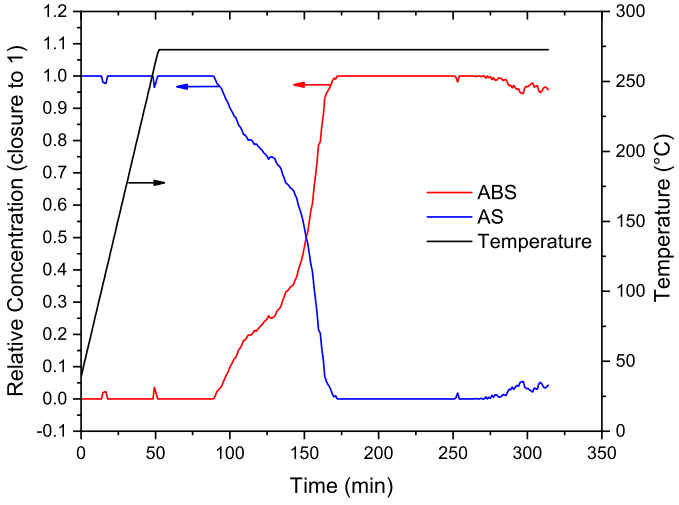

Figure 4.8: In-situ ATR-FTIR measurements of the heating and decomposition of AS into ABS. The measurement was performed by Haldor Topsøe A/S, and the temperature shown is measured a couple of mm. from the crystal, hence the final actual temperature has been calibrated to 300℃±15℃.

Figure 4.8 shows that more than 50 min. at 300℃ is needed before AS starts to decompose into ABS. Part of the delay is probably due to desorption of physiosorbed water, however, the delay seems long to only be the desorption of water.

In the experiments carried out at DTU, in which the probe was only within the exhaust gas for less than an hour and where very thin layers were observed the decomposition of AS into ABS is considered insignificant. The thickness of the layer is of importance to estimate whether the temperature of the surface resembles the cooling probe or the exhaust gas temperature. The decomposition is quite slow taking into account the high temperature compared to the reported decomposition temperature of approximately 240℃[105, 106], which indicate that the decomposition reaction is kinetically hindered.

4.3.4 Conclusion

The formation of AS and ABS have been studied in an exhaust gas containing sulfuric acid and ammonia to simulate marine exhaust gas equipped with an SCR reactor. A steel probe has been constructed and connected to an oil bath to control the surface temperature to between 80-170℃. The condensed materials were analyzed using ATR-FTIR and compared to the pure spectra of AS and ABS.

It was found that the surface temperature of the probe is quite important. At temperatures below 140℃ the collected product was AS even at ASR below 2. The observed temperature dependency of the probe, is expected to be connected with the dew point temperature of sulfuric acid. This could be because the liquid-gas reaction between H_2SO_4 and NH_3 is not kinetically limited, and therefore, produces the thermodynamically most stable product which is AS.

In-situ ATR-FTIR measurements were also performed on the decomposition of AS into ABS at temperatures up to 300℃. The decomposition of AS into ABS was first observed after 50 min. at 300℃ indicating a kinetically hindered reaction of AS into ABS.

4.4 ABS and Soot - A study on Soot Blowing Efficiency

At Alfa Laval's test and training center, the formation of ABS after installation of an SCR reactor was observed, however, the condensed phase observed at the boiler tubes downstream of the SCR reactor was not sticky but instead quite easy to scrape off. It was considered if this could be explained by the presence of soot which acted as a sponge, preventing ABS to become a sticky deposit. Therefore, it was decided to study how easily different mixtures of soot and ABS could be removed from a steel surface by soot blowing using air. The idea was to investigate if soot blowing could be an alternative solution to clean marine boilers compared to the expensive close down followed by water wash. The experiments presented in Section 4.4 were conducted at DTU by senior scientist Brian B. Hansen.

4.4.1 Experimental

A lab scale air blower system was built, to measure the stickiness of different ABS-soot mixtures, as shown in Figure 4.9.

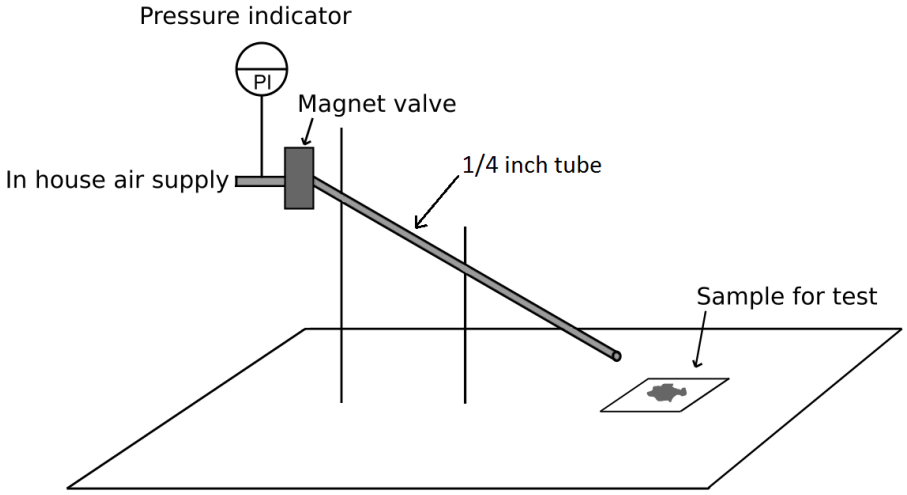

Figure 4.9: The setup used to test the stickiness of soot/ABS mixtures, by soot blowing and measurement of weight loss.

A metal plate of approximately 5 cm x 3 cm was positioned in front of the end of a 1/4 inch tube as shown in Figure 4.9. The tube can be tilted in different angles and the distance to the sample can be changed, as well as the pressure of the air. In the experiments presented here an angle of 45^o from horizontal was used, a distance of 7 cm and a max air pressure of 6 bar. The air pressure was chosen based upon typical available air/steam pressures at ships, and the distance was based upon characteristics known from soot blowers used at power plants[129]. Two types of soot were used, a commercial carbon black product (Printex U) which is more or less pure carbon and an engine soot collected after a diesel generator, which is comprised of ~40 wt% soot, ~55-60 wt% organic content, and a small fraction of ash ($\leq$ 5%). The diesel generator is part of the diesel test setup further discussed in

Section 4.5. An important physical parameter is the porosity of the soot used here, compared to each other and compared to that emitted from marine diesel engines. Further studies should include a determination of the porosity and how it changes depending on the source.

The first mixture of ABS and soot was prepared by mixing and subsequently heating the mixture, however, this resulted in a visible unequal mixing. Therefore, the samples were instead mixed by weighting the desired ABS and soot separately and mixing them with a couple of droplets containing approximately 50/50 water and ethanol solution. ABS is solubility in water and soot is miscible in ethanol, so the mixture of the two made it possible to mix the two substances. The droplets were subsequently dried on a steel surface in an oven at 80℃. The dried sample was stored in a desiccator during the night and the next day installed in the setup, at which the sample was exposed to pressurized air for 200 ms at a pressure of 2 bar, 4 bar and finally 6 bar. Between each blow off test, the loss of material was measured by weighing the plate.

4.4.2 Results

Mixtures from pure soot and down to approximately 20 wt% of soot were prepared. Below 20 wt% of soot the mixture was too sticky, and the sample could not be removed by soot blowing (up to 6 bar). The accumulated loss as a function of initial soot fraction is shown in 4.10.

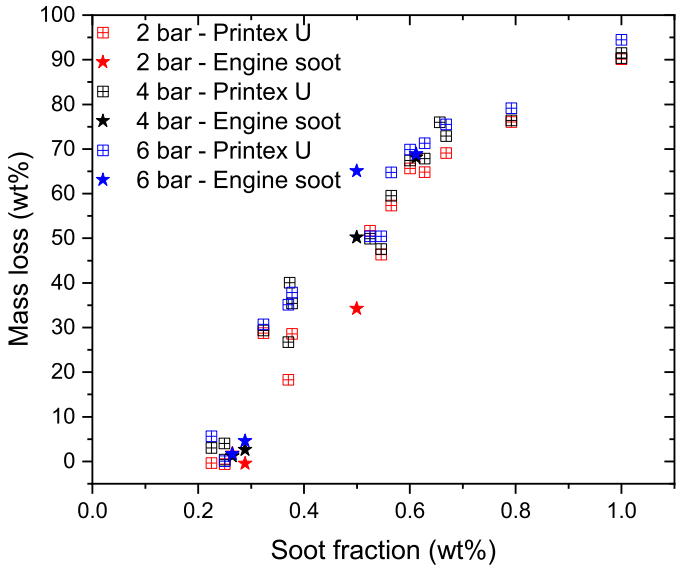

Figure 4.10: Mass loss of different mixtures of ABS and Printex U or engine soot after being exposed to soot blowing for 200 ms using an air pressure of 2, 4 and 6 bar. The engine soot is collected after the diesel engine described in section 4.5 and contains approximately 40 wt% soot.

Figure 4.10 shows that the use of Printex U as a carbon source or soot produced by the diesel generator setup discussed in section 4.5 gives similar results, even though the engine soot also contain condensed volatile organic content.

Figure 4.10 shows that a mixture of 20-30 wt% soot in ABS only loses below 10 wt% even when using 6 bar air pressure for soot blowing. This is unexpected because the soot collected at Alfa Laval's facility in Aalborg only had a soot fraction of 18 wt% and they were quite easily removed. The difference could be because the samples tested here were physically mixed together at cold conditions, however, at Alfa Laval they are produced together within the hot exhaust gas. Another possibility is that the force used to remove the soot by hand from the boiler is underestimated compared to the force from a 6 bar air blow. Or the physical properties, such as porosity, is simply too different causing a deviation between the two results. In order to test if the mixing of soot and ABS does simulate that made from gaseous condensation a condensation plate has been made which can be positioned in the diesel generator setup, however, experiments have not yet been carried out.

From Figure 4.10 it is observed that the mass loss is close to linear with the fraction of soot. To ensure that the mass loss is not only pure soot the amount of soot and ABS were measured by the use of a two stage thermogravimetric experiment. A 1.5 mg sample, which had already been exposed to soot blowing, was first heated in nitrogen to 325℃ (10 ℃/min) followed by a 3 hours isotherm. Secondly the sample was heated in 10% O_2 in nitrogen to 780℃ (10℃/min). The mass loss from 100℃-500℃ was assumed to be a loss of ABS and soot from 500-780℃. This resulted in an ABS fraction of 75 wt% and 25 wt% soot compared to the original content of 71 wt% ABS and 29 wt% soot. A couple of additional tests were performed with similar results. Therefore, the mass loss is expected to be the mixture prepared, and therefore it is concluded that the presence of soot can make it easier to remove condensed ABS, however, the amount of soot needs to be above about 20 wt%. This also explains why Burke et al.[105] reported that installing an ESP before the SCR reactor increased the pressure drop substantially, compared to before.

4.4.3 Conclusion

A lab-scale soot blower system has been constructed, in order to test if the addition of soot to ABS could prevent the formation of a sticky compound.

It was found that when the soot content is less than 20 wt% it could not be removed by an air jet of 6 bar. As the soot fraction increases, the mixture becomes easier to remove by soot blowing, and therefore, a positive effect of adding soot is observed.

The experiments performed here, could not explain why the condensible material observed at Alfa Laval's test facility was so easy to remove, since the collected material only contained ∼19 wt% soot.

4.5 SCR and ABS Deactivation - A Bench-Scale Investigation

The following section describes the experimental work that has been performed to understand how an V-SCR monolith is deactivated by the formation of sulfates due to the presence of SO_3, NH_3, and H_2O. The effects of having soot within the exhaust gas, should also have been studied, however, due to engine malfunction was not performed. The SCR catalyst at Alfa Laval's test and training center is due to legislation, always kept at a high temperature (> 330℃) at which deactivation is not an issue, therefore another experimental facility has been chosen at DTU Chemical Engineering for these investigations.

4.5.1 Experimental

The setup used to study the deactivation of 1 wt% V-SCR catalysts by sulfates is shown in Figure 4.11. Exhaust gas can either be created by using a 5.5 kW diesel generator (DG5500SE-3, from powergenerator.dk) and subsequently diluted with air, and additional SO_2, SO_3, H_2O, NO and NH_3 can be added. Or, a synthetic exhaust gas without particulate matter can be created by using the dilution air as main flow and subsequently add SO_2, SO_3, H_2O, NO and NH_3. Dilution air, NO, NH_3, and SO_2 were all added as pure gases by the use of Bronkhorst High-Tech Mass Flow Controllers. Water was added as steam, by the use of a steam generator (Veit 2365 steam generator), and controlled through a manual needle valve. SO_3 was added by oxidizing SO_2 across a platinum catalyst at 250℃. The formation of SO_3 is measured by the disappearance of SO_2, compared to inlet conditions.

It should be noted that no experiments were carried out in this project using the generator due to malfunctions with the generator in the final stage of this project.

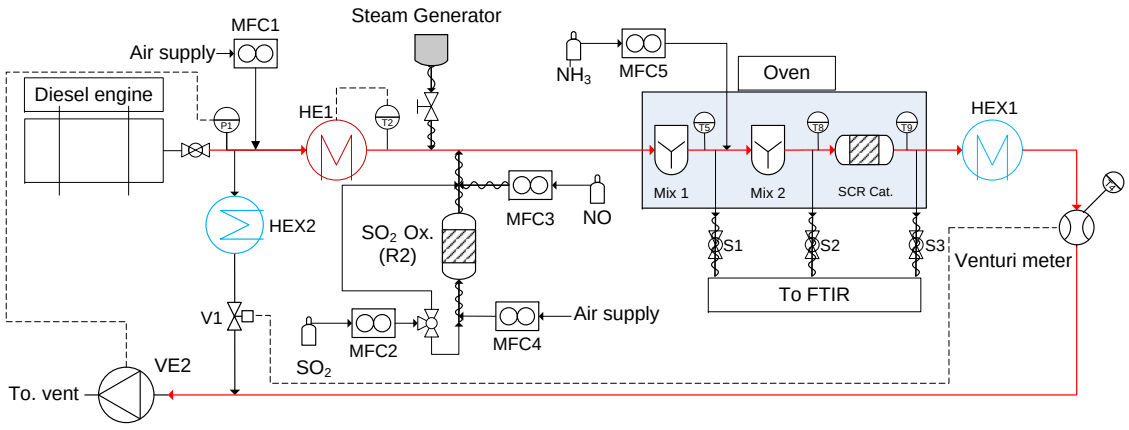

Figure 4.11: Schematic representation of the setup used to study ABS deactivation of marine SCR catalysts. The main flow way, through the catalyst, is marked with red.

Air was added through MFC1, and heated by an electrical heater before NO, SO_2, SO_3, and water were added to the gas. The gas was passed through a static mixer,

after which NH_3 was also added to the gas, which was further mixed across a second static mixer before the exhaust gas reached the SCR catalyst. The SCR catalyst used in the test discussed here, was supplied by Umicore Denmark ApS, as a cylindrical monolith with a diameter of 5 cm and a length of 7.5 cm with an approximate V_2O_5 content of 1 wt%. Both the mixers and the catalyst were placed inside a horizontal oven from Entech, with 6 heating zones, to ensure isothermal conditions. After the oven the exhaust gas was cooled to approximately 30℃ and passed through a venturi meter before reaching the pump (VE2) which ensured that the setup was operated at 5-10 mbar below atmospheric pressure as a safety precaution.

Gas concentrations were measured by a multigas 2030 FTIR analyzer from MKS. Sample point 1 (S1) was used to measure SO_2 oxidation, without any NH_3 in the gas phase, to ensure that sulfates were not produced inside the analyzer. NO_x reduction was measured across the catalyst, by stopping SO_x addition, and measure NO_x before (S2) and after (S3) the catalyst in the center of the tube to calculate the NO_x conversion (X_{NOx}) according to equation 4.12.

$$X_{\mathrm{NOx}} = \frac{\mathrm{NOx}_{in} - \mathrm{NOx}_{out}}{\mathrm{NOx}_{in}} \cdot 100\% \tag{4.12}$$

4.5.2 Clean SCR Profile

The loaded catalyst was initially degreened at 413℃ in dry air for 15 hours. Thereafter, a NO_x conversion profile was measured using a total flow of 110 Nl/min, 5% H_2O, 620 ppm NO, 740 ppm NH_3 in air. The NO_x conversion is shown in Figure 4.12(a), and in Figure 4.12(b) an Arrhenius plot is shown. Figure 4.12(b) was made, by fitting of the intrinsic NO rate constant (K_{SCR}) using the single channel monolith model developed earlier in our group by Olsen[98], the model was further described earlier, in section 2.3.3. This model was used in order to take internal as well as external mass transfer limitations into account, which typically limits the SCR reaction at temperatures above 250℃[130]. The fitted rate constant (1/s) was transformed into an external surface rate constant (m/h) by the use of the specific surface area of the catalyst ($A_{sp} = 885 m^2/m^3$).

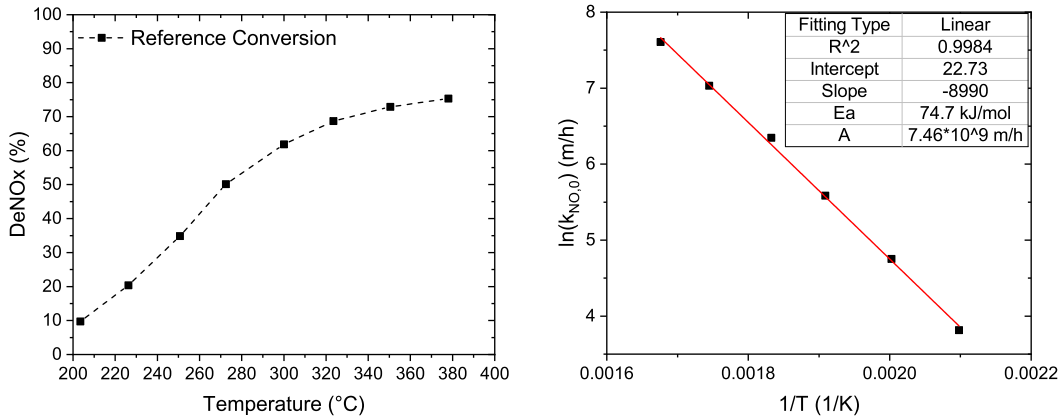

(a) DeNOx profile before deactivation.

(b) Arrhenius plot

Figure 4.12: The DeNOx profile (a) measured before deactivation experiments, using a flow of 110 Nl/min, 5% H_2O, 620 ppm NO, 740 ppm NH_3 in air. The Arrhenius plot (b) of the clean DeNOx profile is also shown, in which the rate was fitted using the monolith model developed by Olsen[98]. The Arrhenius plot is only made for the temperature interval used during deactivation i.e. 200-315℃.

In Figure 4.12(b) the activation energy and preexponential factor is also shown, which will be used to calculate the intrinsic reference rate constant ($k_{NO,0}$) at specific temperatures, and used as a reference during the deactivation experiments. The Arrhenius plot given in Figure 4.12(b) is made for the temperature interval used for deactivation (T=200-315℃).

4.5.3 Test of ABS Bulk Dew Point

The first experiment was done to test how fast the catalyst is deactivated by ABS and to test the three different expressions found for bulk ABS condensation, as already shown in Equation 4.7, 4.8, and 4.9. The experiment was conducted with 478 ppm NH_3, 84 ppm SO_3/H_2SO_4, 5 vol% of H_2O, in air with a total flow rate of 110 Nl/min, and at a temperature of 304℃. The concentration of NH_3 and SO_3, correspond to an ABS potential of 40152 ppm^2, and at a temperature of 304℃ this correspond to just above the bulk dew point of ABS as predicted by Muzio et al.[1] as also shown in Figure 4.13.

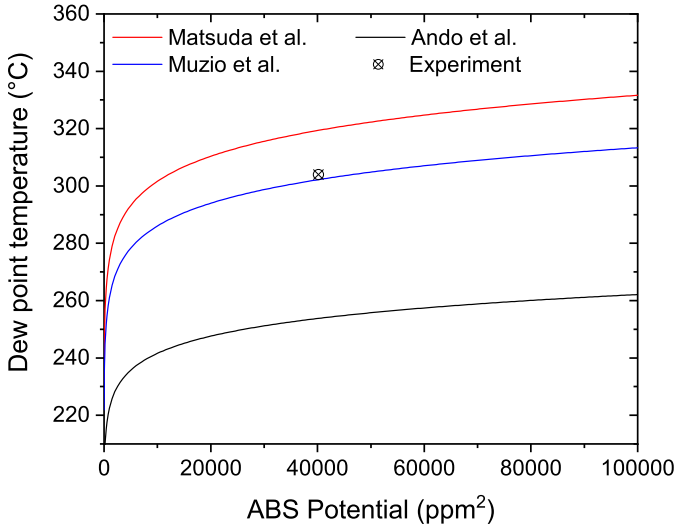

Figure 4.13: The bulk dew point of ABS as a function of the ABS potential. Bulk dew points are calculated based upon Matsadu et al.[106], Muzio et al.[1] and the data by Ando et al.[123], as presented by Thøgersen et al.[107]. The ABS potential of the experiment conducted with 478 ppm NH_3, 84 ppm SO_3/H_2SO_4, 5 vol% of H_2O, in a total flow of 110 Nl/min, and at a temperature of 304℃ is also shown.

In case the bulk dew point of Matsuda et al.[106] is correct, a temperature of 304℃ is below the bulk dew point of ABS, and hence the catalyst and the reactor tubes would become white due to ABS condensation. On the other hand in case the expression derived from the data presented by Ando et al.[123] is correct only a small part of the catalyst is expected to be deactivated since only pores with a radius smaller than 8 Å would be filled with ABS, as calculated by Equation 4.8 and Equation 4.10.

The NO_x conversion was measured without SO_x present, using a total flow of 110 Nl/min, 5% H_2O, 600 ppm NO_x and 740 ppm NH_3. The measurement was done by stopping addition of SO_2 and after 3 minutes an FTIR measurement was started before the SCR catalyst (S2). If SO_2 was flushed from the setup i.e. no SO_2 measured on the FTIR, NO_x was added, and NH_3 was increased to ANR = 1.2, and a steady state measurement was done before (S2) and after the catalyst (S3), from which the NO_x conversion could be calculated. The decrease in DeNOx conversion as a function of deactivation time is shown in Figure 4.14(a), and the relative intrinsic rate constant is shown in Figure 4.14(b).

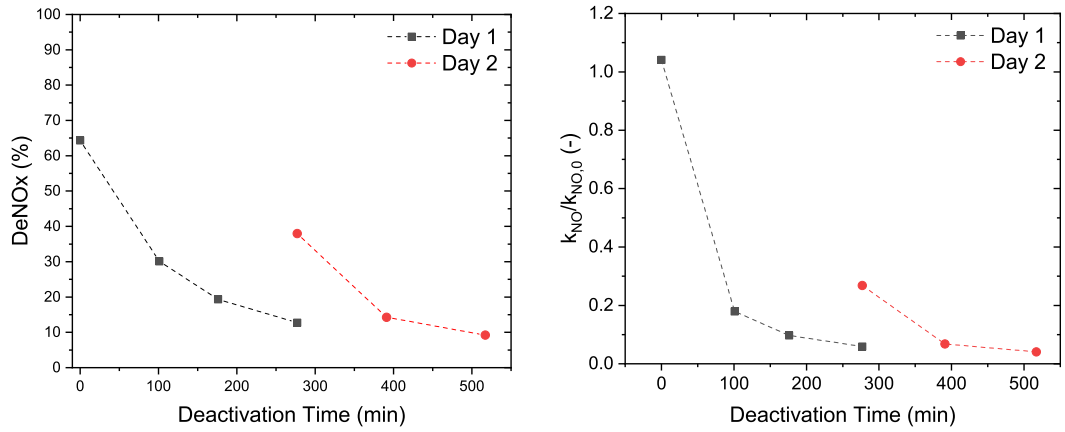

(a) DeNOx Profile (b) Relative intrinsic rate

Figure 4.14: Deactivation of an SCR catalyst using 478 ppm NH_3, 84 ppm SO_4, 5% H_2O, a flow of 110 Nl/min, and at a constant temperature of 304℃. Deactivation time, refers to time with both 478 ppm NH_3 and 84 ppm SO_4 present. The DeNOx profile (a) is measured using standard conditions, also at 304℃, and the intrinsic rate constant (k_{NO}) is fitted using the monolith model[98].

Figure 4.14(a) shows that the catalyst quickly looses the activity when operated at what is expected to be just above the bulk dew point of ABS. The catalyst was left from "Day 1" to "Day 2" at a temperature of 304℃, and a total flow of 110 Nl/min with 5% H_2O. During the 12 hours, the catalyst partly regenerated, however, after only 114 min during the second day (391 min in total) the catalysts activity fell from a NO_x conversion of 38% to 14.3% and continued to decrease to 9.2% after a total deactivation time of 517 min. To ensure that the deactivation observed was not due to bulk condensation, the setup was cooled and tubes around the catalyst inspected. All parts around the catalyst which had been at a temperature of 304℃ was clean, and the part of the setup which was after the oven, and therefore below 304℃ was covered with a thin white layer, as expected from bulk condensation, as shown in Figure 4.15.

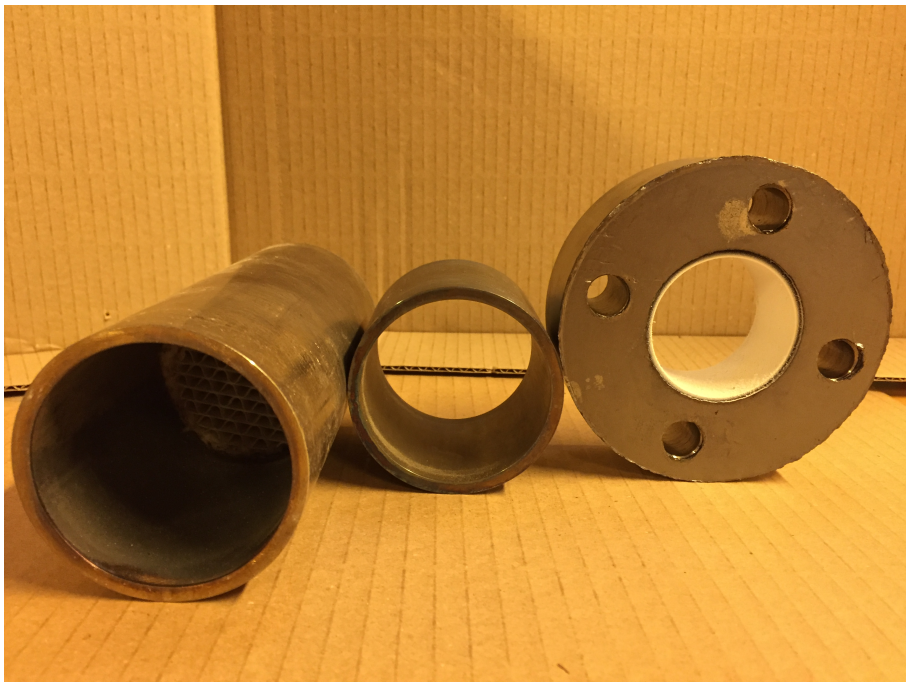

Figure 4.15: From the left: The catalyst tube seen from the inlet side, the tube right after the catalyst, and a downstream tube which is positioned 15 cm after the oven without any isolation.

Based upon Figure 4.15 it was concluded that the catalyst was operated above the bulk dew point, and therefore also that the bulk dew point equation given by Muzio et al.[1] seems likely. It should however be noted, that this experiments does not prove that the expression presented by Muzio et al. is correct, but it does prove that the expression by Matsuda et al.[106] predicts a too high bulk condensation temperature, hence using Matsuda et al. as a design basis would results in a non-deactivated catalyst, however, the higher temperature needed is a problem if the temperature should be increased by auxiliary burners. This is contradictory to what Thøgersen et al.[107] reported, as they found a good agreement with the deactivation profile and Matsuda's bulk dew point expression. The expression based upon the data from Ando et al.[123] seems to predict a too low condensation temperature, hence, as a design basis the low temperature is expected to be below the bulk condensation temperature, and therefore, the catalyst would be completely covered with ABS. Because, the experiment was conducted just above the bulk dew point, this experiments also shows the importance of taking pore condensation into account, when designing an SCR reactor.

The thin white layer observed downstream of the oven was collected. The sample was analyzed using ATR-FTIR and compared to the pure spectra of AS and ABS. Figure 4.16 indicates that the collected material is AS, from which it should be noted that the samples absorbance has been scaled by a factor of 10, due to a very low absorbance. It should be noted that the conclusion does follow the same trends as discussed in Section 4.3, that with such a high ammonia to sulfuric acid ratio (ASR$\sim$ 5.7), AS is the expected condensed material when cooled. At the high temperatures within the catalyst (above 240°C[106]) only ABS is expected to be stable and hence, the deactivation is expected to be due to ABS condensation.

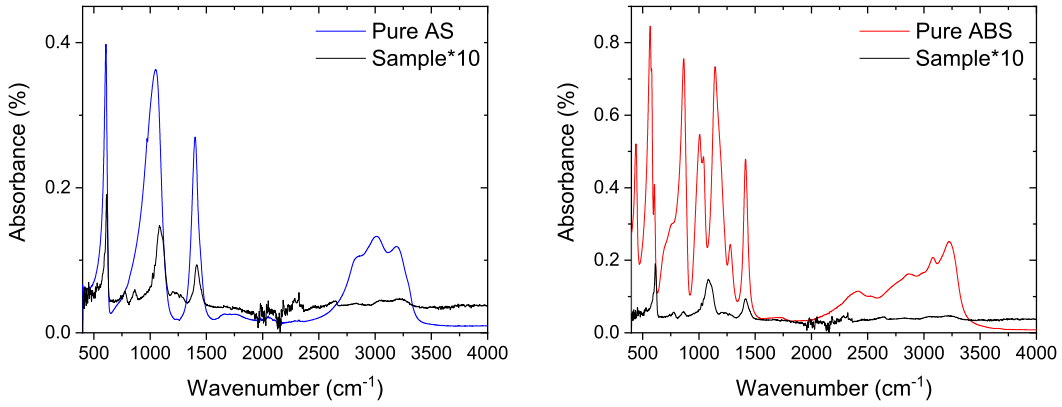

(a) Pure AS and collected sample

(b) Pure ABS and collected sample

Figure 4.16: ATR-FTIR of pure AS (a), pure ABS (b) and the sample collected after the oven. The absorbance of the sample has been multiplied by 10, due to low absorbance.

4.5.4 Regeneration of Deactivated Catalyst

The same catalyst element was used throughout of this study. Therefore, the catalyst was regenerated after each study at temperatures above 350℃ which has been found in the literature to be sufficient to evaporate ABS[105, 107, 121]. The bulk decomposition temperature of ABS was tested using the same two-stage thermogravimetric experiment as presented in Section 4.4. As shown in Figure 4.17 ABS decomposes almost completely at 325℃, the last 3 wt% is of unknown origin. It should be noted that the decomposition temperatures within the pores is expected to be higher.

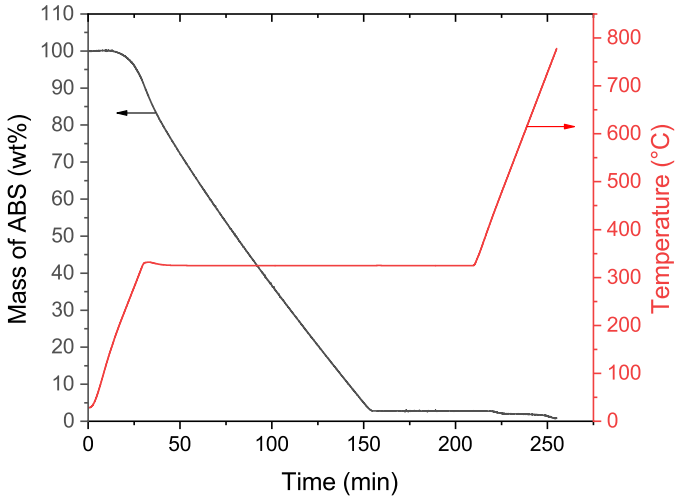

Figure 4.17: A TGA profile from a two-stage thermogravimetric test of ABS. At first ABS is heated to 325℃ (10℃/min) in a flow of nitrogen (100 mL/min), followed by a 3 hours isotherm at 325℃. Secondly the sample is heated in 10% O_2 in nitrogen to 780℃ (10℃/min).

The catalyst was left with heat on the oven, and a flow of air, and additionally in the first regeneration performed, water was also added during the regeneration.

After the regeneration, the setup was cooled and the NO_x conversion was measured at 4 temperatures, from 220℃ to 320℃, using a flow of 110 Nl/min containing 10 % O_2, 5 % H_2O, 630 ppm NO_x, 720 ppm NH_3. The intrinsic rate constant was compared by fitting the rate constant to the measured NO_x conversion using the monolith model[98]. The loss of activity was therefore assumed to be a loss in the intrinsic rate constant as shown in Figure 4.18, however, in reality the loss of activity is expected to be due to a loss of surface area as discussed further below.

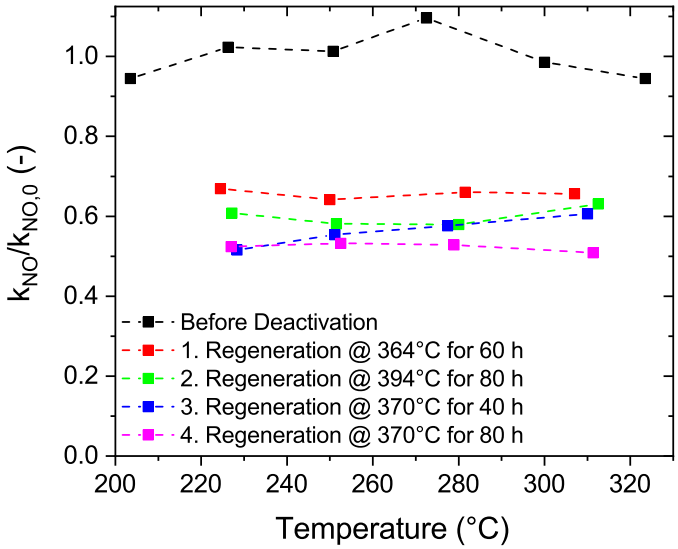

Figure 4.18: Regeneration of the SCR catalyst in air at different temperatures. Between each regeneration, different deactivation experiments have been carried out, as discussed below. $k_{NO,0}$ is the intrinsic rate constant calculated based on the Arrhenius plot shown in Figure 4.12(b).

The black curve ("Before deactivation") in Figure 4.18 should in principle be a horizontal line at 1.00, however, due to small deviations between the fitted intrinsic rate constant (k_{NO}) and the intrinsic rate constant estimated by the Arrhenius equation ($k_{NO,0}$) using the parameters given in Figure 4.12(b), small deviations are observed. Figure 4.18 shows that even 80 hours at 394℃ is not enough to regenerated the catalyst to its original state, which was unexpected. Based upon BET surface area measurements of the fresh catalyst (See Figure 4.19), and the final deactivated catalyst after regeneration 4, the surface area was found to be reduced by 25%, causing a decrease in the intrinsic rate of 50%.

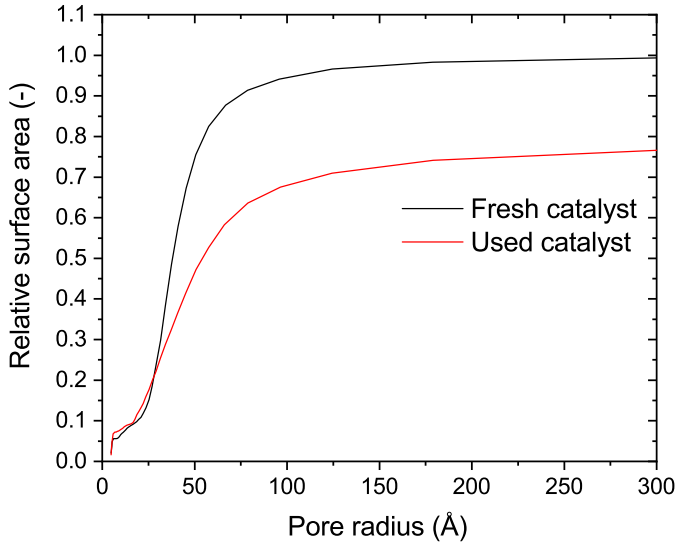

Figure 4.19: The relative surface area of the fresh and used catalyst based on BET measurement. The results are relative to the fresh catalyst.

4.5.5 ABS Deactivation as a Function of Temperature

The next experiment performed was to test how the catalyst deactivates at different temperatures still using synthetic gas mixtures. These experiments were performed after the second regeneration and the deactivation was performed with 471 ppm NH_3, 13 ppm SO_3, 5% H_2O in air, with a total flow rate of 160 Nl/min. The deactivation was performed at four temperatures (310℃, 303℃, 293℃, and 284℃), as shown in Figure 4.20. Using the bulk dew point given by Muzio et al.[1] results in deactivation of pores with a radius less than 16 Å, 21 Å, 40 Å, and 167 Å at the four temperatures respectively.

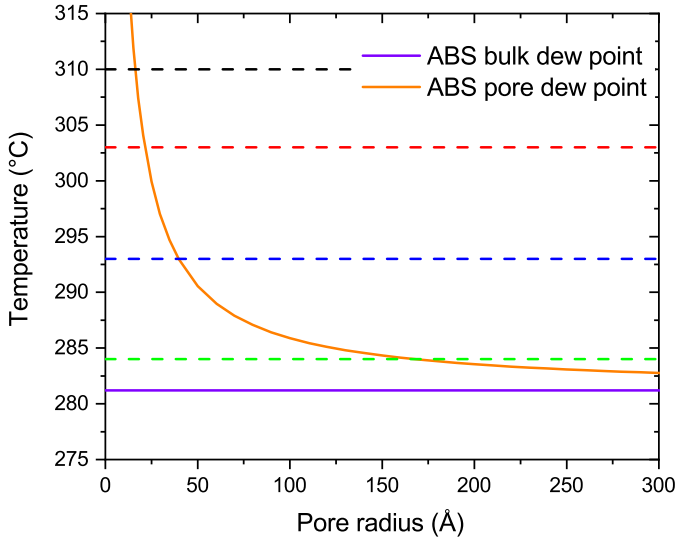

Figure 4.20: The bulk dew point and pore condensation based on Muzio et al.[1]. The four dashed lines indicate the four temperatures at which the experiment was carried out.

The NO_x conversion, was measured without SO_x using standard conditions. The de-

activation experiment was started at the highest temperature investigated (310℃), and was carried out during the day and at the end of the day, the temperature was lowered to the next temperature of interest and the setup was left with a flow of dry air (150 Nl/min) during the night. The measured NO_x conversion and the relative rate is shown in Figure 4.21.

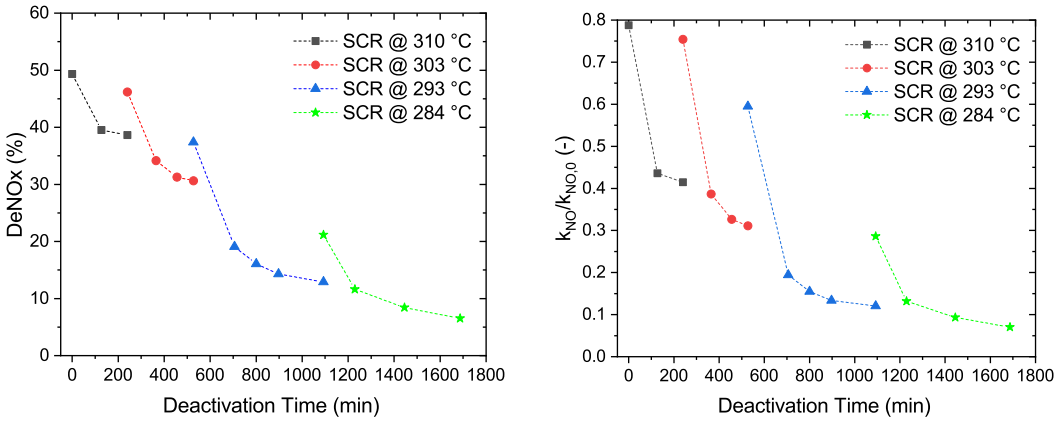

(a) DeNOx profile

(b) Relative intrinsic rate

Figure 4.21: Deactivation by ABS as a function of temperature. The deactivation is shown as a decrease in DeNOx conversion (a) or as a loss in the relative intrinsic rate constant (b). Deactivation was performed with 471 ppm NH_3, 13 ppm SO_3, 5% H_2O in air, with a total flow rate of 160 Nl/min. The DeNOx profile is measured without SO_x using standard conditions, and the intrinsic rate constant is fitted using the monolith model[98]

Figure 4.21 shows that in general the initial deactivation is quite fast, followed by a slower tendency towards steady state. This is probably because the initial deactivation is the smallest pore, and hence the volume of ABS needed to fill these pores is low, but the impact in loss of surface area of the catalyst is great, as also shown by the mercury pore size analysis as shown in Figure 4.22(b). Another trend is that even though the first experiment at 310℃ should only deactivate pores with a radius less than 16 Å, the impact on the DeNOx activity is still a drop from approximately 50% NO_x conversion to 39% NO_x conversion. This clearly shows how important it is to take pore condensation into account, when designing an SCR reactor where sulfur is present.

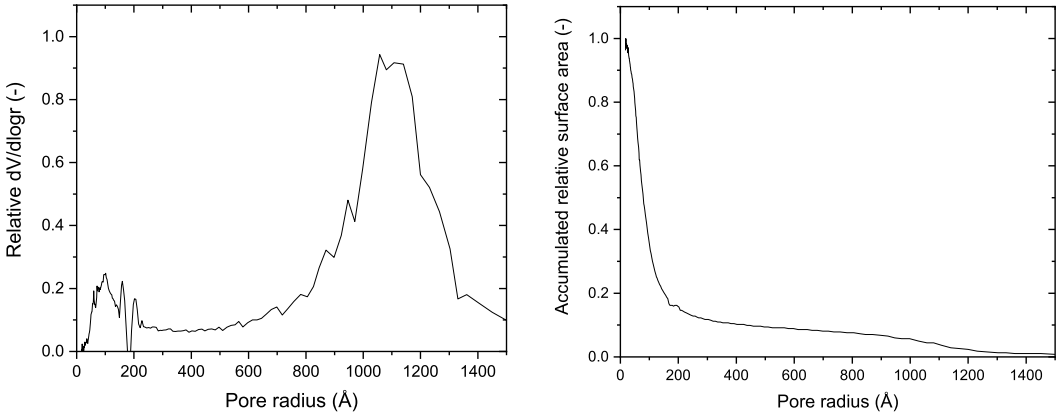

(a) Relative volume of pores as a function of pore size.

(b) Relative accumulated surface area as a function of pore size. Accumulated from right to left.

Figure 4.22: The relative volume (a) and accumulated surface area (b) as a function of pore size determined by Hg porosimetry. The analysis was performed by Haldor Topsøe A/S.

Figure 4.21(b) also shows, that at 303℃ the catalyst almost regenerated during the night to the same state as observed at 310℃ ($k_{NO}/k_{NO,0} = 0.8$ @ 310, and $k_{NO}/k_{NO,0}$ =0.77 @ 303), and as the temperature is decreased, the degree of regeneration during the night is also decreased. The degree of deactivation is as expected increased as the temperature is lowered and the bulk dew point of ABS is approached.

4.5.6 Deactivation with both ABS and NOx

The catalyst was regenerated at 370℃ for 40 hours. After regeneration the four SCR points (See Figure 4.18, "3. Regeneration") was measured, indicating, that it was still not possible to fully regenerate the catalyst. The next deactivation experiment was done to test the effect of also having NO_x present in the synthetic flue gas, resulting in a changing ABS potential throughout the catalyst, due to the consumption of NH_3 by NO_x in the SCR reaction. Initially, before deactivation, the catalyst removes about 44% of the NO_x, which corresponds to 136 ppm NH_3 when 310 ppm of NO_x is fed. This change in NH_3 and hence the ABS potential changes the pore size that will be filled with ABS from the inlet of the catalyst where pores less than 16 Å will be filled to the outlet of the catalyst, where pores less than 14 Å will be filled with ABS. However, as the catalyst becomes deactivated, the ABS potential increases, and hence the higher ABS potential will "travel" through the catalyst as it deactivates.

The experiment was performed with 471 ppm NH_3, 14 ppm SO_3, 310 ppm NO_x (∼ 10-15 ppm NO_2), 5 % H_2O in air with a total volumetric flow of 160 Nl/min. The DeNOx activity was measured without SO_x present and the results are shown in Figure 4.23.

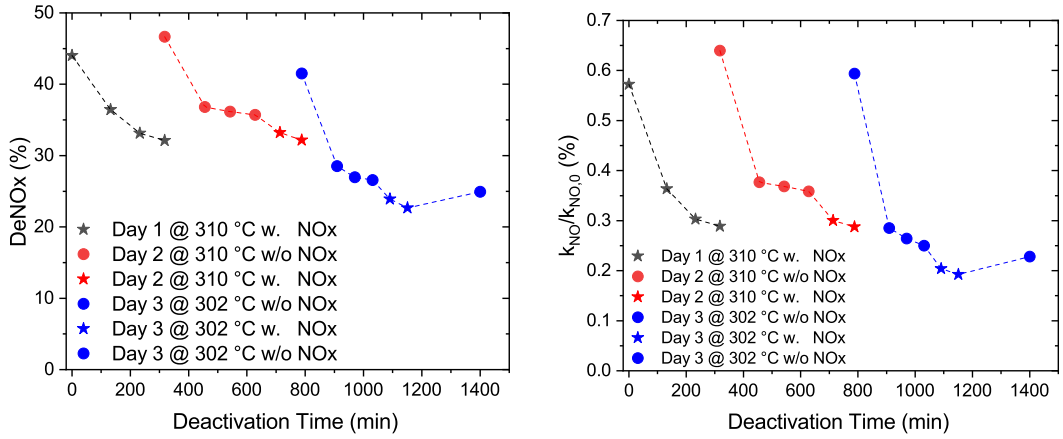

(a) DeNOx Profile

(b) Relative intrinsic rate

Figure 4.23: Deactivation by ABS in the presence of NO_x. The deactivation is shown as a loss in DeNOx conversion (a) and as a loss in the relative intrinsic rate constant (b). Experiment carried out using 471 ppm NH_3, 14 ppm SO_3, 310 ppm NO_x ($\sim$ 10-15 ppm NO_2), 5 % H_2O in air with a total flow of 160 Nl/min. All "$\star$" are made with 310 ppm NO_x present in the gas and all "$\bullet$" are made without NO_x present. Identical colors are made the same day. The DeNOx profile is measured without SO_x using standard conditions, and the intrinsic rate is fitted using the monolith model[98].

Figure 4.23 shows that initially the experiment at 310℃ starts out with a lower activity (DeNOx = 44%) compared to the deactivation experiment performed without NO_x (DeNOx = 49%, Figure 4.21) for unknown reasons. Having this in mind, the initial part of the deactivation looks rather similar, however, while the experiment without NO_x seems to stabilized quite fast, the experiment with NO_x takes longer time, and the final deactivation is lower (33%) compared to the experiment shown in Figure 4.21(b) (38%). However, since the initial points of the two experiments are different it is hard to compare the experiments directly.

The experiment during the second day was, therefore, initially started without any NO_x present and still at 310℃. Initially, it was observed that the catalyst had regenerated during the night, and was now more active than at the beginning of day 1 (Day 2, 47% conversion, vs. Day 1, 44% conversion). This is expected to be due to the catalyst being more acidic due to sulfates on the surface, but now without ABS filling the pores, which would result in a more active catalyst. The first part of the experiment followed the same trend as the one performed earlier, also without NO_x (See Figure 4.21). Initially, the catalyst started with a DeNOx activity of 47% (compared to 49%) and fell to 36% after 224 minutes of deactivation time, compared to an earlier measurement of a drop to 38% after 240 min. also without NO_x. After additional 90 min. (total of 628 min), 310 ppm of NO_x was added to the gas while continuing deactivation. The addition of NO_x resulted in a fast drop in activity, as shown by the two red stars in Figure 4.23 (Day 2, 700-800 min). The addition of NO_x was originally expected to result in an increase in activity. Therefore the temperature was lowered, and the experiment was conducted in the same way at 302℃ on "Day 3".

At 302℃ and without NO_x, the deactivation had a bit sharper slope, indicating

that steady state was not achieved after a total deactivation time of 1000 minutes. However, the addition of NO_x again resulted in a lowered NO_x reduction activity. To test whether this further, NO_x induced, deactivation was reversible the NO_x was shut off, while maintaining both NH_3 and SO_x on. As shown in Figure 4.23, this resulted in partial reactivation, resulting in a conversion of 30% DeNOx compared to a DeNOx of 25% while NO_x was present during the deactivation.

The increased deactivation observed when NO_x is present can either be due to a catalyzed reaction between SO_2 and NO_2 forming SO_3, thereby increasing the ABS potential, as was observed by an earlier study (Christensen et al.[102]). However, the low concentration of SO_2 ($\sim$ 120 ppm) makes it hard to imagine that a large increase in SO_3 happens across the catalyst, since typically less than 1% of SO_2 is oxidized to SO_3, i.e. forming 1.2 ppm extra SO_3. Another possibility is the formation of molecules that originate from NO_x, SO_3, and possible NH_3 which have condensation temperatures lower than ABS, and therefore, increased deactivation is observed. In a review by Zhou et al.[121] the addition of NO_x was reported to increase the ABS dew point temperature, however, the original reference (Louis[131]), originating from Ljungstrom air preheaters, has been requested but so far without success. Therefore, the reason for the proposed increase in ABS bulk dew point due to the presence of NO_x is unknown. Further experiments should be conducted in which NO_2 is added to the gas followed by condensation and characterization of the condensed material, to investigate whether only AS and ABS are condensed or other compounds as well.

4.6 Installation of an SCR reactor on a Ship

It has now been realized that the installation of an SCR reactor at a too cold position, can result in quite a severe deactivation of the SCR catalyst due to condensation of sulfates. This problem might be diminished by the presence of soot, however further experiments are needed to make a conclusion.

Based on the experiment discussed in Section 4.5.5, the bulk dew point expression presented by Muzio et al.[1] was found to give good results. In order to bring these calculation from small scale to real engine scale, the amount of SO_2 emitted from a ship was estimated as a function of the sulfur content of the fuel according to Equation 4.13[126].

$$\text{Fuel S Eq. [\% w/w]} = \frac{\frac{SO_2[\text{ppm, dry}]}{CO_2[\%, \text{dry}]}}{43.3} \tag{4.13}$$

From which the concentration of SO_2 in the exhaust gas could be calculated, under the assumption of a constant CO_2 concentration of 5.5 %, equal to that measured at Alfa Laval's test and training center. The SO_2 emission was found to be 24 ppm SO_2 for a fuel oil containing 0.1 wt% sulfur and 595 ppm SO_2 for a fuel oil containing 2.5 wt% of sulfur. If the SO_3 content of the exhaust gas is assumed to be 5% of the total SO_2, and the NH_3 content of the exhaust gas is assumed to be

480 ppm (ANR = 0.8 for 600 ppm NO_x), the bulk dew point as a function of total pressure could be calculated based on the expression presented by Muzio et al.[1] as shown in Figure 4.24.

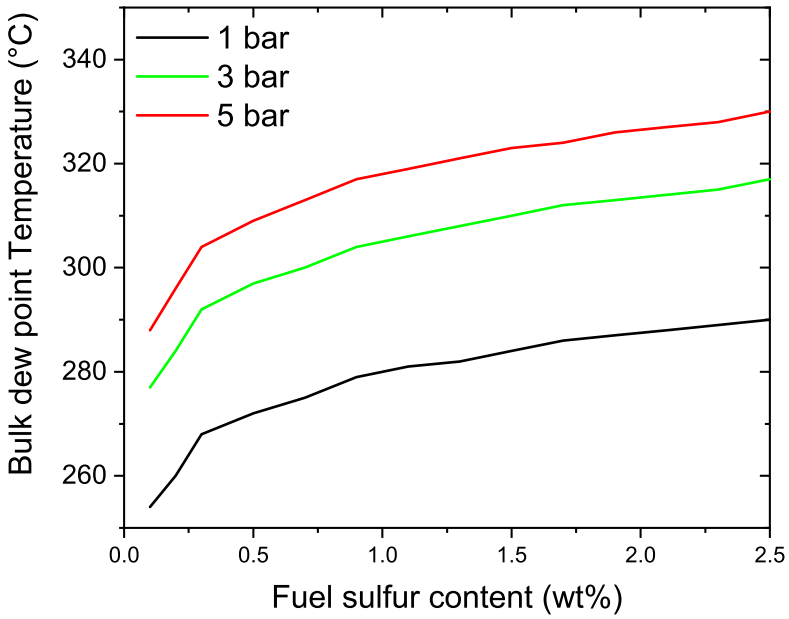

Figure 4.24: The bulk dew point temperature as a function of fuel oil sulfur content, and pressure. The dew point temperature is based on the expression given by Muzio et al.[1]. The SO_2 concentration is calculated using Equation 4.13, and the bulk dew point is calculated based upon 480 ppm NH_3 and SO_3 equals 5% of the total SO_2 concentration.

Figure 4.24 shows that the required temperature even using a low sulfur fuel oil, containing 0.1 wt% sulfur, result in a required minimum temperature of 255℃, which is before pore condensation has been taken into account. Calculating the pore condensation temperature, for pores less than 10 Å, result in a temperature of 298℃. A typical downstream temperature of approximately 200-260℃ has been reported in the literature, depending on the engine load[22, 70, 84]. This clearly shows the need for installation of the catalytic reactor upstream of the turbocharger, where typical temperatures are between 300-450℃, depending on the engine load. At the low engine load of for instance 25%, Sandelin et al.[84] reported an upstream turbocharger temperature of 310℃, and a pressure of 1.4 bar, which would be sufficient according to Figure 4.24. At a load of 75% a temperature of 380℃ and a pressure of 3.3 bar, was measured upstream of the turbocharger, and finally at full load a temperature of 450℃ and a pressure of 4.3 bar was measured upstream of the turbocharger. All of which would be sufficient according to Figure 4.24. It should be noted that the results shown in Figure 4.24 does not take the possible effects of soot, NO_2, pore condensation and consumption of NH_3 across the catalyst into account.

It is therefore proposed that an SCR reactor should be installed upstream of the turbocharger for a two-stroke marine diesel engine.

4.6.1 Conclusion

The deactivation caused by ABS condensation within the pores of a 1 wt% V-SCR catalyst has been studied using a pilot scale reactor. A diesel generator should have been used to test the difference between synthetic gas mixtures and "real" engine exhaust gas, however, due to generator malfunctions only synthetic air has been used.

The bulk dew point as given by Ando et al.[123] was found to estimate a too low bulk dew point, and therefore, if used as design basis the catalyst would become deactivated. The bulk dew point as given by Matsuda et al.[106] was found too high, and therefore, if used as the design basis for an SCR reactor, the minimum temperature would be estimated to high, which in case of auxiliary burners to increase the temperature, would be expensive. The bulk dew point as estimated by Muzio et al.[1] was in this study fond to more closely predict the dew point temperature, also at the high partial pressures interesting for preturbine configuration.

Based on an experiment where the temperature was lowered in steps thereby deactivating larger and larger pores, it was observed, that a large part of the activity originates from the small pores within the catalyst (r<50Å), containing the main part (75%) of the total surface area of the catalyst. This clearly showed the importance of taking pore condensation into account when choosing operation temperatures for SCR catalyst to be used in sulfur rich environments.

The catalyst was attempted regenerated after ABS deactivation using air and temperatures of up to 394℃ for 80 hours, which is conditions where the catalyst should not sinter. However, by measuring the DeNOx activity after multiple regeneration attempts it was concluded that the catalyst could not be completely regenerated to its original state. Furthermore, after the first regeneration step the activity was neither constant and the activity subsequently decreased after each regeneration attempt, which could indicate destruction of the small pores. If this also applies for industrial applications, this should be taken into account during the design phase of the catalytic reactor.

Opposite to expectations, the presence of NO_x during deactivation enhanced the deactivation. This is expected to be due to either an increased SO_3 concentration because of a catalyzed SO_2 oxidation by NO_2 or due to formation of condensible compounds with a lower dew point than ABS. This should be further studied in another study.

5 Conclusion and Future Work

This thesis contributes to the understanding of how selective catalytic reduction (SCR) will perform at increased pressure with respect to the main SCR reactions, but also side reactions such as SO_2 oxidation and ABS formation. These are primary issues that were investigated to ensure competitive and reliable SCR of NO_x on ships, to comply with IMO Tier III.

The main SCR reaction was investigated at an increased pressure of up to 5 bar using vanadium based SCR catalysts ($\sim$1 wt% V_2O_5/10 wt% WO_3/TiO_2) supplied by Umicore Denmark ApS. The experiments were carried out using both granulated catalyst (mesh = 150-300 microns) and a 10 cm. long monolith catalyst (d_h=4.3 mm). Steady state SCR experiments were performed across a packed bed reactor, at a pressure of 1.2 bar up to 4.8 bar. It was found that when the residence time was kept constant, the NO_x conversion across the catalyst was also constant, independent of the pressure. This shows that the main SCR reaction is not affected by the increased pressure.
NH_3 temperature programmed desorption (TPD) was also studied for the granulated catalyst. It was observed that when the pressure was increased, the amount of NH_3 on the surface of the catalyst increased, while it decreased with increasing temperature. The transient NH_3 TPD experiments were fitted using a Temkin isotherm (i.e. a coverage dependent desorption enthalpi), and kinetic rate constants were found similar to literature, and independent of the pressure. The steady state SCR was modeled, using the transient kinetics for the adsorption/desorption of NH_3 on the surface of the catalyst. This showed that the rate of NO disappearance was found not to depend on NH_3 when the surface coverage of the catalyst was higher than 14%. This low NH_3 surface coverage, explains why the steady state SCR experiments were not affected by the increased NH_3 adsorption at increased pressure.
Steady state SCR experiments were also performed across a monolith catalyst to test how pressure affects external and internal diffusion limitations. It was found that when the pressure was increased from 1 bar to 3.1 bar while keeping the residence time within the catalyst constant, a small decrease of up to 5% points in NO_x conversion was observed at temperatures higher than 250℃. The decrease in NO_x conversion is caused by increased mass transfer limitations. If the mass flow rate is kept constant, the total effect of the pressure is positive, due to a significant impact of the increased residence time.

Oxidation of SO_2 across a monolith catalyst containing either 1.2 wt% V_2O_5 or 3 wt% V_2O_5 was studied at pressures of up to 4.5 bar. It was found that when

the residence time was kept constant, the conversion of SO_2 was independent on the pressure. Based on a this observation, and that variations in the SO_2 in inlet concentration lead to the same conversion of SO_2, it is concluded that the rate of SO_2 oxidation, is first order in SO_2 and zero order in SO_3. The oxidation of SO_2 was found to be limited by reaction kinetics, and was, therefore, increased by increasing the concentration of active material in the catalyst, i.e., V_2O_5. Opposite to the SCR reaction, the SO_2 oxidation was therefore not affected by changes in mass transfer. The oxidation of SO_2 was found to be promoted by the presence of NO_2 at increased pressure, due to a direct reaction between SO_2 and NO_2 forming SO_3 and NO.

The formation and deactivation caused by ammonium sulfates were finally investigated. Based on condensation of sulfates from a gas containing NH_3 and H_2SO_4 on the surface of a steel tube, and subsequent analysis of the condensed material, the formation of sulfates was found to be dependent on the NH_3 to sulfate ratio (ASR). When ASR was below one ammonium bisulfate (ABS) was observed, with an ASR of 1-2 a mixture of ABS and ammonium sulfate (AS) was observed and at ASR larger than two AS was observed. Based on literature and an experiment on decomposition of AS, it was found that at temperatures interesting for SCR (300-400℃), the sulfates will be present as ABS.
The deactivation of the SCR reaction caused by condensation of ABS within a monolith catalyst was investigated. The bulk dew point temperature of ABS was found to be best calculated by the expression proposed by Muzio et al.[1]. Furthermore, the pore structure of the catalyst was shown to be important to take into account, because ABS condense at temperatures higher than the bulk temperature in the pores, due to pore condensation. The catalyst was attempted regenerated by heating the catalyst element to temperatures between 350-400℃, however, these temperatures were found insufficient for complete regeneration. BET measurements on the spent catalyst showed that the insufficient regeneration of the catalyst was due to a loss in surface area of the small pores, either still covered with ABS or the small pores were collapsed.

At Alfa Laval's test and training center the deposits were quite easily removed from the boiler, even though they contained ABS. It was therefore considered if the presence of soot could prohibit the stickiness of ABS. Based upon mixtures of ABS and soot deposited on a test element to simulate a surface of a boiler, it was observed that the force needed to remove ABS by air blowing, was lower when the soot fraction was at least 20 wt% of the mixture, which was explained by soot acting as a sponge, preventing ABS from becoming a sticky mass.

Based on the experiments carried out in this thesis, the most critical parameter to ensure reliable SCR is believed to be to ensure that the catalyst is not deactivated by condensation of ABS. In order to achieve high enough temperatures at 2-stroke engines, it is therefore proposed that the SCR reactor is installed upstream of the turbocharger. In such case, it is essential during the design phase to take into account, that the high pressure depends on the engine load and in case the SCR reactor should be used at all loads this also means at both low and high pressure. At

the high pressure, the catalyst will, therefore, be over-sized resulting in increased SO_2 oxidation, however, decreased NH_3 slip. Furthermore, for preturbine SCR configuration, a valve system is needed in order to bypass either the SCR reactor or the cylinder during load change, to prevent the turbine from fluctuating due to the heat capacity of the catalyst.

5.1 Future Work

Based on the work presented in this thesis, a number of future studies could be interesting to perform, to ensure reliable preturbine high pressure SCR. The future work has been divided into four overall issues, i.e. "Pressurized SCR of NO_x", "Pressurized SO_2 Oxidation", "Formation and condensation of AS/ABS", and "Full-Scale Experiments".

Pressurized SCR of NO_x

- Conduct SCR experiments with a high V-SCR catalyst, i.e., 4-5 wt% V_2O_5, to ensure that the results presented in this thesis apply to the full range of vanadia used for SCR catalysts. At the high V_2O_5 loading, NH_3 oxidation at temperatures of 350-500℃ should also be investigated.
- An SCR experiment with a regularly sized monolith catalyst (500-1000 mm[44]), and regular linear velocities (5 m/s[44]) should be performed to test the effects of mass transfer limitations at increased pressure. These experiments should also be performed to test how well the single channel monolith model made by Olsen[98], can predict these experiments. The model has earlier been found to work well at atmospheric pressures, lower velocities (2 m/s) and longer catalyst (400 mm) in our group.
- An SCR experiment using a monolith catalyst, testing the NH_3 adsorption capacity, to evaluate how well the lab-scale TPD results translate into pilot scale, and preferable also full scale. Bank et al.[72] measured a 70% increase in NH_3 capacity, when only increasing the pressure from 1 to 2 bar at 215℃ across a monolith, compared to the 10% increase measured in this study at 200℃ and by changing the pressure from 1 to 2 bar.

Pressurized SO_2 Oxidation

- All measurements of SO_2 oxidation were performed without NH_3 present in the gas, to prevent the formation of AS/ABS. Orsenigo et al.[104] stated that the addition of NH_3 inhibited the oxidation of SO_2, however, Orsenigo et al. did not state how they handled the formation of ABS/AS during the measurements of SO_3 formation. Therefore a study, measuring the pressurized SO_2 oxidation, with NH_3 and/or NO_x present would be interesting.
- The addition of NO_x during SO_2 oxidation, was found to increase the oxidation of SO_2 expected to be caused by NO_2. The aspects of NO_2 induced SO_2 oxidation could also be further investigated.

Formation and condensation of AS/ABS

- All AS/ABS experiments have been conducted at atmospheric pressure. High partial pressures of AS/ABS has been used to simulate high pressure, however, experiments at elevated pressures should be performed, to ensure that the results obtained at atmospheric pressure, also applies at increased pressure. Especially the dew point temperature calculations, are of interest at the increased pressure.

- Regeneration of the SCR catalyst after deactivation by ABS was found to be insufficient at temperatures of 350-400℃. Therefore, it should be further investigated whether it is possible to regain the catalyst activity at a higher temperature (500℃), in order to understand whether the loss in activity is due to destroyed or ABS filled pores. Blank experiments should also be conducted without NH_3 present in the gas, to ensure that the single cause of deactivation is the formation of ABS.

- The stickiness of ABS was found to decrease when mixed with more than 20 wt% soot. Therefore, engine experiments should be performed to investigate if a critical amount of soot can be present, at which the catalyst is not deactivated because the soot absorbs ABS.

- A transient model should be developed in order to predict the deactivation caused by low temperature SCR, and equally important, the temperature needed to restore the catalyst. Thøgersen et al.[107] developed such a model, hence inspiration could be found in their paper.

Full-Scale Experiments

- The effects of using an SCR monolith at an actual engine was not investigated. Especially the contaminants from the engine oil and lube oil, such as alkali metals and vanadia could be interesting to investigate.

- Full-scale tests of the decomposition of urea at the increased pressure and possible short residence time should also be conducted.

Bibliography

[1] L. Muzio, S. Bogseth, R. Himes, Y.C. Chien and D. Dunn Rankin (2017) "Ammonium bisulfate formation and reduced load SCR operation" *Fuel* **206** 180–189, DOI: 10.1016/j.fuel.2017.05.081.

[2] H. Jääskeläinen "Early History of the Diesel Engine" [Online] Available at: https://www.dieselnet.com/tech/diesel_history.php, Accessed: 08/08-18.

[3] D. Woodyard (2009) "Pounder's Marine Diesel Engines and Gas Turbines", *Butterworth-Heinemann*, ISBN: 978-0-7506-8984-7.

[4] CIMAC Working Group 8 "CIMAC Guideline: Cold Corrosion in Marine Two Stroke" [Online] Available at: https://cimac.com/cms/upload/Publication_Press/WG_Publications/CIMAC_WG8_Guideline_2017_Two_Stroke_Engine_Cold_Corrosion.pdf, Accessed: 27/6-18.

[5] K. Mollenhauer and H. Tschöke (2010) "Handbook of Diesel Engines", *Springer Berlin Heidelberg*, ISBN: 978-3-540-89082-9.

[6] S.R. Turns (2012) "An introduction to combustion : concepts and applications", *McGraw-Hill*, ISBN: 9780071086875.

[7] M. Koebel, M. Elsener and G. Madia (2001) "Reaction Pathways in the Selective Catalytic Reduction Process with NO and NO 2 at Low Temperatures" *Industrial & Engineering Chemistry Research* **40(1)** 52–59, DOI: 10.1021/ie000551y.

[8] Å.M. Hallquist, E. Fridell, J. Westerlund and M. Hallquist (2013) "Onboard Measurements of Nanoparticles from a SCR-Equipped Marine Diesel Engine" *Environmental Science & Technology* **47(2)** 773–780, DOI: 10.1021/es302712a.

[9] Man Diesel & Turbo "Exhaust gas emission control today and tomorrow" [Online] Available at: http://marine.man.eu/docs/librariesprovider6/technical-papers/exhaust-gas-emission-control-today-and-tomorrow.pdf?sfvrsn=22.

[10] M.I. Lamas and C.G. Rodríguez (2012) "Emissions from Marine Engines and NOx Reduction Methods" *Journal of maritime research* **9(1)** 77–81.

[11] J. Briggs and J. Mccarney (2013) "Field experience of Marine SCR" in *CIMAC Congress*.

[12] K. Lehtoranta, H. Vesala, P. Koponen and S. Korhonen (2015) "Selective Catalytic Reduction Operation with Heavy Fuel Oil: NOx , NH3, and Particle Emissions" *Environmental Science & Technology* **49(7)** 4735–4741, DOI: 10.1021/es506185x.

[13] Y. Niki, K. Hirata, T. Kishi, T. Inaba et al. (2010) "SCR system for NOx reduction of Medium Speed Marine Diesel Engine" in *CIMAC Congress*.

[14] M. Magnusson, E. Fridell and H. Harelind (2014) "Improved low-temperature activity for marine selective catalytic reduction systems" *Proceedings of the Institution of Mechanical Engineers, Part M: Journal of Engineering for the Maritime Environment*, DOI: 10.1177/1475090214536546.

[15] C. Österman and M. Magnusson (2013) "A systemic review of shipboard SCR installations in practice" *WMU Journal of Maritime Affairs* **12(1)** 63–85, DOI: 10.1007/s13437-012-0034-1.

[16] DieselNet "EU: Cars and light Trucks" [Online] Available at: https://www.dieselnet.com/standards/eu/ld.php#stds, Accessed: 08/08-2018.

[17] Det Norske Veritas (DNV) "Marpol 73/78 Annex VI" [Online] Available at: http://hulpinnood.nl/wp-content/uploads/2015/03/BIJLAGE3_Marpol-annex-VI.pdf, Accessed: 9/5-2016.

[18] IMO "IMO Tier III - Appendix II" [Online] Available at: http://www.marpoltraining.com/MMSKOREAN/MARPOL/Annex_VI/app2.htm, Accessed: 09/08-2018.

[19] IMO "NECAs" [Online] Available at: http://www.imo.org/en/OurWork/Environment/PollutionPrevention/AirPollution/Pages/Emission-Control-Areas-(ECAs)-designated-under-regulation-13-of-MARPOL-Annex-VI-(NOx-emission-control).aspx, Accessed: 09/08-2018.

[20] Lloyd's Register Marine(2015)"Your options for emissions compliance" [Online] Available at: http://www.lr.org/en/_images/213-35826_Your_options_for_emissions_compliance.pdf, Accessed: 19/12-15.

[21] IMO "IMO MEPC 66/6/15" [Online] Available at: http://www.worldshipping.org/industry-issues/environment/air-emissions/MEPC_66-6-15_-_Comments_concerning_potential_amendments_to_the_effective___.pdf, Accessed: 20/11-2017.

[22] Man Diesel & Turbo "Tier III Two-Stroke Technology" [Online] Available at: http://marine.man.eu/docs/librariesprovider6/technical-papers/tier-iii-two-stroke-technology.pdf?sfvrsn=12, Accessed: 10/9-15.

[23] R. Juergens (2013) "First operational experiences with a combined Dry Desulphurization Plant and SCR Unit downstream of a HFO fueled marine engine" in *CIMAC Congress*.

[24] J.P. Hansen and H.T. Jacobsen(2016)"Komplet efterbehandlings- system til skibe" [Online] Available at: http://www2.mst.dk/Udgiv/publikationer/2016/05/978-87-93435-71-1.pdf.

[25] H. Bosch and F. Janssen (1988) "Preface" *Catalysis Today* **2(4)** v, DOI: 10.1016/0920-5861(88)80001-4.

[26] P. Forzatti and L. Lietti (1996) "Recent Advances in DeNOxing Catalysis for Stationary Applications" *Heterogeneous Chemistry Reviews* **3(1)** 33–51.

[27] G. Centi and S. Perathoner (2007) "Chapter 1 Introduction: State of the art in the development of catalytic processes for the selective catalytic reduction of NOx into N2" in *Studies in Surface Science and Catalysis*.

[28] I. Nova and E. Tronconi (2014) "Urea-SCR Technology for deNOx After Treatment of Diesel Exhausts", *Springer*, ISBN: 978-1-4899-8070-0.

[29] "Dieselnet, emission standards" [Online] Available at: https://www.dieselnet.com/standards/eu/hd.php#stds, Accessed: 27/10-15.

[30] M. Koebel, M. Elsener and G. Madia (2001) "Recent Advances in the Development of Urea-SCR for Automotive Applications" *Sae Technical Papers*, DOI: 10.4271/2001-01-3625.

[31] P. Blakeman, K. Arnby, P. Marsh, C. Newman and G. Smedler (2008) "Optimization of an SCR Catalyst System to Meet EUIV Heavy Duty Diesel Legislation" *SAE Technical Paper* **2(724)**, DOI: 10.4271/2008-01-1542.

[32] B. Guan, R. Zhan, H. Lin and Z. Huang (2014) "Review of state of the art technologies of selective catalytic reduction of NOx from diesel engine exhaust" *Applied Thermal Engineering* **66(1-2)** 395–414, DOI: 10.1016/j.applthermaleng.2014.02.021.

[33] O. Kröcher (2007) "Aspects of catalyst development for mobile urea-SCR systems — From Vanadia-Titania catalysts to metal-exchanged zeolites" in *Studies in Surface Science and Catalysis*, Elsevier.

[34] Man Diesel & Turbo "Quality and specifications of HFO and MDO" [Online] Available at: http://www.dma.dk/themes/LNGinfrastructureproject/Documents/Bunkeringoperationsandshippropulsion/51-60DF_IMO_TierII_\OT1\textendash_Marine_partII.pdf, Accessed: 16/1-2016.

[35] S. Amanatidis, L. Ntziachristos, B. Giechaskiel, A. Bergmann and Z. Samaras (2014) "Impact of Selective Catalytic Reduction on Exhaust Particle Formation over Excess Ammonia Events" *Environmental Science & Technology* **48(19)** 11527–11534, DOI: 10.1021/es502895v.

[36] M. Koebel and M. Elsener (1998) "Selective Catalytic Reduction of NO over Commercial DeNO x Catalysts: Comparison of the Measured and Calculated Performance" *Industrial & Engineering Chemistry Research* **37(2)** 327–335, DOI: 10.1021/ie970569h.

[37] M. Koebel, M. Elsener, O. Kröcher, C. Schär et al. (2004) "NOx Reduction in the Exhaust of Mobile Heavy-Duty Diesel Engines by Urea-SCR" *Topics in Catalysis* **30/31(1)** 43–48, DOI: 10.1023/B:TOCA.0000029726.38961.2b.

[38] M. Koebel and E.O. Strutz (2003) "Thermal and Hydrolytic Decomposition of Urea for Automotive Selective Catalytic Reduction Systems: Thermochemical and Practical Aspects" *Industrial & Engineering Chemistry Research* **42(10)** 2093–2100, DOI: 10.1021/ie020950o.

[39] M. Kleemann, M. Elsener, M. Koebel and A. Wokaun (2000) "Hydrolysis of Isocyanic Acid on SCR Catalysts" *Industrial & Engineering Chemistry Research* **39(11)** 4120–4126, DOI: 10.1021/ie9906161.

[40] W.A. Majewski and M.K. Khair (2006) "Diesel emissions and their control", *SAE International*, ISBN: 9780768006742.

[41] G. Cavataio, J. Girard, J.E. Patterson, C. Montreuil et al. (2007) "Laboratory Testing of Urea-SCR Formulations to Meet Tier 2 Bin 5 Emissions" *Sae Technical Papers*, DOI: 10.4271/2007-01-1575.

[42] J.H. Kwak, R.G. Tonkyn, D.H. Kim, J. Szanyi and C.H. Peden (2010) "Excellent activity and selectivity of Cu-SSZ-13 in the selective catalytic reduction of NOx with NH3" *Journal of Catalysis* **275(2)** 187–190, DOI: 10.1016/j.jcat.2010.07.031.

[43] K. Kamasamudram, N. Currier, T. Szailer and A. Yezerets (2010) "Why Cu- and Fe-Zeolite SCR Catalysts Behave Differently At Low Temperatures" *SAE International Journal of Fuels and Lubricants* **3(1)** 664–672, DOI: 10.4271/2010-01-1182.

[44] P. Gabrielsson and H.G. Pedersen (2008) "Flue Gas From Staionary Sources" in *Handbook of heterogeneous catalysis.*, Wiley-VCH.

[45] M. Inomata, A. Miyamoyo and Y. Murakami (1980) "Mechanism of the reaction of NO and NH3 on vanadium oxide catalyst in the presence of oxygen under the dilute gas condition" *Journal of Catalysis* **62(1)** 140–148, DOI: 10.1016/0021-9517(80)90429-7.

[46] N.Y. Topsøe (1994) "Mechanism of the selective catalytic reduction of nitric oxide by ammonia elucidated by in situ on-line fourier transform infrared spectroscopy." *Science (New York, N.Y.)* **265(5176)** 1217–1219.

[47] G.T. Went, L.J. Leu, R.R. Rosin and A.T. Bell (1992) "The Effects of Structure on the Catalytic Activity and Selectivity of V2O5/TiO2 for the Reduction of NO by NH3" *Journal of Catalysis* **134** 492–505, DOI: 10.1016/0021-9517(92)90337-H.

[48] N.Y. Topsøe, M. Anstrom and J.a. Dumesic (2001) "Raman, FTIR and theoretical evidence for dynamic structural rearrangements of vanadia/titania DeNOx catalysts" *Catalysis Letters* **76(1-2)** 11–20, DOI: 10.1023/A:1016715823630.

[49] J. Dumesic, N.Y. Topsøe, H. Topsøe, Y. Chen and T. Slabiak (1996) "Kinetics of Selective Catalytic Reduction of Nitric Oxide by Ammonia over Vanadia/Titania" *Journal of Catalysis* **163(2)** 409–417, DOI: 10.1006/jcat.1996.0342.

[50] L. Arnarson, H. Falsig, S.B. Rasmussen, J.V. Lauritsen and P.G. Moses (2017) "A complete reaction mechanism for standard and fast selective catalytic reduction of nitrogen oxides on low coverage VO x /TiO 2 (0 0 1) catalysts" *Journal of Catalysis* **346** 188–197, DOI: 10.1016/j.jcat.2016.12.017.

[51] E. Tronconi, P. Forzatti, J. Gomez Martin and S. Mallogi (1992) "Selective catalytic removal of NOx: a mathematical model for design of catalyst and reactor" *Chemical Engineering Science* **47(9-11)** 2401–2406, DOI: 10.1016/0009-2509(92)87067-Z.

[52] J.W. Beeckman and L.L. Hegedus (1991) "Design of monolith catalysts for power plant NOx emission control" *Industrial & Engineering Chemistry Research* **30(5)** 969–978, DOI: 10.1021/ie00053a020.

[53] J.W. Girard, C. Montreuil, J. Kim, G. Cavataio and C. Lambert (2008) "Technical Advantages of Vanadium SCR Systems for Diesel NOx Control in Emerging Markets" *SAE International Journal of Fuels and Lubricants* **1(1)** 2008–01–1029, DOI: 10.4271/2008-01-1029.

[54] T. Maunula, A. Viitanen, T. Kinnunen and K. Kanniainen (2013) "Design of Durable Vanadium - SCR Catalyst Systems for Heavy - Duty Diesel Applications" *SAE Technical Papers* **5(2)**, DOI: 10.4271/2013-26-0049.

[55] I. Nova, L. Lietti, A. Beretta and P. Forzatti (2001) "Study of the sintering of a deNOx commercial catalyst" *Studies in Surface Science and Catalysis* **139** 149–156, DOI: 10.1016/S0167-2991(01)80192-0.

[56] S.J. Schmieg and J.H. Lee (2005) "Evaluation of Supplier Catalyst Formulations for the Selective Catalytic Reduction of NOx With Ammonia" in *Powertrain & Fluid Systems Conference & Exhibition*.

[57] J. Gieshoff, A. Schäfer Sindlinger, P.C. Spurk, J.A.A. Van Den Tillaart and G. Garr (2000) "Improved SCR Systems for Heavy Duty Applications" in *SAE 2000 World Congress*, SAE International.

[58] E. Japke, M. Casapu, V. Trouillet, O. Deutschmann and J.D. Grunwaldt (2015) "Soot and hydrocarbon oxidation over vanadia-based SCR catalysts" *Catalysis Today* 16–19, DOI: 10.1016/j.cattod.2015.04.020.

[59] J.Y. Luo, H. Oh, C. Henry and W. Epling (2012) "Effect of C3H6 on selective catalytic reduction of NOx by NH3 over a Cu/zeolite catalyst: A mechanistic study" *Applied Catalysis B: Environmental* **123-124(2)** 296–305, DOI: 10.1016/j.apcatb.2012.04.038.

[60] The Association of European Vehicle Logistics "Sulphur Content in Marine Fuels" [Online] Available at: http://www.ecgassociation.eu/Portals/0/Documentation/Publications/ECGBriefingReport_SulphurContent_Jan2013.pdf, Accessed: 12/11-2015.

[61] W.S. Kijlstra, N.J. Komen, A. Andreini, E.K. Poels and A. Bliek (1996) "Promotion and deactivation of V2O5/TiO2 SCR catalysts by SO2 at low temperature" *Studies in Surface Science and Catalysis* **101** 951–960, DOI: 10.1016/S0167-2991(96)80306-5.

[62] J.P. Chen, M.A. Buzanowski, R.T. Yang and J.E. Cichanowicz (1990) "Deactivation of the Vanadia Catalyst in the Selective Catalytic Reduction Process" *Journal of the Air & Waste Management Association* **40(10)** 1403–1409, DOI: 10.1080/10473289.1990.10466793.

[63] M. Magnusson, E. Fridell and H.H. Ingelsten (2012) "The influence of sulfur dioxide and water on the performance of a marine SCR catalyst" *Applied Catalysis B: Environmental* **111-112(145)** 20–26, DOI: 10.1016/j.apcatb.2011.09.010.

[64] A.P. Walker, P.G. Blakeman, T. Ilkenhans, B. Magnusson and A.C. Mcdonald (2004) "The Development and In-Field Demonstration of Highly Durable SCR Catalyst Systems Reprinted From : Diesel Exhaust Emission Control" *SAE International 2004-01-1289* **(724)**, DOI: 10.4271/2004-01-1289.

[65] J.a. Ura, J. Girard, G. Cavataio, C. Montreuil and C. Lambert (2009) "Cold Start Performance and Enhanced Thermal Durability of Vanadium SCR Catalysts" *SAE Technical Paper Series* **01-0625**, DOI: 10.4271/2009-01-0625.

[66] C. Orsenigo, L. Lietti, E. Tronconi, P. Forzatti and F. Bregani (1998) "Dynamic Investigation of the Role of the Surface Sulfates in NOx Reduction and SO2 Oxidation over V2O5/WO3/TiO2 Catalysts" *Industrial & Engineering Chemistry Research* **37(6)** 2350–2359, DOI: 10.1021/ie970734t.

[67] T. Maunula, T. Kinnunen, K. Kanniainen, A. Viitanen and A. Savimaki (2013) "Thermally Durable Vanadium-SCR Catalysts for Diesel Applications" *SAE Technical Paper* **(4)**, DOI: 10.4271/2013-01-1063.

[68] IMO "IMO MEPC 66/6/6" [Online] Available at: http://www3.epa.gov/otaq/documents/oceanvessels/mepc-66-6-6-comments-mepc-65-amend-nox-tier-3.pdf, Accessed: 15/12-15.

[69] J. Gibson and O. Groene (1991) "Selective catalytic reduction on marine diesel engine.pdf" *Automotive Engineering* **99(10)** 18–22.

[70] T. Fujibayashi, S. Baba and H. Tanaka (2013) "Development of Marine SCR System for Large Two-stroke Diesel Engines Complying with IMO NO x Tier III" in *CIMAC Congress*.

[71] Y. Murayama, T. Tagai, T. Mimura and S. Goto (2013) "Demonstration of emission control technology for IMO NO x Tier III" in *CIMAC Congress*.

[72] R. Bank, B. Buchholz, H. Harndorf, R. Rabe and U. Etzien (2013) "High-Pressure SCR at Large Diesel Engines for Reliable NOx -Reduction and Compliance with IMO Tier III Standards" in *CIMAC Congress*.

[73] P.V. Houten, M. Boons, J. Fogarty, M. Brandmair et al. (2013) "Impact of Marine Lubricant Additives on SCR Catalyst Performance" in *CIMAC Congress*.

[74] G. Lövblad and E. Fridell(2006)"Experiences from use of some techniques to reduce emissions from ships" [Online] Available at: http://cleantech.cnss.no/wp-content/uploads/2011/09/2006-Lovblad-and-Fridell-Experiences-from-use-of-some-techniques-to-reduce-emissions-from-ships.pdf, Accessed: 16/12-15.

[75] H. Christensen and M.F. Pedersen (2013) "Continuous Development of Tier III SCR for Large 2-Stroke Diesel Engines" in *CIMAC Congress*.

[76] G. Zheng, F. Wang, S. Wang, W. Gao et al. (2014) "Urea SCR System Development for Large Diesel Engines" *SAE Technical Paper* 9, DOI: 10.4271/2014-01-2352.

[77] N. Soikkeli, M. Lehikoinen and K.O. Ronnback (2013) "Design aspects of SCR systems for HFO fired marine diesel engines" in *CIMAC Congress*.

[78] G. Zheng, A. Kotrba, M. Golin, T. Gardner and A. Wang (2012) "Overview of Large Diesel Engine Aftertreatment System Development" *SAE Technical Papers* **8**, DOI: 10.4271/2012-01-1960.

[79] G. Zheng, G. Palmer, G. Salanta and A. Kotrba (2009) "Mixer Development for Urea SCR Applications" *SAE Technical Paper*, DOI: 10.4271/2009-01-2879.

[80] V. Jayaram, A. Nigam, W.a. Welch, J.W. Miller and D.R. Cocker (2011) "Effectiveness of Emission Control Technologies for Auxiliary Engines on Ocean-Going Vessels" *Journal of the Air & Waste Management Association* **61(1)** 14–21, DOI: 10.3155/1047-3289.61.1.14.

[81] M. Feng and R. Zhan (2010) "Possible Solutions for Reducing NOx and SOx Emissions from Large Cargo Ships" in *AIChE Annual Meeting, Conference Proceedings*.

[82] Dieselnet "Emission Test Cycles" [Online] Available at: https://www.dieselnet.com/standards/cycles/iso8178.php, Accessed: 21/12-15.

[83] O. Kröcher, M. Elsener, M.R. Bothien and W. Dölling (2014) "Pre-Turbo SCR - Influence of Pressure on NOx Reduction" *MTZ worldwide* **75(4)** 46–51, DOI: 10.1007/s38313-014-0140-x.

[84] K. Sandelin and D. Peitz (2016) "SCR under pressure - pre-turbocharger NOx abatement for marine 2-stroke diesel engines" in *CIMAC Congress*.

[85] W. Schüttenhelm, C. Günther and R. Jürgens (2017) "high pressure SCR for large two-stroke engines and comparison to conventional SCR high dust applications" *VGB Powertech* **8** 58–62.

[86] T. Rammelt, B. Torkashvand, C. Hauck, J. Böhm et al. (2017) "Nitric Oxide Reduction of Heavy-Duty Diesel Off-Gas by NH3-SCR in Front of the Turbocharger" *Emission Control Science and Technology* **3(4)** 275–288, DOI: 10.1007/s40825-017-0078-y.

[87] T. Günter, J. Pesek, K. Schäfer, A. Bertótiné Abai et al. (2016) "Cu-SSZ-13 as pre-turbine NOx-removal-catalyst: Impact of pressure and catalyst poisons" *Applied Catalysis B: Environmental* **198** 548–557, DOI: 10.1016/j.apcatb.2016.06.005.

[88] J.M. Luján, V. Bermúdez, P. Piqueras and Ó. García Afonso (2015) "Experimental assessment of pre-turbo aftertreatment configurations in a single stage turbocharged diesel engine. Part 1: Steady-state operation" *Energy* **80** 599–613, DOI: 10.1016/j.energy.2014.05.048.

[89] D. Chatterjee, T. Burkhardt, M. Weibel, I. Nova et al. (2007) "Numerical Simulation of Zeolite- and V-Based SCR Catalytic Converters" in *Sae Technical Papers*.

[90] I. Nova, C. Ciardelli, E. Tronconi, D. Chatterjee and M. Weibel (2009) "Unifying redox kinetics for standard and fast NH3-SCR over a V2O5-WO3/TiO 2 catalyst" *AIChE Journal* **55(6)** 1514–1529, DOI: 10.1002/aic.11750.

[91] L. Lietti, I. Nova, S. Camurri, E. Tronconi and P. Forzatti (1997) "Dynamics of the SCR-DeNOx reaction by the transient-response method" *AIChE Journal* **43(10)** 2559–2570, DOI: 10.1002/aic.690431017.

[92] M. Koebel, G. Madia and M. Elsener (2002) "Selective catalytic reduction of NO and NO2 at low temperatures" *Catalysis Today* **73(3-4)** 239–247, DOI: 10.1016/S0920-5861(02)00006-8.

[93] H. Tsukahara, T. Ishida and M. Mayumi (1999) "Gas-Phase Oxidation of Nitric Oxide: Chemical Kinetics and Rate Constant" *Nitric Oxide* **3(3)** 191–198, DOI: 10.1006/niox.1999.0232.

[94] O. Levenspiel (1989) "The chemical reactor omnibook", *Distributed by OSU Book Stores*, ISBN: 0882461648.

[95] A.S. Pushnov (2006) "Calculation of average bed porosity" *Chemical and Petroleum Engineering* **42(1-2)** 14–17, DOI: 10.1007/s10556-006-0045-x.

[96] J.B. Rawlings and J.G. Ekerdt (2002) "Chemical reactor analysis and design fundamentals" 2. Edition ed., *Nob Hill Pub*, ISBN: 0615118844.

[97] P. Forzatti, I. Nova and A. Beretta (2000) "Catalytic properties in deNOx and SO2–SO3 reactions" *Catalysis Today* **56(4)** 431–441, DOI: 10.1016/S0920-5861(99)00302-8.

[98] B.K. Olsen (2015) "Deactivation of SCR catalysts in biomass fired power plants", *Ph.D. Thesis, Technical University of Denmark*.

[99] R.K. Shah and A.L. London (1978) "Laminar Flow Forced Convection in Ducts".

[100] H. Tratz and U. Grigull (1965) "Thermischer Einlauf in Ausgebildeter Laminarer Rohrströmung" *International Journal of Heat and Mass Transfer* **8** 669–678.

[101] E. Tronconi and P. Forzatti (1992) "Adequacy of lumped parameter models for SCR reactors with monolith structure" *AIChE Journal* **38(2)** 201–210, DOI: 10.1002/aic.690380205.

[102] S.R. Christensen, B.B. Hansen, K. Johansen, K.H. Pedersen et al. (2018) "SO2 Oxidation Across Marine V2O5-WO3-TiO2 SCR Catalysts: a Study at Elevated Pressure for Preturbine SCR Configuration" *Emission Control Science and Technology*, DOI: 10.1007/s40825-018-0092-8.

[103] J.J. Corbett and P. Fischbeck (1997) "Emissions from Ships" *Science* **278(5339)** 823–824, DOI: 10.1126/science.278.5339.823.

[104] C. Orsenigo, A. Beretta, P. Forzatti, J. Svachula et al. (1996) "Theoretical and experimental study of the interaction between NOx reduction and SO2 oxidation over DeNOx-SCR catalysts" *Catalysis Today* **27(1-2)** 15–21, DOI: 10.1016/0920-5861(95)00168-9.

[105] J.M. Burke and K.L. Johnson(1982)"Ammonium sulfate and bisulfate formation in air preheaters".

[106] S. Matsuda, T. Kamo, A. Kato, F. Nakajima et al. (1982) "Deposition of ammonium bisulfate in the selective catalytic reduction of nitrogen oxides with ammonia" *Industrial & Engineering Chemistry Product Research and Development* **21(1)** 48–52, DOI: 10.1021/i300005a009.

[107] J.R. Thøgersen, T. Slabiak and N. White(2012)"Ammonium bisulphate inhibition of SCR catalysts Contents :" [Online] Available at: http://www.topsoe.com/sites/default/files/ammonium_bisulphate_inhibition_of_scr_catalysts.ashx__0.pdf, Accessed: 1/2-16.

[108] J.P. Dunn, P.R. Koppula, H. G. Stenger and I.E. Wachs (1998) "Oxidation of sulfur dioxide to sulfur trioxide over supported vanadia catalysts" *Applied Catalysis B: Environmental* **19(2)** 103–117, DOI: 10.1016/S0926-3373(98)00060-5.

[109] J. Svachula, L.J. Alemany, N. Ferlazzo, P. Forzatti et al. (1993) "Oxidation of sulfur dioxide to sulfur trioxide over honeycomb DeNoxing catalysts" *Industrial & Engineering Chemistry Research* **32(5)** 826–834, DOI: 10.1021/ie00017a009.

[110] E. Tronconi, A. Cavanna, C. Orsenigo and P. Forzatti (1999) "Transient Kinetics of SO2 Oxidation Over SCR-DeNO x Monolith Catalysts" *Industrial & Engineering Chemistry Research* **38(7)** 2593–2598, DOI: 10.1021/ie980673e.

[111] H. Kamata, H. Ohara, K. Takahashi, A. Yukimura and Y. Seo (2001) "SO2 oxidation over the V2O5/TiO2 SCR catalyst" *Catalysis Letters* **73(1)** 79–83, DOI: 10.1023/A:1009065030750.

[112] M.T. Nielsen "On the relative importance of SO2 oxidation to high dust SCR DeNOx units" [Online] Available at: http://www.topsoe.com/sites/default/files/topsoe_importance_of_so2_oxidation_to_high_dust_scr_april_08.ashx_.pdf.

[113] E. Tronconi, A. Beretta, A.S. Elmi, P.L.D. Vinci et al. (1994) "A complete model of SCR monolith reactors for the analysis of interacting NOx reduction and SO2 oxidation reactions" *Chemical Engineering Science* **49(24)** 4277–4287.

[114] "Plot Digitizer" [Online] Available at: http://plotdigitizer.sourceforge.net/, Accessed: 24/1-18.

[115] N.N. Sazonova, L.T. Tsykoza, A.V. Simakov, G.B. Barannik and Z.R. Ismagilov (1994) "Relationship between sulfur dioxide oxidation and selective catalytic NO reduction by ammonia on V2O5-TiO2 catalysts doped with WO3 and Nb2O5" *Reaction Kinetics & Catalysis Letters* **52(1)** 101–106, DOI: 10.1007/BF02129856.

[116] A.A. Ivanov and B.S. Balzhinimaev (1987) "New data on kinetics and reaction mechanism for SO2 oxidation over vanadium catalysts" *Reaction Kinetics and Catalysis Letters* **35(1-2)** 413–424, DOI: 10.1007/BF02062176.

[117] P. Glarborg (2007) "Hidden interactions—Trace species governing combustion and emissions" *Proceedings of the Combustion Institute* **31(1)** 77–98, DOI: 10.1016/j.proci.2006.08.119.

[118] "NIST database" [Online] Available at: https://www.nist.gov/, Accessed: 22/12-2017.

[119] P. Forzatti (1997) "Kinetic study of a simple chemical reaction" *Catalysis Today* **34(3-4)** 401–409, DOI: 10.1016/S0920-5861(96)00062-4.

[120] Z. Huang, Z. Zhu, Z. Liu and Q. Liu (2003) "Formation and reaction of ammonium sulfate salts on V2O5/AC catalyst during selective catalytic reduction of nitric oxide by ammonia at low temperatures" *Journal of Catalysis* **214(2)** 213–219, DOI: 10.1016/S0021-9517(02)00157-4.

[121] C. Zhou, L. Zhang, Y. Deng and S.C. Ma (2016) "Research progress on ammonium bisulfate formation and control in the process of selective catalytic reduction" *Environmental Progress & Sustainable Energy* **35(6)** 1664–1672, DOI: 10.1002/ep.12409.

[122] I.S. Nam, J.W. Eldridge and J.R. Kittrell (1986) "Deactivation of a Vanadia-Alumina Catalyst for NO Reduction by NH3" *Ind. Eng. Chem. Prod. Res. Dev.* **25** 192–197.

[123] J. Ando(1979)"NOx abatement for stationary sources in Japan" [Online] Available at: https://nepis.epa.gov/Exe/ZyNET.exe/9100BPNI.TXT?ZyActionD=ZyDocument&Client=EPA&Index=1976+Thru+1980&Docs=&Query=&Time=&EndTime=&SearchMethod=1&TocRestrict=n&Toc=&TocEntry=&QField=&QFieldYear=&QFieldMonth=&QFieldDay=&IntQFieldOp=0&ExtQFieldOp=0&XmlQuery=, Accessed: 13/12-16.

[124] J.Y. Wei, L.J. Muzio and D. Dunn Rankin (2007) "Formation temperature of ammonium bisulfate at sumulated air preheater conditions" in *5th US Combustion Meeting 2007*, Curran Associates Inc.

[125] J. Menasha, D. Dunn Rankin, L. Muzio and J. Stallings (2011) "Ammonium bisulfate formation temperature in a bench-scale single-channel air preheater" *Fuel* **90(7)** 2445–2453, DOI: 10.1016/j.fuel.2011.03.006.

[126] J.P. Hansen (2012) "Exhaust Gas Scrubber Installed Onboard MV Ficaria Seaways", *Danish Ministry of the Environment*, ISBN: 9788792903280.

[127] IMO "The 2020 Global Sulfur Limit" [Online] Available at: http://www.imo.org/en/MediaCentre/HotTopics/GHG/Documents/FAQ_2020_English.pdf, Accessed: 12/10-17.

[128] F.H. Verhoff and J.T. Banchero (1974) "Predicting Dew Points of Flue Gases" *Chemical Engineering Progress* **70(8)** 71 – 72.

[129] M.S. Bashir, P.A. Jensen, F. Frandsen, S. Wedel et al. (2012) "Suspension-Firing of Biomass. Part 2: Boiler Measurements of Ash Deposit Shedding" *Energy & Fuels* **26(8)** 5241–5255, DOI: 10.1021/ef300611v.

[130] B. Roduit, A. Wokaun and A. Baiker (1998) "Global Kinetic Modeling of Reactions Occurring during Selective Catalytic Reduction of NO by NH3 over Vanadia/Titania-Based Catalysts" *Industrial & Engineering Chemistry Research* **37(12)** 4577–4590, DOI: 10.1021/ie980310e.

[131] P.B. Louis (1999) "Minimizing the impact of SCR/SNCR retrofits on the Ljungstrom air preheater", *ALS-TOM Power Air Preheater, Inc. Wellsville, NY.*

[132] H.S. Fogler (2016) "Elements of chemical reaction engineering", *Pearson Education,*, ISBN: 9780133887518.

[133] R.B. Bird, W.E. Stewart and E.N. Lightfoot (2007) "Transport phenomena", *J. Wiley*, ISBN: 9780470115398.

[134] D.E. Mears (1971) "Role of axial dispersion in trickle-flow laboratory reactors" *Chemical Engineering Science* **26** 1361–1366.

[135] H. Gierman (1988) "Design of laboratory hydrotraeting reactors - Scaling down of trickle-flow reactors" *Applied Catalysis* **43** 277–286.

[136] N. Wakao, S. Kaguei and T. Funazkri (1979) "Effect of fluid dispersion coefficients on particle-to-fluid heat-transfer coefficients in packed-beds - Correlation of Nusselt numbers" *Chemical Engineering Science* **34** 325–336.

[137] M. Puncochar and J. Drahos (1993) "The tortuosity concept in fixed and fluidized-bed" *Chemical Engineering Science* **48** 2173–2175.

[138] C.F. Chu and K.M. Ng (1989) "Flow in packed tubes with a small tube to particle diameter ratio" *AIChE Journal* **35** 148–158.

[139] G. Marin and G.S. Yablonsky (2011) "Kinetics Of Chemical Reactions", *John Wiley & Sons*, ISBN: 3527317635.

Appendix A SCR Engine Test

Fujibayashi et al.[70] tested how engine dynamics were affected when an SCR reactor was installed upstream of the turbocharger, the results are shown in Figure A.1. The experiments was performed on a 6S46MC-C7 6.78 MW marine diesel engine at a 38000 DWT cargo carrier. The cylinder out temperature which is changed at low load under SCR operation is due to a cylinder bypass made in order to ensure high enough temperature for SCR operation as explained in Section 1.3.2.1. In general it was concluded by Fujibayashi et al. that the ships was maneuverable as usual also after the SCR reactor was installed upstream the turbocharger.

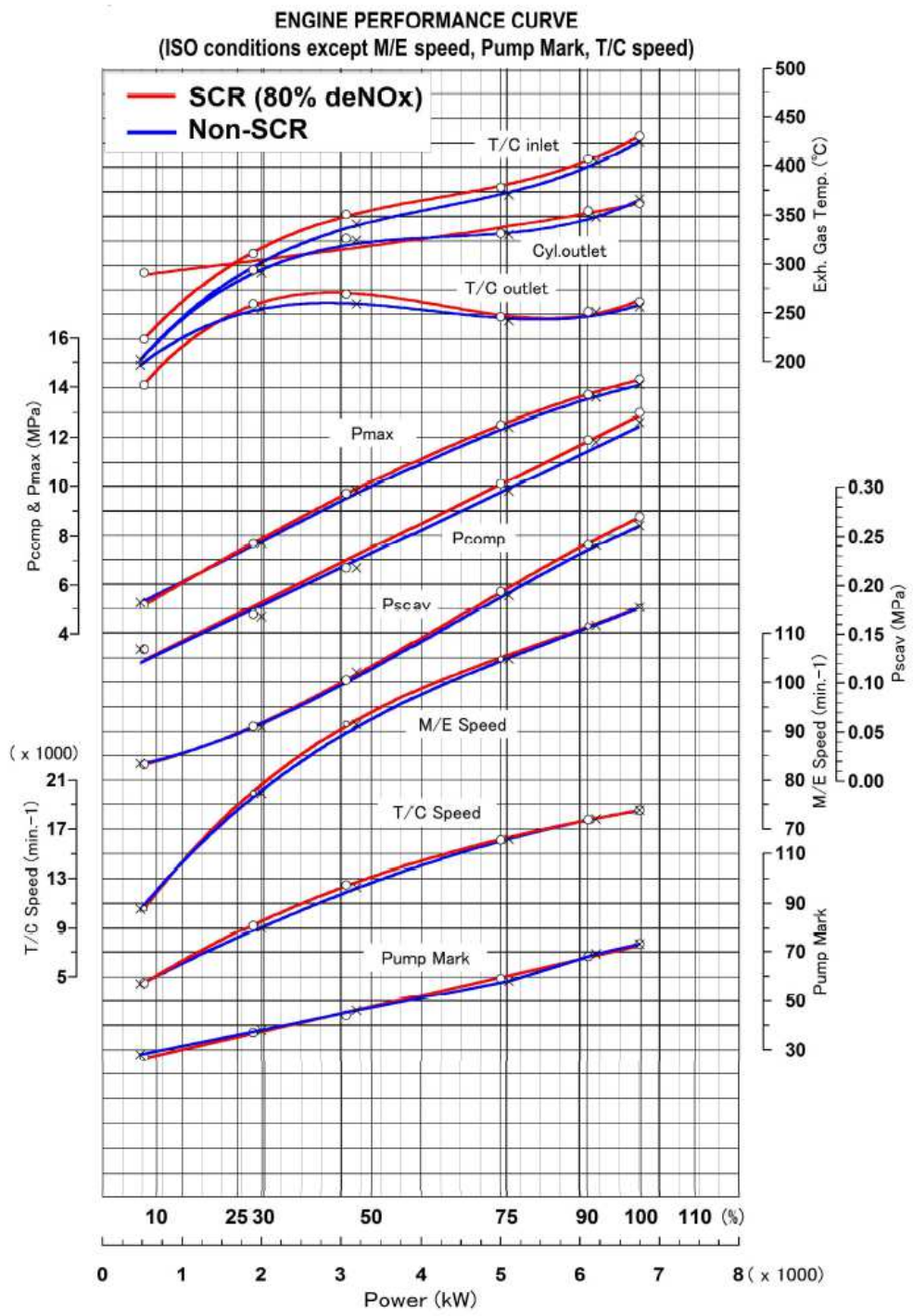

Figure A.1: Test of how engine dynamics are changed when a SCR reactor is installed upstream of the turbocharger[70].

Appendix B NH_3 TPD - Fitting

Based on 80 CSTR's in series the following fitting results were found for the NH_3 experiment.

Table B.1: The fitted adsorption-desorption kinetics parameters including the parameters fitted by Lietti et al.[91] for a Ternary $V_2O_5/WO_3/TiO_2$ catalyst. Ω is in this study calculated based upon the amount of NH_3 adsorbed at 150℃ and 4.5 bar, as shown in Equation 2.9 and Equation 2.11. E_a^0 is assumed to be zero in both studies.

Parameters	k_a^0	E_a^0	k_d^0	E_d^0	α	Ω
Units	$\frac{m^3}{mol \cdot s}$	$\frac{kJ}{mol}$	$\frac{1}{s}$	$\frac{kJ}{mol}$	-	$\frac{mol}{m^3_{\text{reactor}}}$
This Study	6.8	0	$11 \cdot 10^5$	92.8	0.299	372
Lietti et al.[91]	0.487	0	$2.68 \cdot 10^5$	95.8	0.405	270

Based on these parameters the following fitting results can be found for a pressure of 1.2 bar, 2.4 bar, 3.6 bar, and 4.5 bar

1.2 Bar Experiment

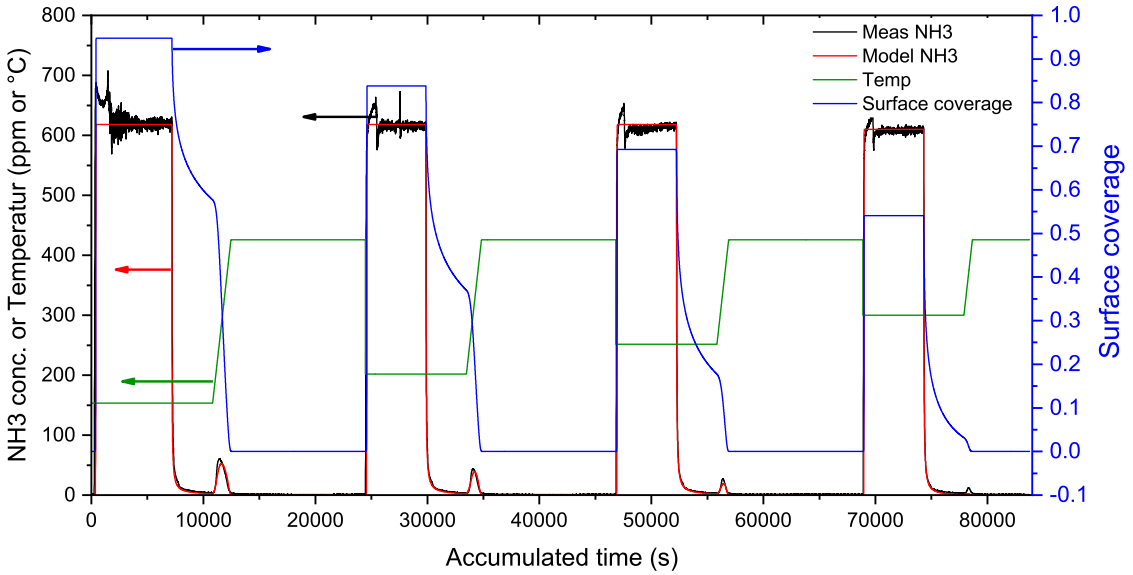

Figure B.1: Measured and model prediction at 1.2 bar based on the fitted parameters shown in Table B.1.

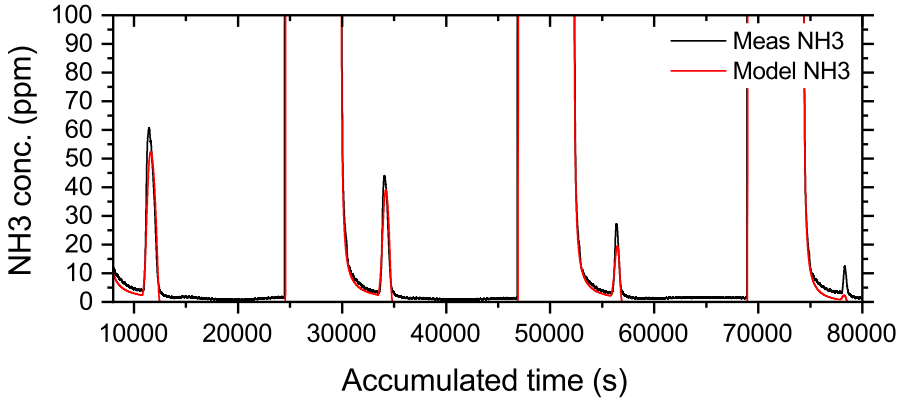

Figure B.2: A zoom of the NH_3 desorption peaks. Measured and model prediction at 1.2 bar based on the fitted parameters shown in Table B.1.

2.4 Bar Experiment

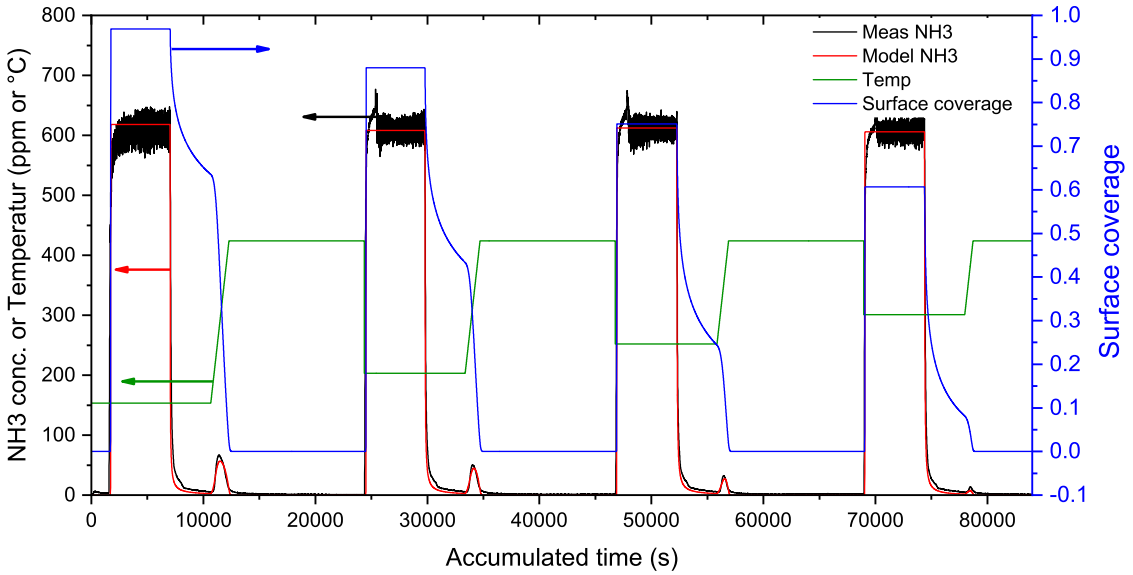

Figure B.3: Measured and model prediction at 2.4 bar based on the fitted parameters shown in Table B.1.

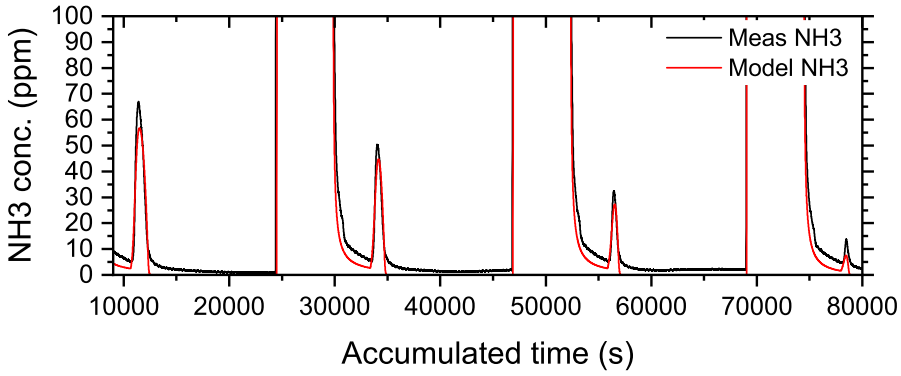

Figure B.4: A zoom of the NH_3 desorption peaks. Measured and model prediction at 2.4 bar based on the fitted parameters shown in Table B.1.

3.6 Bar Experiment

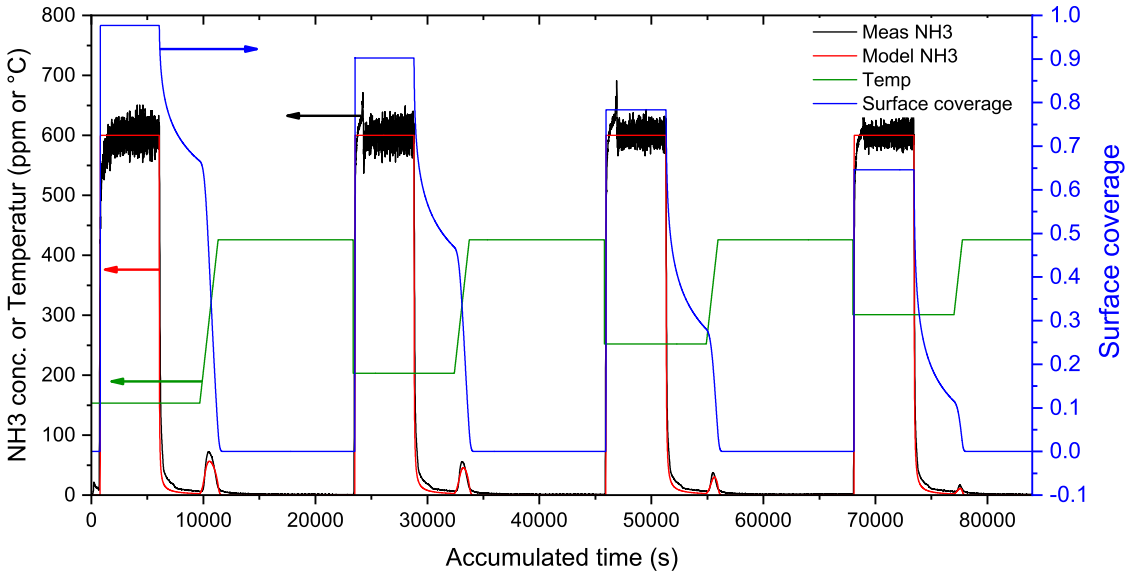

Figure B.5: Measured and model prediction at 3.6 bar based on the fitted parameters shown in Table B.1.

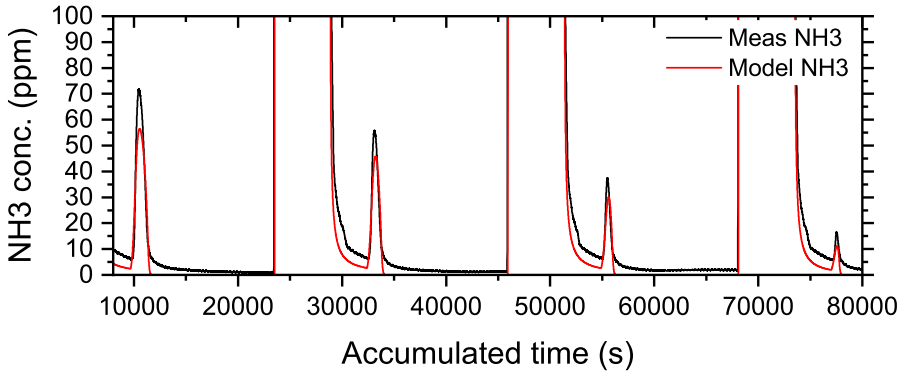

Figure B.6: A zoom of the NH_3 desorption peaks. Measured and model prediction at 3.6 bar based on the fitted parameters shown in Table B.1.

4.5 Bar Experiment

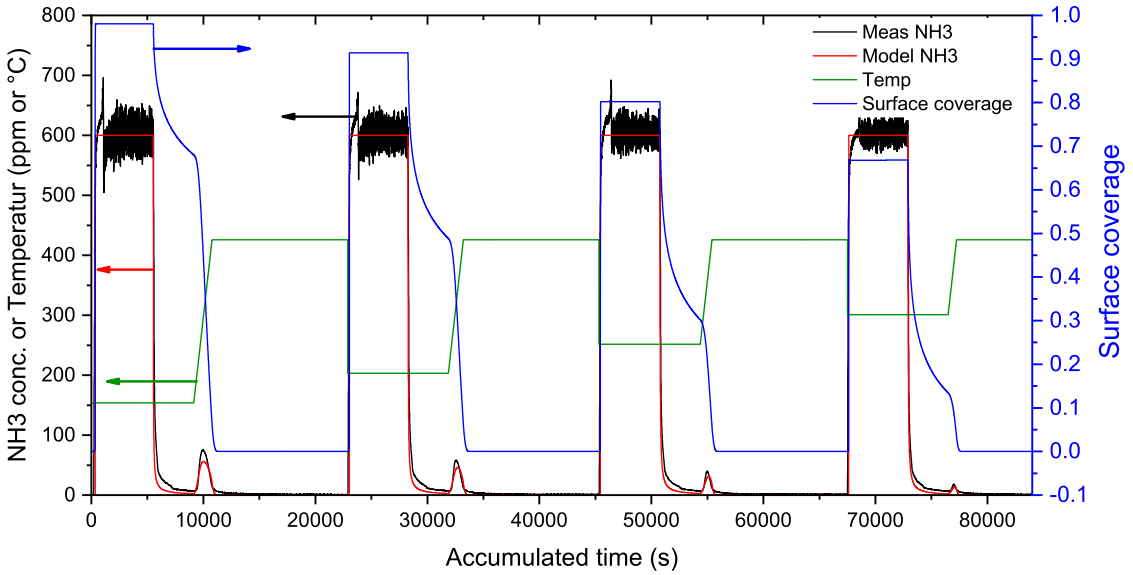

Figure B.7: Measured and model prediction at 4.5 bar based on the fitted parameters shown in Table B.1.

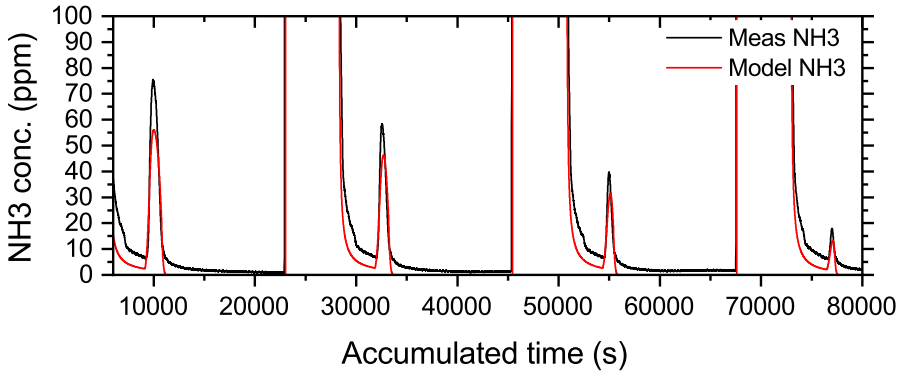

Figure B.8: A zoom of the NH_3 desorptions peaks. Measured and model prediction at 4.5 bar based on the fitted parameters shown in Table B.1.

Appendix C Limitations in a PBR

C.1 Diffusion Limitations

The diffusion limitation for the packed bed reactor is calculated on the basis of the effectiveness factor assuming spherical particles as given in Equation C.1[132].

$$\eta = \frac{3}{\phi^2} \cdot (\phi \cdot coth(\phi) - 1) \tag{C.1}$$

$$\phi = R_p \cdot \sqrt{\frac{k' \cdot \rho}{D_{ab}}} \tag{C.2}$$

In which R_p is the particle radius, k' is the weight based first order rate constant, D_{ab} is the binary diffusivity, and η is the effectiveness factor.

The binary diffusion coefficient is calculated based on the Chapman-Enskog theory as presented by Turns[6] and Bird et al[133]. The binary diffusion coefficient is calculated based on:

$$D_{AB} = \frac{3}{16} \cdot \sqrt{\frac{2 \cdot (R \cdot T)^3}{\pi} \cdot \left(\frac{1}{M_A} + \frac{1}{M_B}\right)} \cdot \frac{1}{N_A \cdot P \cdot \sigma_{AB}^2 \cdot \Omega_{D,AB}} \tag{C.3}$$

In which N_A is Avogrados constant, P is the pressure, σ_{AB} is the hard sphere collision diameters , and $\Omega_{D,AB}$ is the collision integral. σ_{AB} is calculated based Equation C.4 and the Lennard-Jones parameters given in Table C.1 for NO, NH_3 and air.

$$\sigma_{AB} = \frac{\sigma_A + \sigma_B}{2} \tag{C.4}$$

Table C.1: Lennard-Jones Parameters[6].

specie	σ - (Å)	ϵ/k_b - (K)
Air	3.711	78.6
NH_3	2.900	559.3
NO	3.492	116.7

The collision integral, $\Omega_{D,AB}$ is calculated as shown in Equation C.5, and based on

the dimensionless temperature, T^* as given in Equation C.6.

$$\Omega_{D,AB} = \frac{1.06036}{(T^*)^{0.15610}} + \frac{0.19300}{exp(T^* \cdot 0.47635)} + \frac{1.03587}{exp(T^* \cdot 1.52996)} + \frac{1.76474}{exp(T^* \cdot 3.89411)} \tag{C.5}$$

$$T^* = \frac{k_b \cdot T}{\epsilon_{AB}} = \frac{T}{\left(\frac{\epsilon_A}{k_b} \cdot \frac{\epsilon_B}{k_b}\right)^{1/2}} \tag{C.6}$$

Based on the Chapman-Enskog theory the binary diffusion coefficient was calculated at each temperature and pressure, an example of each diffusion coefficient is shown in Table C.2.

Table C.2: The binary diffusion coefficient for NO in air and NH_3 in air at 200 ℃ and 1 bar, calculated based on the Chapman-Enskog theory.

Specie A	Specie B	D_{AB} - m^2/s
NO	Air	$4.6055 \cdot 10^{-5}$
NH_3	Air	$5.2468 \cdot 10^{-5}$

Based on the binary diffusion and the NO rate given in Table 2.3 the diffusion limitation calculated for the mean particle diameter of 225 microns (sieved to 150-300 microns) is shown in Figure C.1.

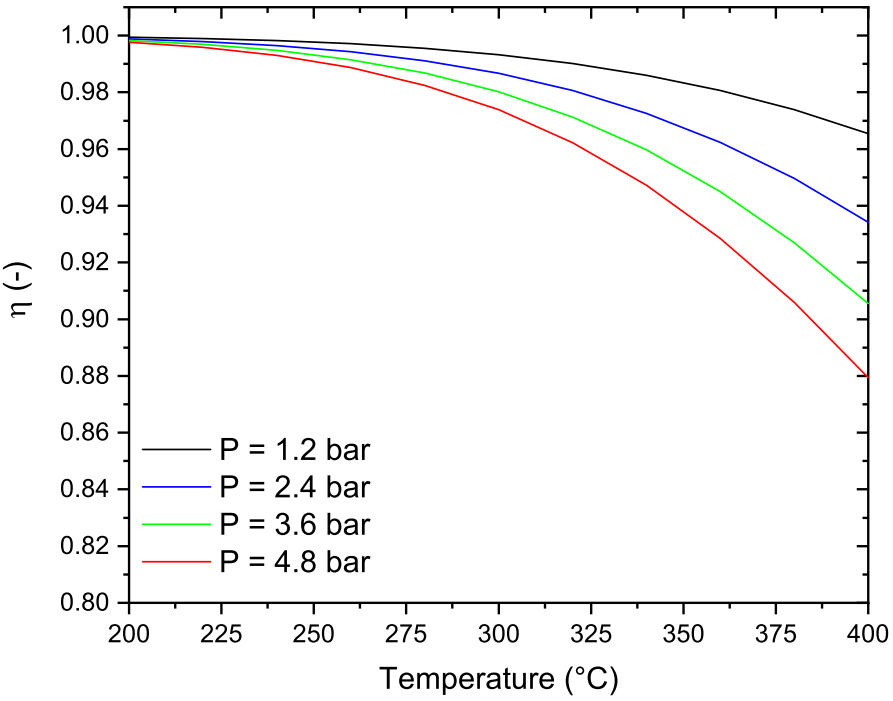

Figure C.1: The diffusion limitations calculated for a mean particle diameter of 225 microns using the NO rate as given in Table 2.3.

As given in Figure C.1, the effectiveness factor is above 0.9 for all cases except at

4.8 bar and 400℃ at which it reaches 0.88, and therefore, the assumption of no diffusion limitation is assumed valid.

C.2 Dispersion

C.2.1 Axial Dispersion

Mears[134] and Gierman[135] defined the following criterion for the bed height allowing neglection of the axial dispersion which is of importance to assume plug flow behavior.

$$\frac{h_{bed}}{d_p} > \frac{8}{Bo} \cdot n \cdot ln\left(\frac{1}{1-X_A}\right). \tag{C.7}$$

In which, h_{bed} is the bed height, d_p is the particle diameter, n is the reaction order and Bo is the bodenstein number which according to Wakao et al.[136] can be calculated based on the following correlation.

$$\frac{1}{Bo} = \frac{\epsilon_b \cdot D_{A,m}}{\tau_b \cdot d_p \cdot u_0} + 0.5 \tag{C.8}$$

At 300℃, the SCR reaction is found to have a conversion of 60% using a flow rate of 300 NmL/min, ANR=1.2 and a pressure of 1.2 bar. The porosity of the bed is 0.38 and the molecular diffusion of air in NO is found to be $D_{air,NO} = 6.28{\cdot}10^{-5}\mathrm{m}^2/\mathrm{s}$ also at 300℃. For the tortuosity the correlation reported by Puncochar & Drahos[137] is used, as given by:

$$\tau_b = \frac{1}{\sqrt{\epsilon_b}} \tag{C.9}$$

The bed height for the SCR experiments was 4 mm, using catalyst particles in a size fraction of 150-300 micron, hence a average diameter of 225 micron, the following can be calculated for the axial dispersion:

$$\frac{h_{bed}}{d_P} = 18 > 0.68 \tag{C.10}$$

Hence no axial dispersion is present.

C.2.2 Radial Dispersion

The radial dispersion, can according to Chu & Ng[138] be evaluated based on the bed diameter and the particle diameter.

$$\frac{d_t}{d_p} > 8 \tag{C.11}$$

The bed diameter used for the SCR experiments are 4 mm and a mean diameter of the particles of 225 micron has been used, therefore the following applies:

$$17.8 > 8 \tag{C.12}$$

Hence no radial dispersion is present.

Appendix D Online Resources for SO_2 Ox. Article

SO_2 Oxidation across Marine V_2O_5-WO_3-TiO_2 SCR Catalysts – A Study at Elevated Pressure for Pre-turbine SCR Configuration

Authors: Steen R. Christensen[a], Brian B. Hansen[a], Keld Johansen[b], Kim H. Pedersen[c], Joakim R. Thøgersen[c], and Anker Degn Jensen[a,*].

[a] *Department of Chemical and Biochemical Engineering, Technical University of Denmark, Søltofts Plads B229, 2800 Kgs Lyngby, Denmark*
[b] *Haldor Topsoe A/S, Haldor Topsøes Allé 1, 2800 Kgs. Lyngby, Denmark*
[c] *Umicore Denmark ApS, Nøjsomhedsvej 20, DK-2800 Kgs. Lyngby, Denmark*
[*] Corresponding author: aj@kt.dtu.dk , +45 4525 2841,
OrCID: 0000-0002-7341-4859

D.1 Mass Transfer Limitations

The mass transfer limitations for the monolith is evaluated using the rate constant estimated when assuming first order dependency of SO2 and zero order dependency of SO3 as given in the last entry in Table 3.4, however, the rate constant are multiplied by (R·T) to convert the units into (m^3/kg/s).

External Mass Transfer Limitations:

The extent of external mass transfer limitations is evaluated based on the Carberry number as given by Equation D.1[139]

$$Ca = \frac{r_w^{obs}}{k_g \cdot A_s \cdot C_{bulk}} = \frac{\frac{k_w \cdot k_g \cdot A_s \cdot C_{bulk}}{k_w + k_g \cdot A_s}}{k_g \cdot A_s \cdot C_{bulk}} \tag{D.1}$$

In which k_w is the mass based rate constant (m^3/kg/s), k_g is the mass transfer coefficient, A_s is the specific surface area of the catalyst, and C_{bulk} is the bulk concentration of SO_2. The mass transfer coefficient is dependent on the flow profile

within the channels, as given through the dimensional Sherwood number. It is assumed that the flow profile is turbulent in the beginning of the channel, and as the flow passes down the length of the monolith the flow profile approaches a laminar flow profile. Tronconi et al.[51, 101] proposed the following correlation for the Sherwood number for a developing laminar flow profile.

$$Sh = Sh_{\infty} + 8.827 \cdot (1000 \cdot Z^*)^{-0.545} \cdot \exp(-48.2 \cdot Z^*) \tag{D.2}$$

Where Sh_{∞}, is the asymptotic Sherwood number which depends on the channel geometry, according to Table D.1.

Table D.1: Asymptotic Sherwood numbers depending on the channel geometry as given by Tronconi et al.[101]

Channel Geometry	Sh_{∞}
Circular	3.659
Square	2.977
Equilateral Triangular	2.494

The lowest Sherwood number must also result in the lowest mass transfer coefficient and therefore also the worst case scenario with respect to mass transfer limitations. Therefore, at a completely developed laminar velocity profile, the lowest Sherwood number will be present ($Sh = Sh_{\infty}$). For the catalyst used in this paper the channel geometry was equilateral triangles. The mass transfer coefficient can therefore be calculated based upon Equation D.3

$$Sh_{\infty} = \frac{k_g \cdot d_h}{D_{AB}} \tag{D.3}$$

In which d_h is the hydraulic diameter as given in Table 3.1 and D_{AB} is the binary diffusivity of A in B, which here is evaluated as SO_2 in air. The Binary diffusivity was calculated based upon the Chapman-Enskog theory as presented by Bird et al.[133] and as given in Equation D.4

$$D_{AB} = \frac{3}{16} \cdot \sqrt{\frac{2 \cdot (R \cdot T)^3}{\pi} \cdot \left(\frac{1}{M_A} + \frac{1}{M_B}\right)} \cdot \frac{1}{\tilde{N} \cdot P \cdot \sigma_{AB}^2 \cdot \Omega_{D,AB}} \tag{D.4}$$

In which M_A, M_B are molecular weight of species "A" and "B" respectively, $\tilde{N}$ is Avogrados constant, σ_{AB} is the mean hard collision sphere, and $\Omega_{D,AB}$ is the collision integral calculated on the basis of Lennard-Jones parameters as given by Turns[6]. Based on the above a diffusivity of $D_{AB} \cdot 10^6 = 43.15 \mathrm{m}^2/\mathrm{s}$ is found at 200℃. Furthermore, based on a bulk concentration of SO_2 of 1000 ppm and a specific surface area of A_s=4.63 m^2/kg the Carberry number is calculated as shown in Figure D.1.

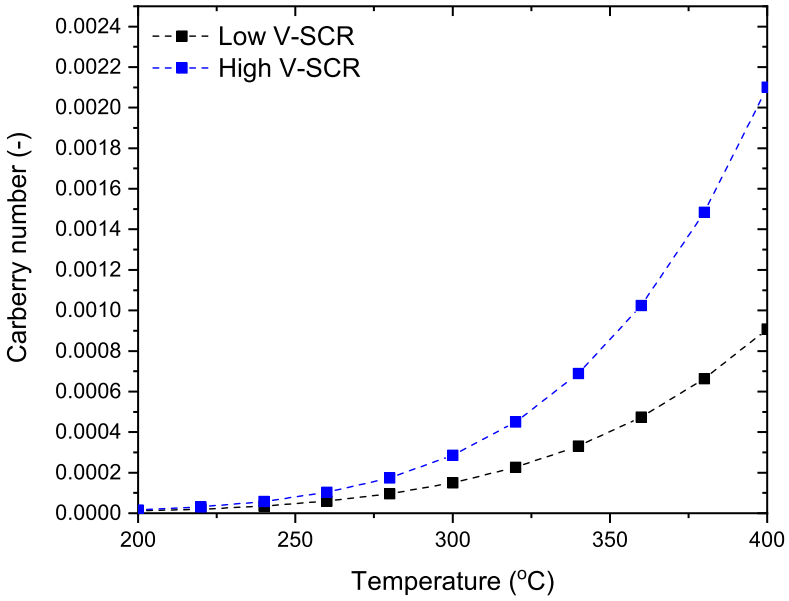

Figure D.1: The Carberry number calculated for the low and high V-SCR catalyst.

Figure D.1 shows that $Ca << 0.05$ indicating that no external mass transfer limitations are present.

Internal Mass Transfer Limitations:

Internal mass transfer limitation can be evaluated based upon the effectiveness factor for a slab, in which the characteristic length "L" is the half thickness of the walls due to symmetry conditions. Based on Fogler[132] the effectiveness factor for a slab is given as in Equation D.5.

$$\eta = \frac{tanh(\phi')}{\phi'} \quad , \quad \phi' = L \cdot \sqrt{\frac{k_w \cdot \rho_{bulk}}{D_{AB}}} \tag{D.5}$$

In which ρ_{bulk} is the bulk density. Based on Equation D.5 the effectiveness factor was found to $\eta > 0.99$ for the temperature interval investigated, and hence internal mass transfer can be neglected, and the reaction must therefore be kinetic limited. At increasing pressure the binary diffusion will be lowered, and the reaction will therefore also be kinetic limited at increased pressure.